INVESTIGATION OF THE STRUCTURAL AND ELECTRO-OPTICAL PROPERTIES OF CHEMICALLY DEPOSITED ZnS AND CdS THIN FILMS AND THE THERMOLUMINESCENCE PROPERTIES OF ZnS THIN FILMS

Ph. D. Thesis

in

Physics Engineering
University of Gaziantep

By
Mustafa Oztas
December 1996

Approval of the Graduate School of Natural and Applied Science.

Prof.Dr.Mazhar UNSAL
Director

I certify that I have read this thesis and that in my opinion it is fully adequate, in scope and quality, as a dissertation for the degree of Doctor of Philosohy.

Assoc.Prof.Dr. Refik KAYALI
Chairman of the Department

I certify that I have read this thesis and that in my opinion it is fully adequate, in scope and quality, as a dissertation for the degree of Doctor of Philosophy.

Assoc. Prof. Dr. Ramazan ESEN

Assoc.Prof.Dr. Refik KAYALI

Supervisors

Examinig Committee in Charge

Prof.Dr.Selami KILINCKAYA ……………………

Assoc.Prof.Dr.Refik KAYALI ……………………

Assoc.Prof.Dr.Ramazan ESEN ……………………

Assist.Prof.Dr.Zihni OZTURK ……………………

Assist.Prof.Dr.Andrew Beddall A. J. Beddall ……………………

ABSTRACT

INVESTIGATION OF THE STRUCTURAL AND ELECTRO-OPTICAL PROPERTIES OF CHEMICALLY DEPOSITED ZnS AND CdS THIN FILMS AND THE THERMOLUMINESCENCE PROPERTIES OF ZnS THIN FILMS

OZTAS, MUSTAFA
Ph. D. in P.E., University of Gaziantep
Supervisor:Assoc.Prof.Dr.Refik KAYALI
Co-adviser: Assoc.Prof.Dr.Ramazan ESEN
December 1996, 140 Pages

In this work, ZnS and CdS thin films have been developed onto glass substrates with different concentrations and at different substrate temperatures using the spraying pyrolysis method and electric, electronic, optic, structural, and thermoluminescence properties of these films have been investigated.

The resistivities and Hall mobilities of the CdS and ZnS thin film samples were obtained using Van der Pauw method in the dark and under the illumination. The transit time of the CdS thin films was measured using the Haynes-Shockley experiment and the drift mobility of these films was calculated using these results. The carrier lifetimes of the CdS thin films was determined using photoconductive decay method. The trap density in CdS thin films was calculated using the space-charge limited current method. The optical absorption coefficients of both the CdS and ZnS films were found from optical measurements and using these results the energy bandgap of these films was calculated. It was shown that both of these films have a wurtzite crystal structure by employing the X-ray diffraction powder method.

Finally, the thermoluminescence property of ZnS thin films was examined. The trap density, activation energy and frequency factor values of these thin films were found from their glow curves. Then, the lifetime of the electrons trapped , using the values of activation energy and frequency factor, has been calculated.

Keywords: Spray pyrolysis, thin film, ZnS and CdS

ÖZET

ZnS VE CdS İNCE FİLMLERİNİN YAPISAL, ELEKTRİKSEL VE OPTİK VE ZnS İNCE FİLMLERİNİN TERMOLUMİNESANS ÖZELLİKLERİNİN İNCELENMESİ

ÖZTAS, MUSTAFA
Ph. D. in P.E., University of Gaziantep
Supervisor:Assoc.Prof.Dr.Refik KAYALI
Co-adviser: Assoc.Prof.Dr.Ramazan ESEN
Aralık 1996, 140 sayfa

Bu çalışmada, ZnS ve CdS ince filmleri değişik derişimlerde ve değişik sıcaklıklarda püskürtme yöntemiyle elde edilmiş ve bu filmlerin elektrik, elektronik, optik, yapısal ve termolüminesans özellikleri incelenmiştir.

CdS ve ZnS ince film örneklerinin dirençleri ve Hall mobiliteleri (karanlıkta ve aydınlıkta) Van Der Pauw metoduyla bulunmuştur. CdS ince filmlerde geçiş zamanı (transit time) değerleri Haynes-Schokley deneyinden elde edilmiş ve bu değerler kullanılmak suretiyle bu filmlerin sürüklenme hareketliliği (drift mobility) değerleri hesaplanmıştır. CdS ince filmlerin taşıyıcı yaşama süreleri (carrier lifetime) fotoiletkenlik sönüm methoduyla tespit edilmiştir. CdS ince filmlerdeki tuzak yoğunluğu ise uzay-yük sınırlı akım yöntemiyle (space-charge limited current method) bulunmuştur. Ayrıca, hem CdS hemde ZnS ince filmlerin optik soğurma katsayıları optik ölçümlerle bulunmuş ve bu değerler kullanılarak bu filmlerin enerji band aralıkları tespit edilmiştir. Buna ilaveten, x-ışınları toz kırınım yöntemi kullanilarak her iki filmin Wurtzite kristal yapıya sahip oldukları gösterilmiştir.

Son olarak, ZnS ince filmlerin termoluminesans özellikleri incelenmiştir. Bu filmlerin, tuzak yoğunluğu, aktivasyon enerjisi ve frekans faktör değerleri bu filmlerin ışıldama eğrilerinden bulunmuştur. Sonra, bunlardan aktivasyon ve frekans faktörü değerlerinden yararlanarak elektronların tuzaklarda kalma süreleri hesaplanmıştır.

Anahtar Kelimeter: Püskürtme Yöntemi, İnce Film, CdS ve ZnS

ACKNOWLEDGEMENTS

The author would like to express his sincerest gratitude and thanks to his supervisor Assoc.Prof.Dr.Refik Kayali for his guidance, encouragement, assistance, advice, suggestions in the course of this work, and above all, for his warm friendship.

He would like to thank to all his friends, and Gaziantep University Physics Engineering department staff for their kind help, especially research assistant Metin Bedir and Mr. Ziya Gesoglu.

TABLE OF CONTENTS

LIST OF TABLES

LIST OF FIGURES

LIST OF SYMBOLS

ε_O : free space permittivity
q : electronic charge
h : planck constant
p : particle momentum
m_o^* :effective mass
k :propagation vector
N(E) : density of states
n(E) : density of energy states
F(E) : Fermi-Dirac distribution
E_F : Fermi level
k_b : Boltzman constant
T : temperature
F(E) : Fermi distribution function
N_v : effective density of states
n_i : intrinsic carrier density
E_g : energy bandgap
N_D : donor concentration
N_A : acceptor concentration
n : electron concentration
p : hole concentration
a : accelaration
E : electric field
m_e : electron mass
v : velocity
t : time
v_{th} : thermal velocity

μ_{drift} : drift mobility

v_D : drift velocity

t_r : transit time

σ : conductivity

ρ : resistivity

μ_n : electron mobility

μ_p : hole mobility

H : magnetic field intensity

V_H : Hall voltage

E_H : Hall field

μ_H : Hall mobility

α : absorption constant

I_o : intensity

λ : wavelength

d : thickness

η : quantum efficiency

I_p : photocurrent

τ : carrier lifetime

I_{ph} : primary photocurrent

ϕ : work function

χ : electron affinity

CHAPTER 1

LITERATURE SURVEY

1.1 Introduction

ZnS and CdS are very important semiconducting II-VI compounds which are widely used in different fields due to their optical and electronic properties. ZnS is especially used in monochrome display devices since it has luminescent behaviour, and CdS is commonly used in photodetection and solar cell applications. There are many fabrication techniques for producing these materials. Among them are chemical(wet), spray pyrolysis, vacuum evaporation, and plasma reactive methods. Every process has some distinct advantages and disadvantages in terms of material quality, suitability to device fabrication, and cost. Among them the method of spray pyrolysis (or solution spraying) is a convenient and economical method for the production of such materials.

The ZnS and CdS have been most extensively studied because of their luminescent properties and photoconductive properties. As a general rule, the electrical properties of the group II-VI compounds are between those of the group I-VII and III-V compounds. For example, the energy gaps of ZnS and

CdS are, respectively, 3.7 eV and 2.4 eV, compared to 9.4 eV for KCl and 1.4 eV for GaAs. The best estimate of the nature of the binding seems to indicate that the ZnS lattice is about 75% covalent, which is intermediate between predominantly ionic KCl and predominantly covalent GaAs. Because the gap energy in ZnS and CdS is either close to or in the visible region, the materials are useful for generation and detection of visible radiation. The luminescent and photoconductive process in these materials may involve the band states as well as the impurity states. The group II-VI compounds are activated by suitable impurities known as activators to produce luminescence in the desired spectral range.

Because of their large optical absorption coefficients at above bandgap wavelenghts, a II-VI semiconductor of about 1mm thickness is sufficient to absorb 99% of the impinging radiation with photon energy higher than the bandgap energy. Thus, they are well-suited for thin film optical devices. The short optical absorption length in II-VI compounds also renders the carrier diffusion length in minority carrier devices relatively unimportant. In addition to the diffusion length requirment, II-VI compounds also have the advantage that they can be prepared in the form of high quality polycrystalline films from inexpensive raw materials by several low-cost method. Thus, the use of thin film II-VI compounds is an economically viable approach to the terrestrial utilization of solar energy.

In this study, a certain number of CdS and ZnS thin films, having different concentrations of $CdCl_2$, $ZnCl_2$ and $SC(NH_2)_2$ salts, have been developed by employing the spray pyrolysis method at different substrate temperatures and their electrical, optical and structural properties have been investigated. These studies are presented in the chapters as follows: In chapter 1, a general introduction about ZnS and CdS materials is given and experimental and theoretical studies done by the other researchers are reviewed. In chapter 2, the theory of the semiconductor materials which include crystal structure, the crystal imperfections effecting electrical properties of the materials, diffusion of the impurities through a semiconductor, the mobility and electical conductivity, electronic transitions in photoconductors, excess carriers in semiconductors, the electrode effects, and thermoluminescence is given. In chapter 3, the construction of the apparatus used for the production of the thin film samples, the production of thin film samples, and the experimental set-ups established for resistivity, transit time, absorption coefficients, carrier lifetime, photocurrent, and Hall mobility measurements are given. The results obtained from the experimental measurements and their discussion are given in chapter four. Finally, the conclusion and recommendations for the further studies appear in the last chapter.

1.2. Literature Survey

1.2.1. History of spray pyrolysis

The process of spray pyrolysis was first introduced in the 1940's for the preparation of transparent oxide films , when groups developed the technique as a low cost thin film deposition method. Since it has become one of the more extensively used low cost and readily scalable techniques, spray pyrolysis has been reviewed several times in the literature [1]. However, a brief summary of progress with the technique will be given, including some recent developments. One of its early applications was the deposition of thin films of sulphide by Chamberlin and his co-workers [2]. Subsequently they extend the process to the preparation of thin film $CdS/Cu_{2-x}S$ photovoltaic cells with the achievement of 2% efficiency . The technique was then adopted by the Stanford University group led by Bube, who eventually used the method to deposit a wide range of compound semiconductors . Starting with thin films of CdS [3], they were able within a short period to prepare solar cells by the spray pyrolysis of CdS films and single crystal CdTe substrates and thereby produced devices with 6% efficiency [4]. Also Touskova et al.[5] investigated the photovoltaic cells on CdS/CdTe heterojunctions. They prepared the cadmium sulphide and cadmium telluride thin layers which are sprayed and electrodeposited, respectively, for n-CdS/p-CdTe solar cells. They also obtained the photovoltaic properties of these solar cells. As their confidence in the technique grew, Bube and his co-workers successfully attempted the preparation of the complete range of solid solution films of (Cd,Zn)S and Cd(S,Se) by this process [6]. They then extended the work to the deposition of (Cd,Zn)S films onto p-type single crystal CdTe substrates, thus forming solar cells and achieving efficiencies between 6% and 8% [7]. Latterly they have investigated the spray pyrolysis of ZnO films onto glass and single crystals of CdTe and InP [8] with equal success.

In parallel with Bube's and his co-workers similar investigations have been carried out by the group at the University of Montpellier . This work commenced in 1978 when work began on the II-VI familly of compound semiconductors with particular emphasis being placed on the spray pyrolysis of CdS and Cu_2S. In 1980 the Montpellics group launch a programme to improve and stabilize Cu_2S/CdS solar cells based on sprayed CdS films. In their pilot plant the technique was applied to the successive depositions of ITO and CdS layers on pyrex substrates. This was followed by the formation of Cu_2S layers by the well established " wet plating " method to complete the fabrication of the solar cell structure [9]. Under this project the best reported efficiency is 7.5% with the open circuit (V_{oc}) short circuit (I_x) and fill factor (ff) values of V_{oc}=0.45V. I_x=24mA, ff=0.66f or cm^2 area cells. Sprayed (Cd,Zn)S thin films have also been investigated by the Bube group as an alternative to CdS in an attempt to improve the efficiency [10]. However, the limitations on the performance and the operational lifetime of Cu_2S/CdS and Cu_2S/(Cd.Zn)S solar cells have prompted this group to apply expertise in spray pyrolysis to alternative new materials, and recently they reported studies of the chemical spray pyrolysis of $CuInSe_2$, and the direct polymerisation of $(CH)_x$ onto a sprayed CdS layer [11].

The spray pyrolysis technique has also been studied extensively by Krunks and his co-workers for photovoltaic applications[12]. Their early studies in 1977 were similarly focused on the characterization and the improvement of (Cd,Zn)S films , and on solar cells prepared on them by the topotaxial growth of Cu_2S using both the "wet plating" and the "dry barrier" methods .They also applied the technique to the deposition of metal oxides namely In_2O_3:Sn and ZnO. Moreover I-II-VI ternary semiconductors namely $CuInS_2$ and $CuInSe_2$ have also been prepared by the same institute using the spray technique and they recently extended this work to the preparation of totally sprayed $CuInSe_2$/(Cd,Zn)S and CuInSe/(Cd,Zn)S solar cells yielding efficiencies up to 3% [13].

Besides the continuing investigations carried out by these three leading groups, there is now considerable research activity world-wide into the development of the technique for the deposition of thin semiconducting films for photovoltaic applications. Kwok and his co-workers [14] at the Chinese University of Hong Kong have reported a series of detailed studies of Cu_2S/(Cd,Zn)S solar cells prepared on spray pyrolysed CdS and (Cd,Zn)S thin films using the "wet plating"method.

Tomer and Garcia at the University of Simon Bolivar(Venezuela) have also dealt with the spray pyrolysis of II-VI compounds [15] and demonstrated the feasibility of preparing ZnO/$CuInSe_2$ heterojunction solar cells entirely by spray pyrolysis with efficiencies exceeding 2%. The group led by Vedel in France have adapted the "airless-spray pyrolysis" technique to yield a higher deposition rate for CdS and (Cd,Zn)S films , while Siefert [16] has introduced new coating technique called "corona spray pyrolysis" to improve the deposition rate of metal oxides. This has increased the deposition rate by 80% for In_2O_3 and SnO_2.

1.2.2. Historical perspective of CdS and ZnS thin films.

In the original description of spray pyrolysis for sulphides and selenides [1] the starting materials used were an aqueous solution of $CdCl_2$ and $SC(NH_2)_2$ (thiourea) and selenourea prepared with concentrations between 0,001M and 0.05M. The quantities of these constituents were chosen such that they were present in equal numbers. Although $CdCl_2$ and $SC(NH_2)_2$ are still the most commonly used starting materials for CdS deposition, for the deposition of CdS, several different spray nozzles have been used in various laboratories and spray rates of between 2 and 30 ml/min have been reported. Although passive substrates such as glass have usually been used, there have also been studies of the deposition of CdS on CdTe single crystal substrate[6]. And also, Lo Savio and Oliveri [17] have studied the novel preparation method and investigation of sprayed CdS films using starting materials such as $CdCl_2$ and $SC(NH_2)_2$.

During the early days of the study of spray pyrolysis it was generally assumed that intermediate complex ions of $CdCl_2$ and $SC(NH_2)_2$ were formed in the solution and CdS was deposited by the decomposition of these complex ions on the heated substrate[2]. However, later it was demonstrated that intermediate chemical reactions also take place during the formation of the final layer. These led to the production of intermediate complex compounds of either $[Cd(SCN_2H_4)]Cl_2$ or $[Cd(SCN_2H_4)]Cl_2$ depending on the pH of the solution, the molar ratio of the source components and also on $CdCl_2$ being anhydrous. Savio, and Oliveri [18] have described a new experimental "solution spraying" procedure that prevents the restrictions which will be resulted controlling the substrate temperature. And they described a perform a systematic investigation of the properties of sprayed films. Recently Krunks et al.[12] have shown that the formation of CdS passes through the intermediate complex compound $[Cd(SCN_2H_4)]Cl_2$ for various molar ratios of precursor component in neutral aqueous solution, but at substrate temperatures higher than 230 °C this complex compound breaks up into a new compound $[Cd(SCN_2H_4)]Cl_2$ which undergoes the pyrolytic reaction to form final CdS layer. Brown, Bates, and Clayton [19] have investigated the similarities in the chemical mechanism of $CuInSe_2$ and CdS thin film formation by chemical spray pyrolysis. This paper provides a mechanistic model for the formation of $CuInSe_2$ and CdS thin films by chemical spray pyrolysis. They demonstrated similarities between the two mechanisms. Albin and Risbud [20] investigated the nucleation and the growth characteristics of spray pyrolysed

CdS thin films and they identified droplet impingement, surface pyrolysis and incorporation of impurity phases as the major mechanism of film growth.

From a structural study of CdS films deposited by spray pyrolysis, Ma and Bube[3] demonstrated the coexistence of hexagonal and cubic phases. This has been reported independently by Kolhe et al.[21] and Gupta et al. [22]. Ma and Bube[3] have also reported that the proportion of hexagonal to cubic phases were dominant in layers deposited on substrates at temperatures <400 °C and with increasing temperature the proportion of hexagonal phase as well as the degree of preferred orientation were found to increase. Furthermore, rapid cooling of sprayed layers also resulted in the preferential formation of the cubic of CdS[3] and this was thought to be the result of a phase transformation from hexagonal to cubic by stress-induced faults. In contrast to these results [3], the studies of Krunks et al [12] suggest that the effect of the substrate temperature on the crystallographic structure of sprayed films is not as significant as was previously believed.

At the very beginning of the application of this technique to amorphous substrates, Chamberlin the Skarman [2] indicated that the use of $CdCl_2$ as one of the starting materials gave rise to highly crystalline CdS films with a large grain size, whereas layers grown using cadmium acetate were amorphous. Although reported grain size for sprayed CdS films are generally less than a micron, the achievement of a grain size up to several microns has been claimed [14]. As far as the effect of doping on crystal structure is concerned, reported results indicated that; (i) heavy Cu doping reduces the degree of preferred orientation [3], (ii) Al_2O_3 doping reduces the preferred orientation and results in smaller grain size as well, (iii) the incorporation of In or Ag improves grain growth , (iv) the effect of excess cadmium is to reduce the degree of preferred orientation of crystallines, due to the tendency to form stacking faults associated with the corresponding sulphur vacancies [16-19], and the desirable columnar growth can only be achieved as the CdS ratio approaches unity [8]. Chow et al.[23] have presented a detailed study on the chemically sprayed CdS thin films used in the fabrication of low cost solar cells. They investigated the physical properties of the films as well as their conditions of preparation. It was observed that the substrate temperature plays a vital role on grain structure and the transport properties of the samples. In addition to these effects, a fast spray rate is also found to have an adverse effect on the crystallinity and grain size by introducing defects during the deposition [22].

Chamberlin and Skarman [2] made the earliest study of the electrical properties of CdS films prepared by spray pyrolysis, reporting the preparation of n-type CdS films with a carrier concentration of 10^{21}-10^{23} m^{-3} and a carrier mobility as high as 9.0 x 10^{-3} m^2/Vs. Subsequently Micheletti and Mark [24] demonstrated the importance of oxygen chemiabsorption effects on these films, with the conclusions that; (i) the Hall mobility and the electron density were reduced by chemiabsorbed oxygen, (ii) the activation energy for the electron was not affected, (iii) the value of activation energy for Hall mobility was increased by chemisorption.

Valyomana, Vijayakumar and Purushothama [25] have studied the effect of annealing temperatures on the electrical transport properties of spray-pyrolysed CdS films. Annealing of the films at 373 K results in maximum conductivity whereas annealing at 473 K produces a minimum value. The charge carriers are reduced from cadmium-sulphur vacancy complexes in films annealed at temperatures up to 473 K. The conductivity due to these carriers is maximum when films are annealed at 373 K. There is a steady decrease of conductivity as annealing temperature increases at or above 473 K. This supports the photoconductivity results that the number of carriers causing photoconductivity is maximum in number for films annealed at 373 K, and this number is reduced when the films are annealed at or above 473 K. A small increase in the photoconductivity of the films are carried out in spray-pyrolysed CdS thin films using photoconductivity techniques. Special attention was given to examine the influence of annealing temperatures on the dark and photoconducting properties of this material. The electrical properties of these films have been extensively studied by the Stanford group. Bube et al. [3] investigated the electrical transport properties and concluded that dark electron mobilities are thermally activated and transport is controlled by the grain boundary barrier heights and barrier widths which are highly sensitive to the chemisorption of oxygen. Furthermore, they reported that Cu impurities decrease with the dark electron concentration and mobility. The crystalline grain sizes and the film thickness as a function of the deposition temperature and the spraying rate have been investigated[17]. Kolhe et al.[26] have studied the electrical conduction in sprayed CdS films. An excess of cadmium was incorporated in sprayed CdS films by appropriately varying the solution composition. It appears that excess cadmium segregates at the grain boundaries, thereby changing the electrical properties. It is inferred that the electrical properties are sensitive function of the grain boundary potential. Kwok[14] has also studied the carrier concentration and the mobility in chemically sprayed CdS films and has demonstrated that all the films had high carrier concentrations but low dark mobilities. However, as the film thickness increases, the dark mobilities and the grain sizes are found to be significantly improved yielding chemically and structurally stable grains of large grain size over 2 mm in thickness. And also Kwok and Siu [27] have studied the carrier concentration and mobility in chemically sprayed cadmium sulphide thin films. Thermoelectric and photothermoelectric measurements were used to study the effects of film thickness on the electronic properties of chemically sprayed cadmium sulphide films. All films had high carrier concentrations and low dark mobilities. They were chemically and structurally more stable and seemed to be more resistant to environmental effects than the thinner films. In a study of electrical properties in relation to thickness, Bougnot et al [11] have shown that, as the thickness of the film increases, the resistivity first decreases drastically for very thin layers (0.5 mm) but subsequently remains fairly constant before it exhibits a further more gradual decrease as the thickness exceeds 3 mm. These improvements in conductivity are thought to be result of better structural order [8]. In fact, this behaviour is similar to that of vacuum evaporated CdS films. Pence et al.[28]

have studied the substrate temperature effects on the electrical properties of CdS films prepared by chemical spray pyrolysis. The effects of heat treatments in H_2 on electrical properties of $Cd_{1-y}Zn_yS$ ($0<y<0.15$) and In-doped CdS spraying films were studied, and also the influence of Zn concentration on layer physical properties. The activation energy of the impurity level is computed from the slope of the dark resistance and current versus temperature. The electrical and physical properties change remarkably when Zn concentration increases[29].

The dark conductivity, electron mobility, and electron carrier concentration of sprayed films as a function of substrate temperature exhibit significant fluctuations for differences in substrate temperature of 20-30 °C [9]. Ma and Bube [3] have correlated these variations with those in crystallite orientation, cubic/hexagonal phase ratio and morphology. Techniques of thermoelectric and photothermoelectric analysis have been applied to investigate the electrical transport of both solution-sprayed and evaporated polycrystalline CdS films by Wu and Bube [30]. They have investigated the structure and characteristic of intergrain boundaries that dominate the transport process in these polycrystalline films.

The effects of annealing sprayed CdS films in different ambients and at different temperatures have been extensively investigated. Annealing in air at elevated temperature considerably increases the resistivity and photoconductivity of the films, while re-annealing the same films in vacuum at similar temperatures reverses the effect by decreasing the resistivity and quenching the photoconductivity. These effects are usually attributed to absorption and desorption of oxygen. Annealing in a hydrogen atmosphere increases the carrier density and the electron mobility of sprayed CdS films by at least an order of magnitude, reaching a carrier concentration of $10^{18}cm^{-3}$ and an electron mobility of $90cm^2/Vs$ at room temperature [10]. It is also thought that hydrogen annealing will modify the stoichiometry of films producing excess cadmium, which in turn increase the carrier concentration in the layer, and as a result of this,the inter-grain barrier heights are reduced. In addition to this, hydrogen annealing also removes any vestige of chemisorbed oxygen with similar consequences [10]. The influence of annealing temperature on photoconductivity of spray pyrolysed CdS has been investigated. The annealing of films at 373 K resulted in maximum photoconductivity. The results are discussed with the help of ellipsometric data, visible and IR spectra of these samples. Also the variation in photoconductivity of these samples were studied during heating to analyze the effect of trapping [31]. And also Valyomana et al.[32] have studied the effect of annealing temperatures on the electrical transport properties of spray-pyrolysed CdS films. They shown that annealing of the films at 373 K results in maximum conductivity whereas annealing at 473 K produces a minimum value. They observed that the charge carriers are released from cadmium-sulphur vacancy complexes in films annealed at temperatures up to 473 K. Recently Kolhe et al [21] have also indicated that the electrical properties of sprayed CdS films, especially their mobilities, are governed by inter-grain barrier heights which are very sensitive to the absorption or desorption of oxygen.

The optical properties of spray pyrolysed CdS films are particularly important for solar cell applications and are mainly determined by the microstructure of the layers. It has been demonstrated that the optical transmission of films improves as the substrate and the relative concentrations of sulphur in the spray solution are increased. However, annealing procedures do not affect the optical transmission significantly [8]. With the spray pyrolysed films the fundamental optical absorption edge is found to be increasingly less well defined as the grain size decrease and the absorption coefficient for films of thickness 2-3 mm becomes larger than that of bulk single crystal CdS at the bandgap for wavelengths greater than 1.0 mm. There are only few reports on the optical properties of spray pyrolysed CdS films which reflects the fact that these have not been studied as much as the other characteristics of these layers [33]. However, intense room temperature photoluminescence observations suggest the possibility of the application of these films to low cost electro-optical devices. Despite the significant decrease in interest in Cu_2S/CdS heterojunction cells, studies on their preparation by spray pyrolysis have still been carried out worldwide for low cost terrestrial photovoltaic applications. In recent new approaches to the spray pyrolysis of CdS layers [34], an improved film quality and a high degree of reproducibility have been reported. And the effect of nickel doping on the photoelectrochemical behaviour of sprayed CdS has been investigated. These results showed that the photoreactivity of sprayed CdS films is governed by their electronic and optical properties[35].

CdS thin films with different compositions were deposited using the electro-spray pyrolysis of $CdCl_2$ and $(NH_2)_2CS$ solutions mixed in different proportions by Golovanov, Lantto, Leppavuori, Uusimaki, Remes, and Frantti [36]. The diverse morphology of the films was analyzed using AFM(atomic force microscopy) and SEM observations. The relative atomic concentrations of Cd and S species in the bulk and at the surface of the films were estimated using EDS and XPS(X-ray photoelectron spectroscopy) quantification routines, respectively. Hill [37] has described a method which has been used successfully for the production of CdS layers in thin film solar cells. The structural, optical, and electrical properties of the resulting layers are discussed and related to the properties required in a high-efficiency thin film solar cell. A description is also given of some less commonly used methods that might be developed into successful techniques for the production of large-area low-cost solar cells.

Polycrystalline ZnS films of cubic phase were prepared using spray pyrolysis on amorphous substrate by Ashour, Afifi, and Mahmoud [38]. The films were found to be uniform and to adhere well to the substrate. The effects of deposition time (10-30 min) and substrate temperature (300-500 °C) on their electrical and optical properties were studied. Afifi, Mahmoud and Ashour [39] have studied the structural properties of ZnS thin films prepared by spray pyrolysis. The effect of substrate temperature as well as deposition time and annealing in air and in a nitrogen atmosphere on some structural features were investigated by X-ray diffraction. In their study, they showed that at a substrate temperature of 300 °C, ZnS appears almost in amorphous form with rising substrate temperature the crystallinity is improved, and at 550 °C, a well-crystallized cubic phase of ZnS is obtained. Falcony, Garcia, Ortiz, and Alonso [40] have reported the photoluminescent properties of manganese-doped zinc sulphide films deposited by spray pyrolysis at room temperature. These films are deposited on pyrex glass substrates at atmospheric pressure using air as a carrier gas. All films are polycrystalline with a wurtzite structure. The photoluminescence spectra is measured at room temperature as a function of the different deposition parameters and the Mn concentration.

Fine particles of ZnS were able to be prepared using ultrasonic spray pyrolysis of an aqueous solution containing $Zn(NO_3)_2$ and $SC(NH_2)_2$ in appropriate molar ratios, the carrier gas being N_2 . Tohge, Tamaki, and Okuyama [41] have prepared CdS thin films using this method and also they investigated the crystalline structure of these films. And also Pike et al.[42] prepared ZnS thin films by ultrasonically spraying a toluene solution of bis(diethyldithiocarbamato)Zinc(II) ($Zn(S_2CN(C_2H_5)_2)_2$) onto silicon, sapphire, and gallium arsenide substrates at 460-520 °C. The films prepared on silicon or sapphire were found to have a highly oriented hexagonal structure, while those deposited onto cubic (100) gallium arsenide showed a highly oriented cubic structure. The films were characterized by X-ray diffraction analysis, ellipsometry, scanning electron microscopy and IR spectroscopy.

CHAPTER 2

THEORY

2.1.Semiconductor Crystals

2.1.1. Introduction

Semiconductors are an important class of materials both for industrial use and for scientific study. Over the last two decades, semiconductors have come to be used in a wide range of electronic devices, such as transistors, switching devices, voltage regulators, photocells, and photodetectors. The rapid growth of the semiconductor industry has stimulated the demands for better material understanding and material quality. The technology of crystal growth developed during this period has made it is possible to produce crystals of exceedingly high purity and crystal perfection. In the meantime, the list of semiconductor materials has expanded steadily. The availability of new and good quality materials and the demand for a better understanding of material properties have permitted scientists to make concerted efforts in many directions. The interplay between technology and science in this area has been one of the most fruitful and rewarding experiences in human endeavor.

2.1.2. Semiconductor Materials

Semiconductors are a group of materials having electrical conductivities intermediate between metals and insulators. It is significant that the conductivity of these materials can be varied over wide ranges by changes in temperature, optical excitation, and impurity content. This variability of electrical properties makes the semiconductor materials natural choices for electronic device investigations.

Semiconductor materials are found in column IV and neighboring columns of the periodic table (Table 2.1). The column IV semiconductors, silicon and germanium, are called elemental semiconductors because they are composed of single species of atoms.

Table 2.1: Common semiconductor materials: (a) the portion of the periodic table where semiconductors occur; (b) elemental and compound semiconductors.

(a)	II	III	IV	V	VI
		B	C		
		Al	Si	P	S
	Zn	Ga	Ge	As	Se
	Cd	In	Sn	Sb	Te

(b) Elemental	IV compounds	III-V compounds	II-VI compounds
Si	SiC	AlP	ZnS
Ge		AlAs	ZnSe
		AlSb	ZnTe
		GaP	CdS
		GaAs	CdSe
		GaSb	CdTe
		InP	
		InAs	
		InSb	

In addition to the elemental materials, compounds of column III and column V atoms, as well as certain combinations from II and VI, make up the intermetallic, or compound, semiconductors.

As Table 2.1 indicates, there are numerous semiconductor materials. Among these, Si is used for the majority of semiconductor devices; rectifiers, transistors, and integrated circuits. The compounds are used most widely in devices requiring the emission or absorption of light. For example, semiconductor light emitters are commonly made of such compounds as GaAs, GaP, and mixed compounds such as GaAsP. Fluorescent materials such as those used in television screens usually are II-VI compound semiconductors such as ZnS. Light detectors are commonly made with InSb, CdSe, or other compounds such as the lead salts PbTe and PbSe; Si and Ge are also widely used as infrared and nuclear radiation detectors. An important microwave device, the Gunn diode, is usually made of GaAs. Thus, the wide range of semiconductor materials offers considerable variety in properties and provides device and circuit engineers with much flexibility in the design of electronic functions.

The electronic and optical properties of semiconductor materials are strongly affected by impurities, which may be added in precisely controlled amounts. Such impurities are used to vary the conductivities of semiconductors over wide ranges and even to alter the nature of the conduction processes from conduction by negative charge carriers to positive charge carries. For example, an impurity density of one part per million can change a sample of Si from a poor conductor to a good conductor of electric current. This process of controlled addition of impurities, called doping, will be discussed in detail in subsequent sections.

To investigate these useful properties of semiconductors, it is necessary to understand the atomic structure of the materials. Obviously, if slight alterations in purity of the original material can produce such dramatic changes in electrical properties, then the nature and specific arrangement of atoms in each semiconductor must be of critical importance. Therefore, we begin our study of semiconductors with a brief introduction to crystal structure.

2.1.3. Crystal Lattice

In this section, we discuss the arrangements of atoms in various solids. We shall distinguish between single crystals and other forms of materials and then investigate the periodicity of crystal lattices. Certain important crystallographic terms will be defined and illustrated in reference to crystals having a basic cubic structure. These definitions will allow us to refer to certain planes and directions within a lattice of arbitrary structure. Finally, we shall investigate the diamond lattice; this structure, with some variations, is typical of most of the semiconductor materials used in devices.

2.1.3.1 Periodic Structure

A crystalline solid is distinguished by the fact that the atoms making up the crystal are arranged in a periodic fashion. That is, there is some basic arrangement of atoms which is repeated throughout the entire solid. Thus, the crystal appears exactly the same at one point as it does at a series of other equivalent points, once the basic periodicity is discovered. However, not all solids are crystals (Fig.2.1); some have no periodic structure at all (amorphous solids), and others are composed of many small regions of single-crystal material (polycrystalline solids). The semiconductor materials we shall study are polycrystals, as seen in Fig.2.1c.

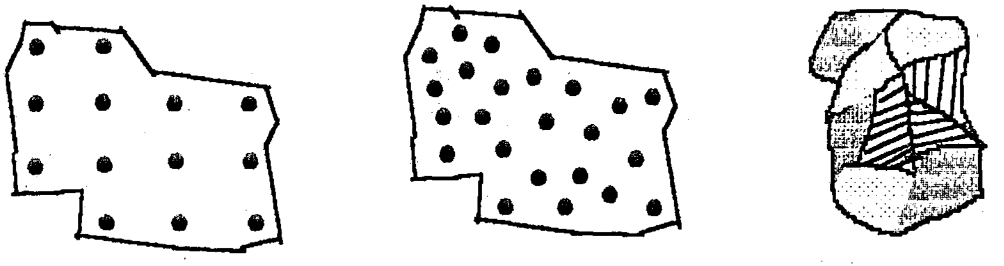

(a) Crystalline (b) Amorphous (c) Polycrystalline

Figure 2.1. Three types of solids, classified according to atomic arrangement: (a) crystalline and (b) amorphous materials are illustrated by microscopic views of the atoms, whereas (c) polycrystalline structure is illustrated by a more macroscopic view of adjacent single-crystalline regions, such as (a).

The periodic arrangement of atoms in a crystal is called the lattice. Since there are many different ways of placing atoms in a volume, the distances and orientation between atoms can take many forms. However, in every case the lattice contains a volume, called a unit cell, which is representative of the entire lattice and is regularly repeated throughout the crystal. As an example of such a lattice, Fig.2.2 shows a two-dimensional arrangement of atoms with a unit cell ODEF.

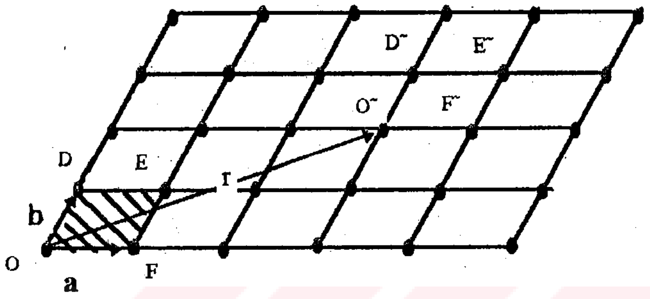

Figure 2.2. A two-dimensional lattice showing translation of a unit cell by $\mathbf{r}=3\mathbf{a}+2\mathbf{b}$.

This cell has an atom at each corner shared with adjacent cells. Notice that we can define vectors a and b such that if the unit cell is translated by integral multiples of these vectors, a new unit cell identical to the original is found (e.g.,O'D'E'F). These vectors **a** and **b** and **c** (if the lattice is three dimensional) are called the basis vectors for the lattice. Points within the lattice are indistinguishable if the vector between the points is

$$\mathbf{r}=p\mathbf{a}+q\mathbf{b}+s\mathbf{c} \tag{2.1}$$

where p,q, and s are integers. A unit cell which contains lattice points only at the corners is called a primitive cell. In Fig.2.2 the shaded area ODEF is a primitive cell. In many lattices, however, the primitive cell is not the most convenient to work with. Therefore, we shall deal primarily with unit cells which contain atoms in addition to those at the corners.

The importance of the unit cell lies in the fact that we can analyze the crystal as a whole by investigating a representative volume. For example, from the unit cell we can find the distances between nearest atoms and next nearest atoms for calculation of the forces holding the lattice together; we can look at the fraction of the unit cell volume filled by atoms and relate the density of the solid to the atomic arrangement. But even more important for our interest in electronic devices, the properties of the periodic crystal lattice determine the allowed energies of electrons which participate in the conduction process. Thus the lattice determines not only the mechanical properties of the crystal but also its electrical properties.

2.1.3.2 Cubic Lattice

The simplest three-dimensional lattice is one in which the unit cell is a cubic volume, such as the three cells shown in Fig.2.3. The simple cubic structure has an atom located at each corner of the unit cell.

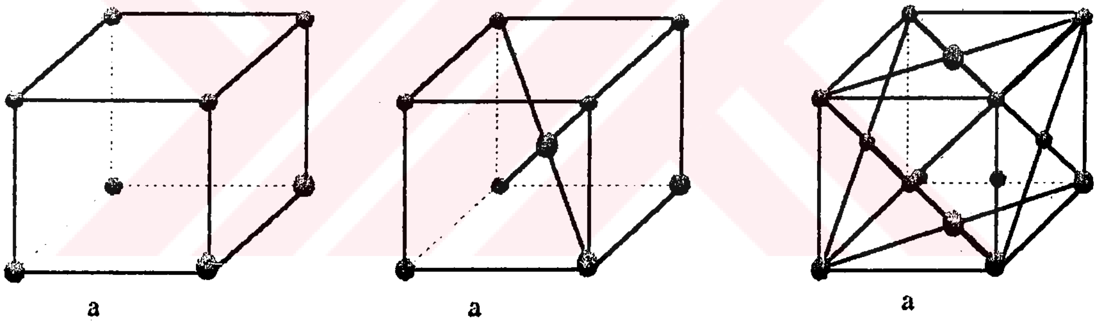

Figure 2.3. Unit cells for three types of cubic lattice structures.

The body-centered cubic (bcc) lattice has an additional atom at the center of the cube, and the face-centered cubic (fcc) unit cell has atoms at the eight corners and centered on the six faces.

2.1.3.3 The Diamond Lattice

The basic lattice structure for many important semiconductors is the diamond lattice, which is characteristic of Si and Ge. In many compound semiconductors, atoms are arranged in a basic diamond structure but are different on alternating sites. This is called a zinc blende lattice and is typical of the III-V compounds. One of the simplest ways of stating the construction of the diamond lattice is the following: The diamond lattice can be thought of as an fcc structure with an extra atom placed at a/4+b/4+c/4 from each of the fcc atoms.

Figure 2.4a illustrates the construction of a diamond lattice from an fcc unit cell. We notice that when the vectors are drawn with components one-of the cube edge in each direction, only four additional points within the same unit cell are reached. Vectors drawn from any of the other fcc atoms simply determine corresponding points in adjacent unit cells. This method of constructing the diamond lattice implies that the original fcc has associated with it a second interpenetrating fcc displaced by 1/4, 1/4, 1/4. The two interpenetrating fcc sublattices can be visualized by looking down on the unit cell of Fig.2.4a from the top (or along any <100> direction). In the top view of Fig 2.4b, atoms belonging to the original fcc are represented by open circles,

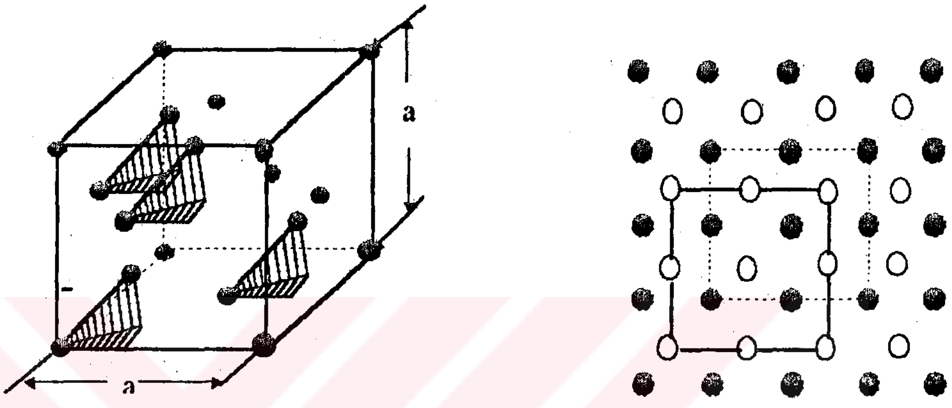

(a) (b)

Figure 2.4. Diamond lattice stucture: (a) a unit cell of the diamond lattice constructed by placing atoms 1/4, 1/4, 1/4 from each atom in a fcc; (b) top view (along any <100> direction of an extended diamond lattice. The open circles indicate one fcc sublattice and the solid circles indicate the interpenetrating fcc.

and the interpenetrating sublattice is shaded. If the atoms are all similar, we call this structure a diamond lattice; if the atoms differ on alternating sites, it is a zinc blende structure. For example, if one fcc sublattice is composed of Ga atoms and interpenetrating sublattice is As, the zinc blende structure of GaAs results. Most of the compound semiconductors have this type of lattice, although some of the II-VI compounds are arranged in a slightly different structure called the wurtzite lattice. We shall restrict our discussions here to the diamond and zinc blende structures since they are typical of most of the commonly used semiconductors.

All atoms are identical in a diamond lattice, and each atom in the diamond lattice is surrounded by four equidistant nearest neighbors that lie at the corners of a tetrahedron (refer to the spheres connected by darkened bars in Fig.2.5a). Most of the II-VI compound semiconductors (e.g.,ZnS) have a zinc blende lattice, shown in Fig.2.5b, which is identical to a diamond lattice excepted that one fcc sublattice has column II atoms (Zn) and the other has column VI atoms (S).

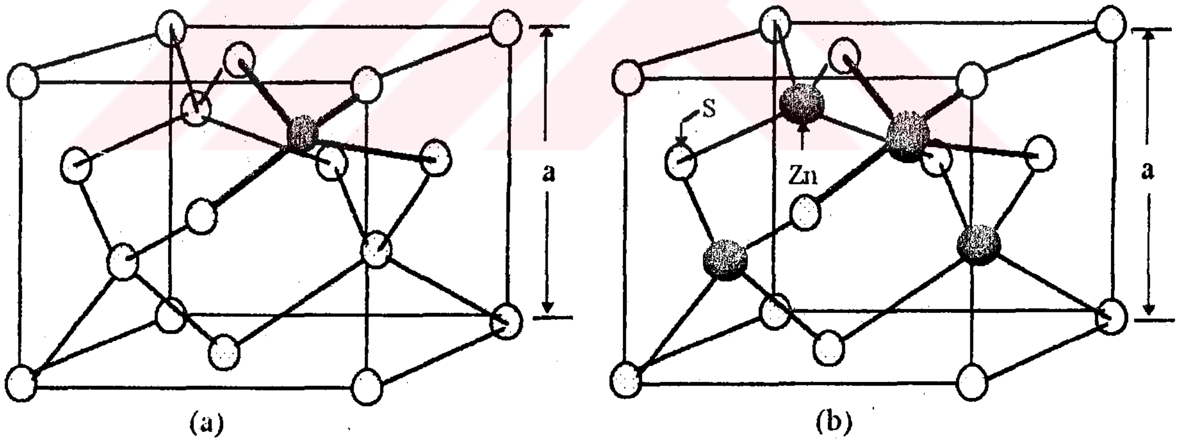

Figure 2.5 (a) Diamond lattice (b) Zincblende lattice.

2.1.4. Valence Bonds

As discussed in the previous section, each atom in a diamond lattice is surrounded by four nearest neighbors. Fig.2.6a shows the tetrahedron configuration of a diamond lattice. A simplified two-dimensional bonding diagram for the tetrahedron is shown in Fig.2.6b. Each atom has four

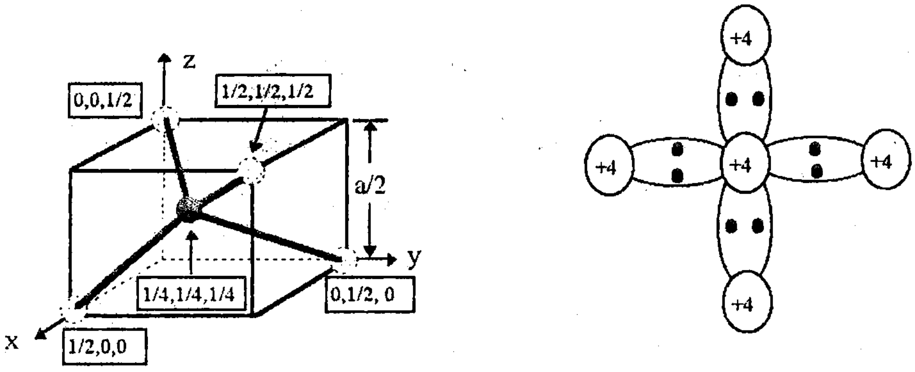

(a) (b)

Figure 2.6. (a) A tetrahedron bond. (b) Schematic two-dimensional representation of a tetrahedron bond.

electrons in the outer orbit, and each atom shares these valence electrons with its four neighbors. This sharing of electrons is known as covalent bonding; each electron pair constitutes a covalent bond. Covalent bonding occurs between atoms of the same element or between atoms of different elements that have similar outer-shell electron configurations. Each electron spends an equal amount of time with each nucleus. However, both electrons spend most of their time between the two nuclei. The force of attraction for the electrons by both nuclei holds the two together.

At low temperatures, the electrons are bound in their respective tetrahedron lattice; consequently, they are not available for conduction. At higher temperatures, thermal vibrations may break the covalent bonds. When a bond is broken, a free electron results that can participate in current conduction. Figure 2.7a shows the situation when a valence electron becomes a free electron. An electron deficiency is left in the covalent bond. This deficiency may be filled by one of the neigboring electrons, which results in a shift of the deficiency location, as from location A to location B as seen in Fig.2.7b. We may therefore consider this deficiency as a particle similar to an

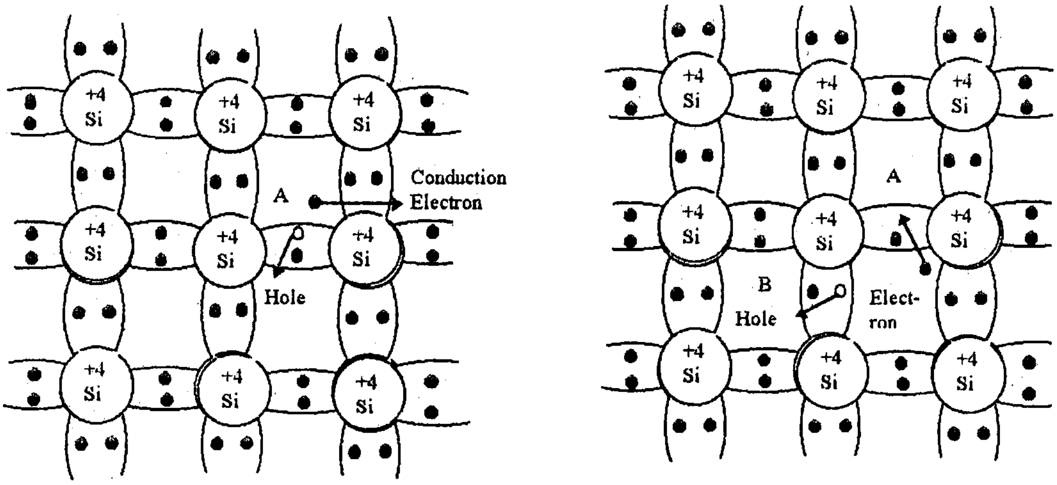

(a) (b)

Figure 2.7 The basic bond pictures of intrinsic silicon. (a) A broken bond at position A, resulting in a conduction electron and a hole. (b) A broken bond at position B.

electron. This fictitious particle is called a hole. It carries a positive charge and moves, under the influence of an applied electric field, in the direction opposite to that of an electron. The concept of a hole is analogous to that of a bubble in a liquid.

2.1.5. Energy Bands

For an isolated atom, the electrons of the atom can have only discrete energy levels. For example, the energy levels for an isolated hydrogen atom are given by the Bohr model:

$$E_H = (-m_o q^4)/(3\varepsilon_o^2 h^2 n^2) = -13.6/n^2 \text{ eV} \tag{2.2}$$

where m_o is the free electron mass, q is the electronic charge, ε_o is the free-space permittivity, h is the planck constant, and n is a positive integer called the principal quantum number. The discrete energies are -13.6 eV for the ground level(n=1), -3.4 eV for the first excited level(n=2), etc.

We now consider two identical atoms. When they are far apart, the allowed energy levels for a given principal quantum number (e.g., n=1) consist of one doubly degenerate level, that is, each atom has exactly the same energy (e.g., -13.6 eV for n=1). As the two atoms approach one another, the doubly degenerate energy level will split into two levels by the interaction between the atoms. When we bring N atoms together to form a crystal, the N-fold degenerate energy level will split into N separate but closely spaced levels due to atomic interaction. This results in an essentially continuous band of energy.

The detailed energy band structures of crystalline solids have been calculated using quantum mechanics. Figure 2.8 is a schematic diagram of the formation of a diamond lattice crystal from isolated silicon atoms. Each isolated atom has its discrete energy levels (two levels are shown on the far right of the diagram). As the interatomic spacing decreases, each degenerate

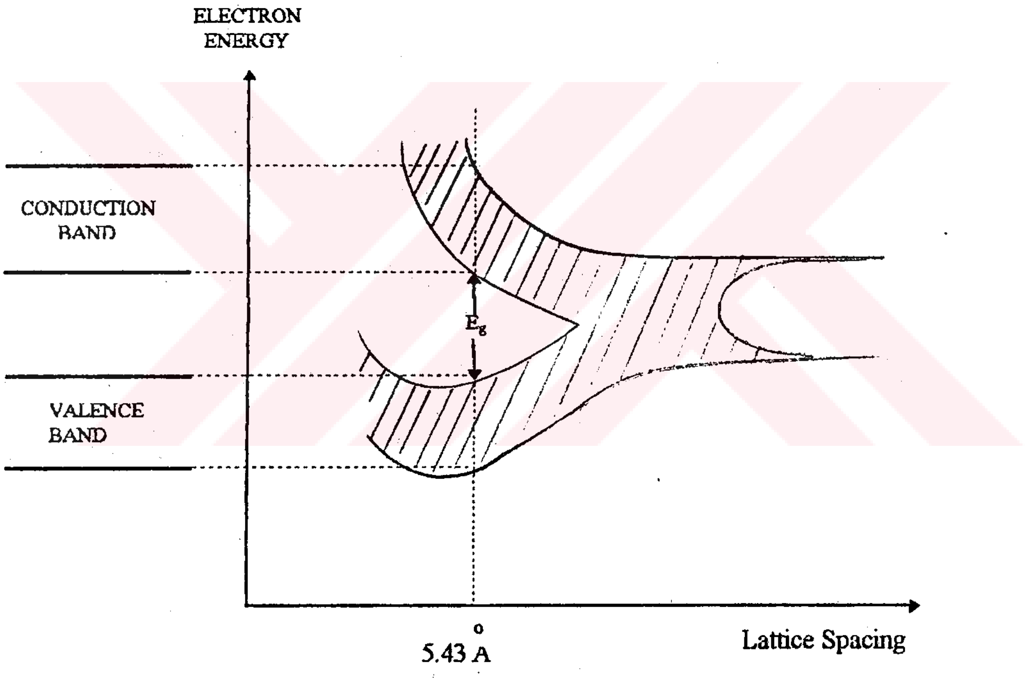

Figure 2.8. Formation of energy bands as a diamond lattice crystal is formed by bringing together isolated silicon atoms.

energy level splits to form a band. Further decrease in spacing causes the bands originating from different discrete levels to lose their identities and merge together, forming a single band. When the distance between atoms approaches the equilibrium interatomic spacing of the diamond lattice (with a lattice constant of 5.43 °A for silicon), this band splits again into two bands. These bands are separated by a region which designates energies that the electrons in the solid can not possess. This is called the forbidden gap, or bandgap E_g. The upper band is called the conduction band, while the lower band is called the valence band, as shown on the far left of Fig.2.8 [43].

A conductor is a solid containing many electrons in the conduction band at room temperature. In fact, there is no forbidden region between the valence and conduction bands on a good conductor's energy band diagram. The two bands actually overlap as shown in Fig. 2.9a. Since the valence band energies are the same as the conduction band energies for a conductor, it is very easy for a valence electron to become a conduction (free) electron. Thus conductors have many conduction electrons available to conduct electric current without the need for applied energy, such as heat or light.

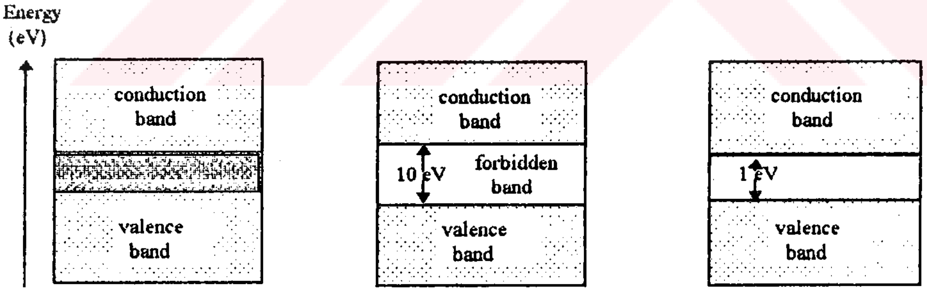

(A)Conductor (B)Insulator (C)Semiconductor

Figure 2.9. Energy band diagrams of matter: (A)Conductor; (B)Insulator; (C)Semiconductor.

An insulator material has an energy band diagram with a very wide forbidden energy band, such as that in Fig. 2.9b. The forbidden energy band is so wide that practically no electrons can be given sufficient energy to jump the gap from the valence band to the conduction band. In the ideal insulator, all the levels of the valence band are occupied by electrons and the conduction band is empty. Thus a perfect insulator has no conduction electrons and will not conduct an electric current; practical insulator, of course, have a few conduction electrons and conduct a very small current.

A semiconductor is a solid which has a forbidden energy band as shown in Fig. 2.9c. Its forbidden energy is much smaller than that for an insulator but larger than that for a conductor. Normally, since it has this forbidden energy band, it would be considered that a semiconductor has no electrons in its conduction band. However, the energy provided by the heat of room temperature is sufficient to overcome the atomic bonding forces on a few valence electrons so that some can jump the gap into the conduction band. Therefore, at room temperature, semiconductors are capable of conducting some electric current. It is this class of materials which shall be of interest to us [44].

For a free electron, the kinetic energy E is given

$$E = \frac{\vec{p}^{\,2}}{2 m_o^*} \qquad (2.3)$$

where p is the particle momentum and m_o^* is the effective mass of free electron. An electron in the conduction band is similar to a free electron in that it is relatively free to move about in a semiconductor. However, because of the periodic potential of the nuclei, the effective mass of a conduction electron is different from the mass of a free electron. The energy-momentum relationship of a conduction electron can be written as

$$E = \frac{\hbar^2 \bar{k}^2}{2m_n^*} \qquad (2.4)$$

where **k** is the propagation vector and h is Planck constant. A similar expression can be written for holes (with effective mass m_p^*, where the subscript p refers to the positive charge on a hole). The crystal momentum is analogous to the particle momentum. The effective-mass concept is very useful because it enables us to treat holes and electrons essentially as classical charged particles.

2.1.6. Density of States

As we can see from the bandstructure of semiconductors, the bands are not parabolic in general. We will now develop a more general formulation for the density of states. The number of electrons in the energy interval E and E+dE are N(E)dE (per unit volume), where N(E) is the density of states:

$$N(E)dE = \frac{2}{V}x \text{ (number of allowed k-vectors between E and E+dE)} \qquad (2.5)$$

The k-space volume per state is $\Delta k = (2\pi)^3/V$. Thus,

$$N(E)dE = \int \frac{d^3\vec{k}}{4\pi^3} x \frac{1 \rightarrow \text{if} E \leq E(k) \leq E + dE}{0 \rightarrow \text{otherwise}} \qquad (2.6)$$

To evaluate the integral, we define a surface of constant energy S(E) where all surface points have the energy E. Around it we have a different surface S(E+dE) where the k-space points have energy E+dE as shown in Figure 2.10. The volume element in k-space can be written as

$$d^3k = d\vec{S}.\delta\vec{k} \qquad (2.7)$$

where δk is the perpendicular distance between S(E) and S(E+dE) at the point k and dS is the surface element on the constant energy surface.

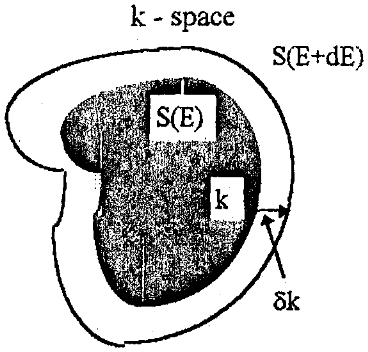

Figure 2.10. Constant energy surfaces S(E) and S(E+dE) separated by energy dE, and a k-vector dk as shown.

We may write

$$E + dE = E + \left|\nabla_{\vec{k}} E(\vec{k})\right| . \delta\vec{k}(\vec{k})$$

$$\delta\vec{k}(\vec{k}) = \frac{dE}{\left|\nabla_{\vec{k}} E(\vec{k})\right|} \qquad (2.8)$$

Thus

$$N(E) = \int_{S(E)} \frac{dS}{4\pi^3} \frac{1}{\left|\nabla_{\vec{k}} E(\vec{k})\right|} \qquad (2.9)$$

If the E vs. **k** relation is simple, the integral can be evaluated analytically. In general, however, one has to carry out a numerical integration.

We note that in the E vs. **k** relation, there may be regions where $\nabla_k E(\mathbf{k})$ approaches zero. At these points the density of states increases rapidly giving spikes in the density of states. Such points are called van Hove singularities. The van Hove singularities occur around high symmetry points and since most physical properties of the semiconductor are determined by the density of states, their presence is reflected in these properties.

The energy versus crystal momentum relations are quite complex in semiconductors but for many important processes one can use the simplifications that arise near the band edges. Near band edges one can describe the E vs. **k** relation by simple relations, the simplest of which is the free electron parabolic relation with an effective mass.

2.1.7. Intrinsic Carrier Concentration

At finite temperatures, continuous thermal agitation results in the excitation of electrons from the valence band to the conduction band and leaves an equal number of holes in the valence band. An intrinsic semiconductor is one that contains relatively small amounts of impurities compared to the thermally generated electrons and holes. To obtain the electron density (i.e., the number of electrons per unit volume) in an intrinsic semiconductor, we first evaluate the electron density in an incremental energy range dE. This density n(E) is given by the product of the density of allowed energy states per unit volume N(E) and by the probability of occupying that energy range F(E). Thus, the electron density in the conduction band is given by integrating N(E)F(E)dE from the bottom of the conduction band (E_C initially taken to be E=0 for simplicity) to the top of the conduction band E_{top}:

$$n = \int_0^{E_{top}} n(E)dE = \int_0^{E_{top}} N(E)F(E)dE \qquad (2.10)$$

and

$$N(E) = 4\pi[\frac{2m_n^*}{h^2}]^{3/2} E^{1/2} \qquad (2.11)$$

The probability that an electronic state with energy E is occupied by an electron is given by the Fermi-Dirac distribution function (which is also referred to as the Fermi distribution function)

$$F(E) = \frac{1}{1 + e^{(E - E_F)/kT}} \qquad (2.12)$$

where k_b is the Boltzmann constant, T is the absolute temperature in Kelvin, and E_F is the Fermi level. The Fermi level is the energy at which the probability of occupation by an electron is exactly one half. The Fermi distribution function can be approximated by simpler expressions:

$$F(E) \approx e^{-(E-E_F)/kT} \qquad \text{for} \quad (E - E_F) > 3kT \qquad (2.13a)$$

and

$$F(E) \approx 1 - e^{-(E-E_F)/kT} \qquad \text{for} \quad (E - E_F) < -3kT \qquad (2.13b)$$

Fig. 2.11 shows schematically from left to right the band diagram, the density of states (which varies as √E), the Fermi distribution function, and the carrier concentrations for an intrinsic semiconductor. The carrier concentrations can be obtained graphically from Fig.2.11 using Eq.2.10; that is, the product of N(E) in Fig.2.11b and F(E) in Fig.2.11c gives the n(E)-versus-E curve (upper curve) in Fig.2.11d. The upper shaded area in Fig.2.11d corresponds to the electron density.

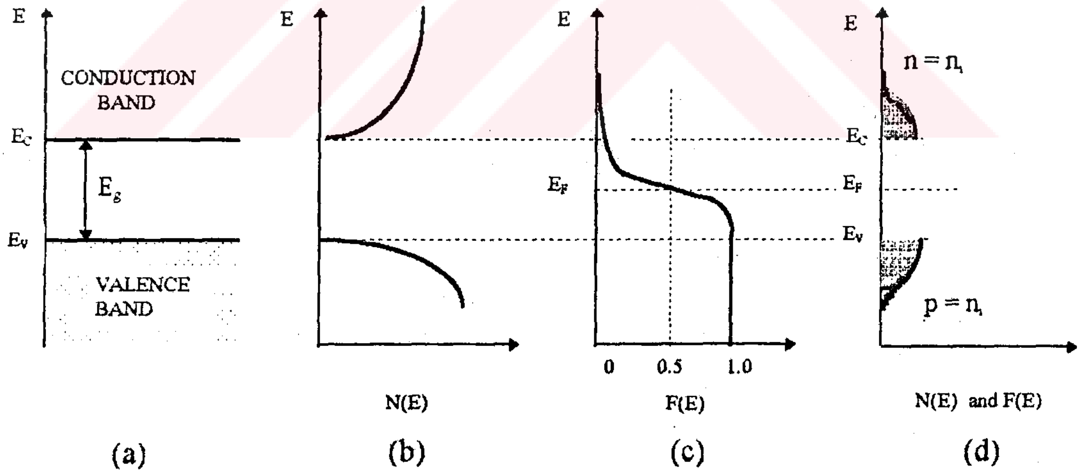

Figure 2.11. Intrinsic semiconductor. (a) Schematic band diagram. (b) Density of states. (c) Fermi distribution function. (d) Carrier concentration.

In the conduction band there is a large number of allowed states. However, for intrinsic semiconductors there will be only a few electrons in the conduction band, hence the probability of an electron occupying one of these states is small. There also are a large number of allowed states in the valence band. By contrast most of these are occupied by electrons. Thus, the probability of an electron occupying one of these states in the valence band is nearly unity. There will be only a few unoccupied electron states, that is, holes in the valence band. As can be seen, the Fermi level is located near the middle of the bandgap (i.e.,E_F is many kT below E_C). Because F(E) is an exponentially decreasing function of E (Eq.2.13a), the value of E_{top} can be replaced by infinity. Substituting Eqs.2.11 and 2.13a into Eq.2.10 yields.

$$n = 4\pi[\frac{2m_n^*}{h^2}]^{3/2}\int_0^{\infty} E^{1/2}\exp[-\frac{E-E_F}{kT}]dE \tag{2.14}$$

If we let x≡E/kT, Eq.2.14 becomes

$$n = 4\pi[\frac{2m_n^*}{h^2}]^{3/2}(kT)^{3/2}\exp[\frac{E_F}{kT}]\int_0^{\infty} x^{1/2}e^{-x}dx \tag{2.15}$$

The integral in Eq.2.15 is of the standard form and equals $\sqrt{\pi}/2$. therefore Eq.2.15 becomes

$$n = 2[\frac{2\pi m_n^* kT}{h^2}]^{3/2}\exp[\frac{E_F}{kT}] \tag{2.16}$$

If we refer to the bottom of the conduction band as E_C instead of E=0, we obtained for the electron density in the conduction band

$$n = 2[\frac{2\pi m_n^* kT}{h^2}]^{3/2}\exp[-\frac{E_C-E_F}{kT}] \tag{2.17}$$

$$n = N_C\exp[-\frac{E_C-E_F}{kT}] \tag{2.18}$$

and

$$N_C = 2[\frac{2\pi m_n kT}{h^2}]^{3/2} \tag{2.19}$$

where N_C is the effective density of states in the conduction band.

Similarly, we can obtain the hole density p in the valence band:

$$p = 2[\frac{2\pi m_p^* kT}{h^2}]^{3/2} \exp[-\frac{E_F - E_V}{kT}]$$

$$= N_V \exp[-\frac{E_F - E_V}{kT}] \tag{2.20}$$

and

$$N_V = 2[\frac{2\pi m_p^* kT}{h^2}]^{3/2} \tag{2.21}$$

where N_V is the effective density of states in the valence band.

For an intrinsic semiconductor as defined previously, the number of electrons per unit volume in the conduction band is equal to the number of holes per unit volume in the valence band, that is, $n = p = n_i$, where n_i is the intrinsic carrier density. This relation of electrons and holes is depicted in Fig.2.11d.

The Fermi level for an intrinsic semiconductor is obtained by equating Eqs.2.17, 2.18 and 2.20:

$$E_F = E_i = \frac{E_C + E_V}{2} + \frac{kT}{2} \ln[\frac{N_V}{N_C}]$$

(2.22)

$$= \frac{E_c + E_v}{2} + \frac{3kT}{4} \ln[\frac{m_p^*}{m_n^*}]$$

At room temperature, the second term is much smaller than the bandgap. Hence, the intrinsic Fermi level E_i , that is, the Fermi level of an intrinsic semiconductor, generally lies very close to the middle of the bandgap.

The intrinsic carrier density is obtained from Eqs.2.17,2.18, and 2.22:

$$np=n_i^2 \tag{2.23}$$

$$n_i^2 = N_C N_V \exp[-\frac{E_g}{kT}] \tag{2.24}$$

and

$$n_i = \sqrt{N_C N_V} \exp[-\frac{E_g}{2kT}] \tag{2.25}$$

where $E_g \equiv (E_C - E_V)$. Equation 2.23 is called the mass action law, which is valid for both intrinsic and extrinsic semiconductors under thermal equilibrium condition.

2.1.8. Impurities and Extrinsic Semiconductors

Solids are materials that are crystalline in form but not perfectly regular. The irregularities are called imperfections, defects or faults. Imperfections are extremely important for the electrical and other transport properties as well as for the structural properties of solids. For example, the idealized model of an electron in a solid for all of the interactions of that electron with the regular lattice atoms and all of the other electrons. Interactions with the regular crystalline atoms and all of the other electrons have already been taken into account. It is the interaction of the charge carriers with the irregularities of the structure that plays the primary scattering role of collisions.

If there are not too many of these irregularities we can base a model of a real solid on that of a perfect solid assuming that the small number of imperfections perturb the idealized model only sligthly.

2.1.8.1. Imperfections

Basically, there are two general classes of irregularities by which real crystals differ from their idealized models, essential and nonessential imperfections. An essential imperfection is one that always exists regardless of how ideally the solid is prepared. Nonessential imperfections exist because the material cannot be prepared with perfect regularity by imperfect men and machines. Conceptually, however, the nonessential imperfections need not exist if techniques could be perfected. The essential imperfections,as we shall see, must always exist independently of manufacturing skills.

One type of essential imperfection that perturbs the periodic potential of a uniform regular array of lattice atoms or ions occurs because real crystals are of finite size whereas the mathematical lattice is infinite in extent. Surfaces represent essential imperfections not only because of the end of the periodicity of the crystal but also because of their physical or chemical condition. Mechanical polishing or chemical treatment of a solid alters its surface. When a solid is exposed to an atmosphere, atoms or molecules may be absorbed on its surfaces. Because these effects alter the configuration of the energy bands as do nonessential irregularities, we shall postpone our discussion momentarily until we have completed a categorization of the other irregularities.

When a solid is heated, phonons are created. The vibration of crystal atoms about their lattice sites is chiefly responsible for the specific heat of solids. Electrons may also interact with vibrations. Such an interaction may transfer energy either from the electron to the vibrational energy, thus creating phonons, or from the lattice to the electron, thus destroying phonons. Naturally, during an electron phonon interaction, the electron must change state so the interaction can occur only if an unoccupied allowed state is available into which the electron may transfer. Electron phonon "collisions" are the principle effects that cause a disturbed electron distribution to relax toward equilibrium in the sense of nonequilibrium statistical mechanics. These are the interactions principally responsible for Ohm's law in solids.

The second general class of imperfections is the nonessential of which there are types:point, line and plane imperfections. An ordinary solid is not crystal but is composed of many small cyrstallites packed together. The orientation of adjacent crystallites may differ, giving rise to an irregularity in the potential along their interface. The interface is called a grain boundary and the defect a plane imperfection. Most semiconductor crystals prepared for solid-state devices are in the form of single crystals. Among the line imperfections is a variety of dislocations due, for example, to slip or to shear in the crystal.

2.1.8.2. The Effects of Imperfections on Electronic States

Recall that the solution of *Schrodinger's equation for the perfectly* periodic potential of an ideal crystal yields eigenenergies and wave functions for a single electron in the entire system of coupled atoms. The allowed energies fall into bands. If the density of defects is so large as to destroy the fundamental periodicity of the lattice, then the solution for the allowed states is very difficult. If, on the other hand, the density of defects is low and does not alter the crystal periodicity, the solution for the allowed states can be obtained by considering the imperfections as a perturbation on the perfect crystal.

For the case of interstitial defects, states may be added to the system without the removal of any original states from the bands depending on whether or not vacancies also occur.

If impurities of the same atoms are present with sufficient density that the impurity wave functions overlap, the defect states will split in energy, forming an allowed energy band of impurity states. The wave functions of impurity band states are not localized.

2.1.8.3. Donors and Acceptors

When a semiconductor is doped with impurities, the semiconductor becomes extrinsic and impurity energy levels are introduced. Fig.2.12a shows schematically that a silicon atom is replaced by an arsenic atom with five valence electrons. The arsenic atom forms covalent bonds with its four neighboring silicon atoms. The fifth electron becomes a conduction electron that is 'donated' to the conduction band. The silicon becomes n-type because of the addition of the negative charge carrier, and the arsenic atom is called a donor. Similarly, Fig.2.12b shows that when a boron atom with three valence electrons substitutes for a silicon atom, an additional electron is 'accepted' to form four covalent bonds around the boron, and a positively charged 'hole' is created in the valence band. This is a p-type semiconductor, and the boron is an acceptor.

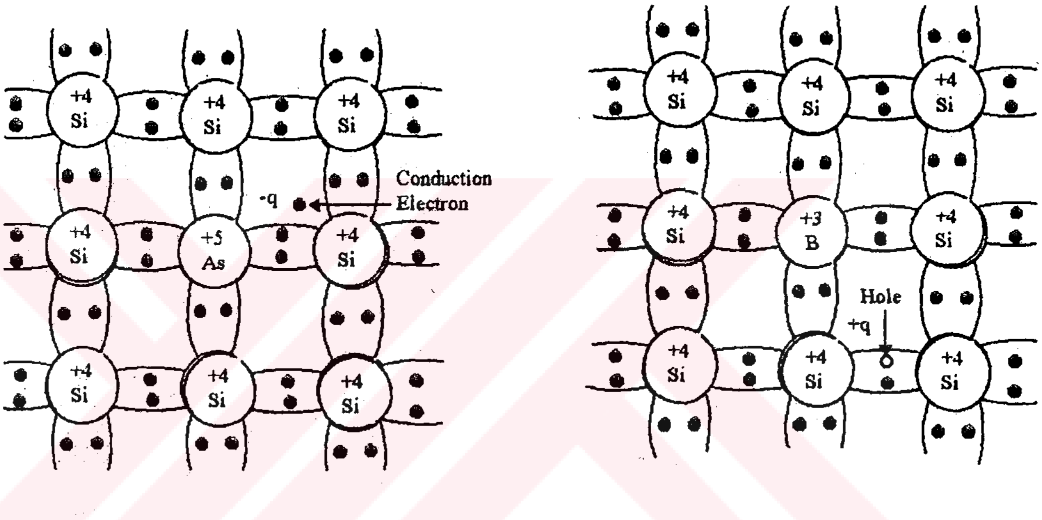

(a) (b)

Figure 2.12 Schematic bond pictures for (a) n-type Si with donor (arsenic) and (b) p-type Si with acceptor (boron).

For shallow donors in silicon and gallium arsenide, there usually is enough thermal energy to supply the energy E_D to ionize all donor impurities at room temperature and thus provide an equal number of electrons in the conduction band. This condition is called ionization. Under a complete ionization condition, we can write the electron densitiy as

$$n = N_D \tag{2.26}$$

where N_D is the donor concentration. Fig.2.13a illustrates complete ionization where the donor level E_D is measured with respect to the bottom of the conduction band equal

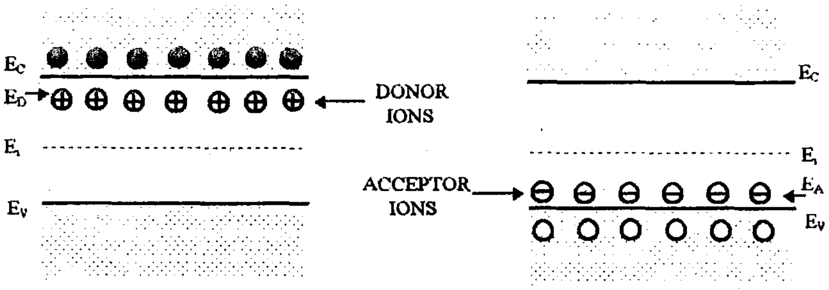

(a) (b)

Figure 2.13 Schematic energy band representation of extrinsic semiconductors with (a) donor ions and (b) acceptor ions.

concentrations of electrons (which are mobile) and donor ions (which are immobile) are shown. From Eqs.2.17, 2.18, and 2.26, we obtain the Fermi level in terms of the effective density of states N_C and the donor concentration N_D:

$$E_C - E_F = kT\ln[\frac{N_C}{N_D}] \qquad (2.27)$$

Similarly, for shallow acceptors as shown in Fig.2.13b, if there is complete ionization, the concentration of holes is

$$p = N_A \qquad (2.28)$$

where N_A is the acceptor concentration. We can obtain the corresponding Fermi level from Eqs.2.20 and 2.28:

$$E_F - E_V = kT\ln[\frac{N_V}{N_D}] \qquad (2.29)$$

From Eq.2.27 it is clear that the higher the donor concentration, the smaller the energy difference (E_C - E_F), that is, the Fermi level will move closer to the bottom of the conduction band. Similarly, for higher acceptor concentrations, the Fermi level will move closer to the top of the valence band. Fig.2.14 shows the graphic procedure to obtain the carrier concentration. This is similar to that shown in Fig. 2.11. However, the Fermi level is closer to the bottom of the conduction band, and the electron concentration (upper shaded area) is much larger than the hole concentration (lower shaded area). Because of the mass action law (Eq.2.23), the product of n and p is the same as that for the intrinsic case(i.e.,$np=n_i^2$).

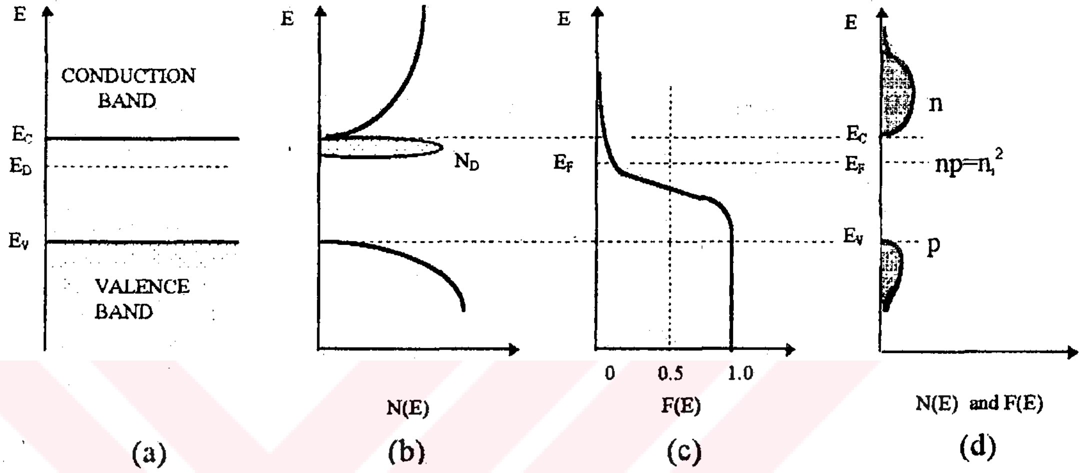

(a) (b) (c) (d)

Figure 2.14 n-type semiconductor. (a) Schematic band diagram. (b) Density of satates. (c) Fermi distribution function. (d) Carrier concentration. Note $np=n_i^2$.

It is useful to express electron and hole densities in terms of the intrinsic carrier concentration n_i and intrinsic Fermi level E_i , since E_i is frequently used as a reference level when discussing extrinsic semiconductors. From Eqs.2.17, 2.18 and 2.20 we obtain

$$n = N_C \exp[-\frac{E_C - E_F}{kT}]$$
$$n = N_C \exp[-\frac{E_C - E_i}{kT}]\exp[\frac{E_F - E_i}{kT}] \qquad (2.30)$$
$$n = n_i \exp[\frac{E_F - E_i}{kT}]$$

and

$$p = N_V \exp[-\frac{E_F - E_V}{kT}]$$
$$p = n_i \exp[\frac{E_i - E_F}{kT}] \qquad (2.31)$$

If both donor and acceptor impurities are present simultaneously, the impurity that is present in a greater concentration determines the type of conductivity in the semiconductor. The Fermi level must adjust itself to preserve charge naturality, that is, the total negative charges (electrons and ionized acceptors must equal the total positive charges holes and ionized donors):

$$n + N_A = p + N_D \qquad (2.32)$$

Solving Eqs.2.23 and 2.32 yields the equilibrium electron and hole concentrations in an n-type semiconductor:

$$n_n = \frac{1}{2}[N_D - N_A + \sqrt{(N_D - N_A)^2 + 4n_i^{\,2}}\,] \qquad (2.33)$$

$$p_n = \frac{n_i^2}{n_n} \qquad (2.34)$$

The subscript n refers to the n-type semiconductor. Because the electron is the dominant carrier, it is called the majority carrier. The hole in the n-type semiconductor is called the minority carrier. Similarly, we obtain the concentration of holes (majority carrier) and electrons (minority carrier) in a p-type semiconductor:

$$p_p = \frac{1}{2}[N_A - N_D + \sqrt{(N_A - N_D)^2 + 4n_i^2}] \tag{2.35}$$

and

$$n_p = \frac{n_i^2}{p_p} \tag{2.36}$$

The subscript p refers to the p-type semiconductor.

An acceptor (p-type) impurity must be an atom with a valence less than four. The most common are indium, boron, aluminum, and gallium which all have a valency of plus three. These atoms produce one hole each. Impurity atoms with two valence electrons produce two holes each, and so on. It is important to note that an acceptor atom becomes a negative ion when its empty covalent bond is filled by a neighboring valence electron. These negative ions, however, are locked into the crystal structure and cannot move. The characterization of n-type and p-type semiconductors are given in Table 2.2

Table 2.2: Summary of n-type and p-type materials.

Characteristics	N-type	P-type
Number of valence electrons of impurity atom	Greater than 4	Less than 4
Name of impurity	Donor	Acceptor
Typical impurities	Arsenic, phosphors, antimony, bismuth	Indium, boron, gallium, aluminum
Majority carrier	Electron	Hole
Minority carrier	Hole	Electron
Energy band in which majority move	Conduction band	Valence band

2.2. Mobility and electrical conductivity

2.2.1. Scattering mechanism

If a constant voltage source is connected to the two sides of a semiconductor chip, an electric field **E**(V cm^{-1}) is created in it. This field acts upon the free charge carriers and causes them to drift in the direction of the force it applies, thereby creating a current called drift current.

When a charge carrier, say an electron, is acted upon by a constant electric field in a vacuum its ensuing acceleration, **a**, is (Newton's law):

$$\vec{a} = \frac{q\vec{E}}{m_e} \qquad (2.37)$$

and its velocity **v** at time t, if it started from rest:

$$\vec{v}=\int_0^t \vec{a}dt=\frac{q\vec{E}t}{m_e} \qquad (2.38)$$

i.e. velocity increases linearly with time.

Inside a semiconductor, on the other hand, the movement of the charge carrier is not smooth but is perturbed by various obstacles, causing what is known as scattering. There are two main types of scattering mechanism: (a) Lattice scattering is caused by collisions of the moving carrier with disturbances in the periodic internal potential inside the semiconductor crystal. These disturbances are due to the vibrations of the crystal lattice atoms around their 'proper' place in the lattice because of their thermal energy. The effect of the internal periodic potential itself, which exists in any crystal, can be taken into consideration by assigning an effective mass m^* to the moving electron or hole. These masses are different from the mass m_0 of the electron outside the crystal. Therefore, it is only the disruptions in the periodic potential, caused by the thermal vibrations of the atoms, that scatters the drifting free carrier: at a certain moment an electron can bump into a region where the crystal atoms are more densely packed than usual, yet a moment later it may find itself in a sparsely packed region. The dense and sparse regions form pressure waves existing inside crystal. (b) Impurity scattering is caused by the presence of ionized impurity atoms in various in the crystal lattice. Due to their net charge, they exert a force on the free carrier passing nearby, causing it to change its direction. This type of scattering is less severe if the free carrier is moving faster (i.e. at higher temperatures), and spends less time in the vicinity of the ionized impurity atom [45].

2.2.2. Mobility and conductivity

We have already seen that the charge carriers occupy levels in energy bands, with the free electrons in the conduction band and the holes in the valence band. If the crystal is absolutely perfect, with every atom occupying its exact position, the conduction electrons and holes would in fact behave very like perfectly free charges in a vacuum. This is a most surprising result of the quantum mechanical treatment of solids because it means that the electrons and holes can move right through a very dense medium of closely spaced atoms just as if the atoms were not there. From knowledge of the scattering of electrons in a low-pressure gas (as compared with a vacuum) we might have expected that the electrons moving in a solid would be severely scattered and suffer frequent collisions with the atoms themselves. But this is another situation in which the electron has to be treated more as a wave than a particle and it turns out that electrons with energies in the valence and conduction bands of the crystal have wavelenghts that can be propagated through the perfectly periodic lattice without attenuation. The electron waves can be thought of as fitting exactly into the lattice, with wavelengths as integral multiples of the atomic spacing. On the particle picture these waves correspond to discrete electrons which can move freely right through the lattice without scattering. The motion of conduction electrons in a perfect crystal would then be very similar to that in a vacuum except that in the crystal we have to allow for a small residual influence of the lattice by replacing the real mass of the electron by a slightly different 'effective mass' in carrying out exact calculations. Similar reasoning applies to the positive holes in the valence band. In a perfect crystal these could move freely as positively charged particles having a positive effective mass that is not very different from that of the electron.

Other crystal imperfections also contribute to the scattering of the conduction electrons in semiconductors. The most important is scattering by the donor and acceptor impurity atoms that are deliberately added to many materials. At room temperature the impurities are ionized in the crystal and this increases their scattering power. The impurity concentrations are so small, however, that 'ionized impurity scattering' is less important than thermal scattering in most device materials at room temperature.

The effect of crystal imperfections on the motion of the holes in the valence band is practically the same. The holes are mainly scattered by the thermal vibrations of the lattice at room temperature, but they still move with comparatively large free paths which are only slightly less than those of the conduction electrons.

In this description of the scattering process the motion of the charge has been taken for granted. Two types of motion have to be distinguished: the random thermal motion of the carriers, and their directed movement in an applied field. The thermal motion is similar to that of the molecules of a gas. Although most of the thermal energy of a solid resides in the lattice vibrations, a small part is in the form of kinetic energy distributed statistically among the free charge carriers. As a result, the carriers have considerable velocities even at room temperatures. The velocities are widely distributed about the mean value, since the kinetic energy of any individual electron or hole changes each time it is scattered and energy is transfered to or from the lattice. At low densities the electrons and holes behave independently .

Let us now consider a semiconductor crystal at temperature T. The electrons and holes in the crystal are in random motion because of their thermal energy. We can visualize the motion of an electron as shown in Fig.2.15(a). The trajectory consists of a series of straight lines between collisions. The free times between collisions are denoted by t_1, t_2, t_3 and so on and the average of these times is the mean free time between collisions. Each scattering event causes an energy exchange between the electron and the lattice. In some collisions, the electrons loses energy to the lattice, while in others it gains energy from the lattice atoms. Since no energy is being supplied from outside, the net rate of energy exchange is zero. Because the motion of the electrons as well as the collisions are random each electron effectively returns to its original position after a large number of collisions. Thus, the average velocity of the electron is zero. The thermal velocity is:

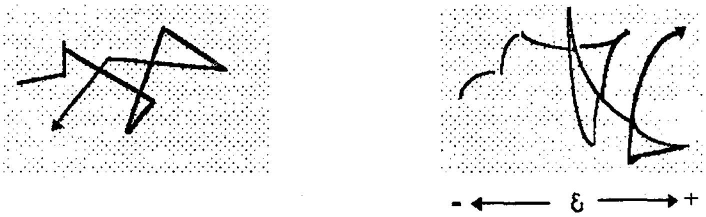

(a) (b)

Figure 2.15. Motion of an electron in the conduction band:(a) no field, (b) with electric field.

$$v_{th} = \sqrt{3\frac{kT}{m_e}} \tag{2.39}$$

When an electric field is applied to the crystal, the electrons are accelerated by the field during their motion between the collisions. As a result, the free paths become curved, like the trajectory of a projectile moving under gravity (Fig.2.15(b)). It is now seen that after a number of collisions, the electron has traversed a distance along the direction of the applied force. This motion is known as the drift motion. During its free flight between two collisions, the electron gains kinetic energy from the electric field and transfers this energy to the lattice upon collision at the end of its field. This energy is dissipated as joule heating in the crystal.

It is possible to measure the drift mobility, μ_{drift}, and the transit time of the minority carriers, t_r. The basic arrengment of a simple technique is shown in Fig.2.16. Thus, it is clear that in the presence of an electric field an electron acquires a drift velocity. Since the average distance between collisions (the mean free path) is not altered by the field, the effect of increase in the electron velocity is to make the collisions more frequent. The drift mobility of a charged particle moving in an electric field is by definition,

$$\mu_{drift} = \frac{\vec{V_D}}{\vec{E}} \tag{2.40}$$

where V_D is the drift velocity of the particle and **E** is the electric field intensity.

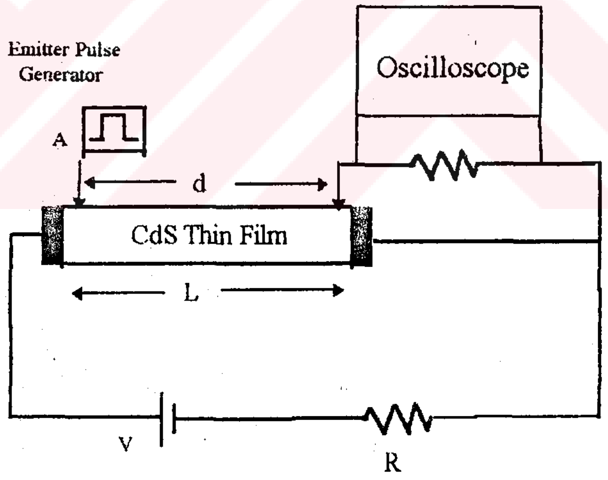

Figure 2.16. Measurement of the transit time and drift mobility.

The average drift velocity of the holes is equal to the distance of the ohmic contacts d, which is fixed at 2 mm, divided by the transit time t_r, is given by

$$\mu_{drift} = \frac{d}{E\,t_r} \tag{2.41}$$

Since E=V/L, where V is the voltage between two ohmic contacts, the new form of the Eq.2.41 which gives the values of the drift mobility of the minority carriers was obtained as [46, 60],

$$\mu_{drift} = \frac{Ld}{V\,t_r} \tag{2.42}$$

The mobility concept implies that the average drift velocity is constant in a given field, and that the electrons do not accelerate over large distances as they do in a vacuum. A high mobility is required in semiconductors used for making devices, and this is another advantage, of germanium and silicon which have comparatively large mean free paths.

The movement of holes in an applied field is similar to that of the free electrons except that they drift in the opposite direction because of their positive charge. As for electrons, the drift velocity is small compared with the thermal velocity, and averaged over a large number of collisions it can be related to the field by means of the hole mobility, μ_p. The mobility is usually somewhat less than the electron mobility because of the slightly different mass and thermal velocity. The hole mobility decreases with temperature and impurity content in much the same way as the electron mobility.

The conductivity of a semiconductor follows immediately from the mobility concept. The holes and electrons, drifting in opposite directions in an applied field, both contribute to the total current. Consider a block of metal, of length L and cross-sectional area S, which contains n free electrons per cubic meter (Fig.2.17). If a voltage V is applied across it, a field E=V/L will be set up, causing the electrons to move with a drift velocity v_D metres per second and in one second they will sweep out a volume v_DS cubic metres. Hence, the total charge passing through a given material slab in one second will be nev_DS coulombs which is also the current I,

$$I = nev_D S \qquad (2.43)$$

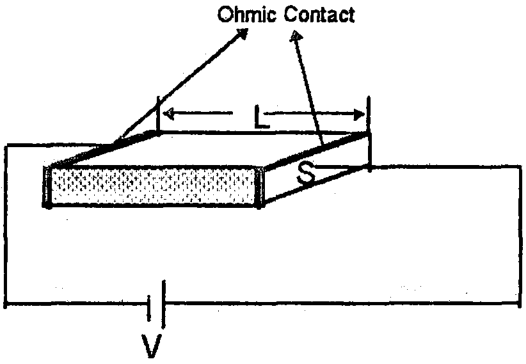

Figure 2.17. Consider a block of metal, of length L and cross sectional area S, and applied voltage V.

The current density, J=I/S ampers per square metre, is therefore given by

$$\vec{J} = ne\vec{v}_D = ne\mu\vec{E} \qquad (2.44)$$

since $V_D = \mu_{drfft}E$. This may be shown to be a form of Ohm's law, corresponding to the familiar expression;

$$I = \frac{V}{R}; R = \rho\frac{1}{A}; J = \frac{V}{RS} = \frac{V}{\rho L} = \frac{E}{\rho} \qquad (2.45)$$

$$\vec{J} = \sigma\vec{E} \qquad (2.46)$$

where σ is the conductivity of the material.

$$\vec{J}=\sigma\vec{E}=ne\mu\vec{E} \tag{2.47}$$

$$\sigma=ne\mu$$

and

$$\rho=\frac{1}{\sigma}=\frac{1}{ne\mu} \tag{2.48}$$

This conductivity is a function both of mobilities and of carrier densities,

$$\sigma=e(n\mu_n+p\,\mu_p) \tag{2.49}$$

We have already seen that in impurity semiconductors there are many more carriers of one type than the other so that one term of Eq.2.49 predominates and the conductivity is determined largely by the density of the majority carriers [61].

2.2.3. Hall mobility

It is possible to determine drift mobility by generating electrons (and holes) by exposure to light. The electrons drifting down a length of the material under the influence of a field of known strength and their arrival at some point detected by a collector. If the light is attenuated by a shutter, the time between the light exposure and arrival of the electrons at the collector can be used to determine the drift mobility.

In practice, it is usually more convenient to determine a mobility termed the Hall mobility. For silicon and germanium, these two mobilities are approximately equal. If a charge moves in a magnetic field, then it experiences a force acting at right angles to both its direction and the direction of the magnetic field. This is the well-known left-hand rule or motor rule for the force exerted by a magnetic field on a conductor carrying a current. If the thumb and first and second fingers of the left hand are made mutually perpendicular and if the forefinger indicates the direction of the magnetic field and the second finger the direction of the current then the thumb indicates the direction of the resultant force. Since the conventional current flow is from high to low potential this is also the direction of movement of positive charges.

If we now consider the carriers in a semiconductor, they will move under the influence of an electric field: electrons against the field, holes with the field. If we apply a magnetic field at right angles to the electric field, an additional vector will be introduced instead of traveling straight toward the ends of the bars, the electrons or holes will also move in a direction mutually perpendicular to the two fields. They will take paths shown by in Fig.2.18. Both holes and electrons will move transversely in the same direction since although the action of the magnetic field is reversed, the motions laterally are in opposite directions. A space charge builds up at the lower surface and at equilibrium an electric field is set up across the crystal such that its magnitude and direction balance the space charge and the charge carriers flow straight through the crystal. If we connect a potentiometer across this field, i.e., at A and B, the polarity will indicate whether holes or electrons are the majority carrier and the magnitude of the potential difference will indicate the Hall field induced.

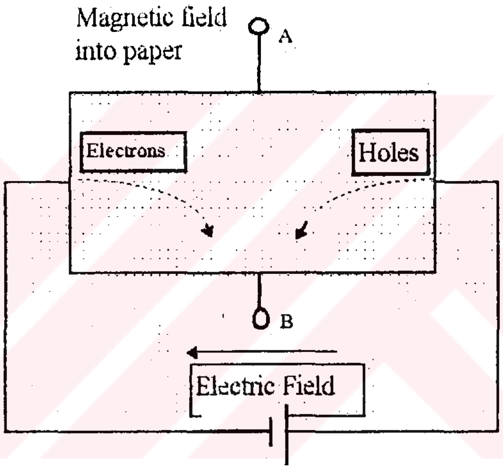

Figure 2.18. Hall effect.

As might be expected the force exerted on the charge is proportional to the magnetic field and to the electric field and the velocity of the charge. In fact, these last two are related, the stronger the field the higher the velocity for any particular crystal, and this is the relationship used to define mobility in Sec.2.2.2.

$$\mu_n = \frac{\vec{v}_D}{\vec{E}} \tag{2.50}$$

If we consider the condition necessary for charge to move undeflected through the crystal, then the Hall field E_H must exactly compensate the force exerted by the magnetic field, for any charge carrier

$$eE_H = ev_D H \tag{2.51}$$

where e is the charge on electron, v_D is velocity of charge carrier, and H is the magnetic field, or E_H can be obtained from the above equation as,

$$E_H = v_D H \tag{2.52}$$

The Hall voltage will depend on the Hall field and distance across it,

$$V_H = E_H d \tag{2.53}$$

By combining these various equations, it can be seen that Hall mobility

$$\mu_H = \frac{V_H}{EHd} \tag{2.54}$$

or, since

$$E = \frac{V}{l} \tag{2.55}$$

where V_a is the applied voltage and l is length of bar,

$$\mu_H = \frac{V_H l}{V_a H d} \tag{2.56}$$

Since all the parameters on the right can be measured, Hall mobility can be calculated [62].

2.3. Electronic Transitions

2.3.1. Transitions

Some of the electronic transitions commonly found in photoconductors are shown schematically in the energy-band diagram of Fig.2.19. These transitions can conveniently be divided into three types: (1) absorption and excitation (Fig.2.19(a)) ; (2) trapping and capture (Fig.2.19(b)) ; and (3) recombination and generation (Fig.2.19(c)).

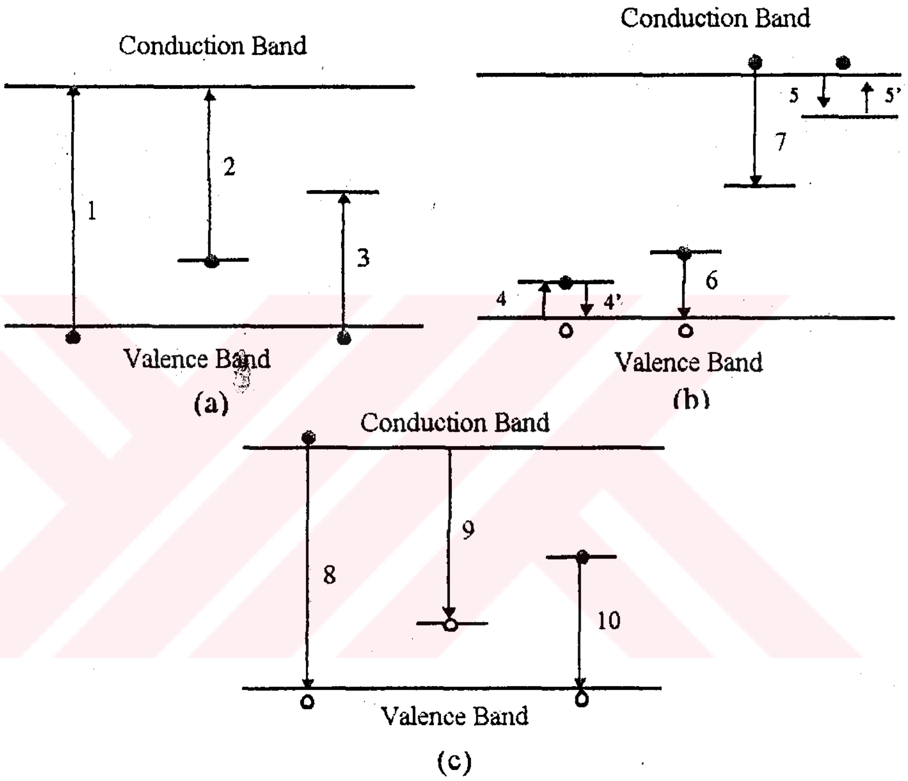

Figure 2.19. Common electronic transitions in photoconductors. (a) Absorption and excited; (b) trapping and capturing; (c) recombination.

2.3.1.1. Absorption and excitation

There are three possible types of absorption transitions resulting in photoconductivity. Transition 1 corresponds to absorption by the atoms of the crystal itself, producing a free electron and a free hole for each photon absorbed. Transition 2 corresponds to absorption at localized imperfections in the crystal, producing a free electron and a hole bound in the neighborhood of the imperfection for each photon absorbed. Transition 3 correspond to absorption, raising an electron from the valence band to an unoccupied imperfection level, producing a free hole and an electron bound in the neighborhood of the imperfection for each photon absorbed. We have omitted transitions (a) resulting in excitation formation, (b) between the ground state and excited states of an imperfection and (c) within allowed bands since these transitions do not directly produce free carriers.

2.3.1.2. Trapping and capture

Transitions from trapping levels to near bands and vice versa are quite likely but there is far less probability of transition between trapping levels and distant bands. Thus as a trapping level gets further away from one band and closer to the other band, it reaches a point where there is an equal probability of transition to either band, although the probability in either case may be relatively low.

Trapping levels near to the valence band are generally refered to as hole-trapping centers since electrons in these levels may easily capture(trap) holes in the valence band. Trapping levels close to the conduction band are generally refered to as electron-trapping centers since these may easily capture electrons in the conduction band. As the centre of the energy gap is approached by trapping levels, we reach a region where there is virtually equal probability of transition in either direction hence the centers cannot be really named hole or electron trapping centers specially. At these levels we may draw lines in the gap known as demarcation levels. Thus the upper line is the electron demarcation level and the lower line the hole demarcation level. These are shown in Fig.2.20 [63].

Once electrons and holes have been freed by absorption of a photon of sufficient energy they will remain free until they are captured at an imperfection (omitting for the moment the alternative possibilities that they may recombine directly or pass out of the crystal at the electrodes). We may

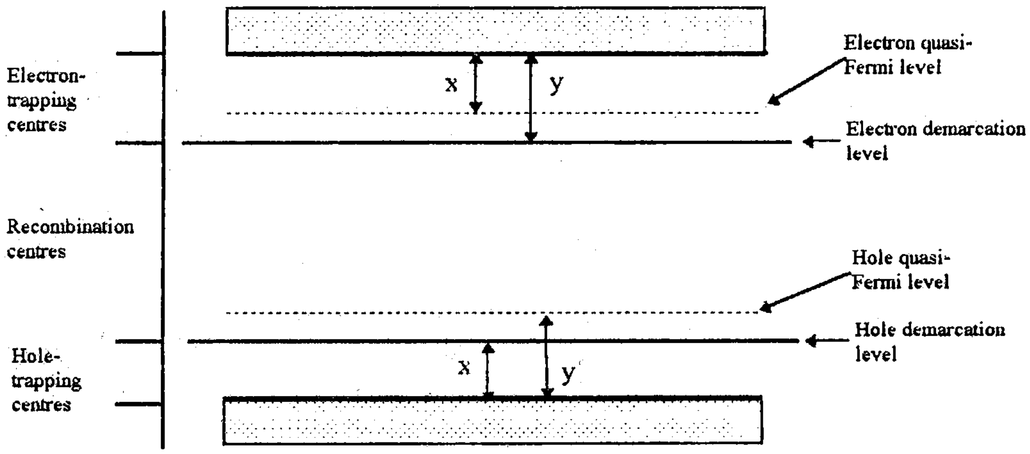

Figure 2.20. Demarcation levels and quasi-Fermi levels .

classify these capturing centers in two groups: (1) trapping centers, if the captured carrier has a greater probability of being thermally re-excited to the free state than of recombining with a carrier of opposite sign at the imperfection; (2) recombination centers, if the captured carrier has a greater probability of recombining with a carrier of opposite sign at the imperfection than of being re-excited to the free state. Fig.2.19b pictures trapping and thermal release of electrons in electron traps (transisitons 5 and 5') and trapping and thermal release of holes traps (electron transitions 4 and 4') also capture of an electron (transition 7) and of a hole (electron transition 6) in recombination centers.

Although a center with an energy level lying near one of the band edges will be more likely to act as a trap or as a recombination center (and vice versa for centers with levels lying near the middle of the forbidden gap), the distinction between traps and recombination centers is a distiction drawn on the basis of the relative probability of thermal ejection versus recombination, i.e., on kinetic conditions and not on basis of the intrinsic nature of themselves. A recombination center at one condition of light level and temperature may act as a trap at another condition of light level and temperature [63].

2.3.1.3. Recombination

Many semiconductor devices are based upon the principle of injection of holes into n-type material or injection of electrons into p-type material. Such injection carriers are called minority carriers to distinguish them from the majority carriers. These minority carriers will sooner or later recombine with the majority carriers and thus be permanently removed. In principle, such a recombination might take place in a single step according to the process: Free electron + free hole ⟷ electron bound in valence band, but in many cases such a recombination occurs in a two step process involving recombination centers.

Three simple types of recombination transitions are pictured in Fig.2.19c. The free electron may combine directly with the free hole, according to transition 8; the probability of this transition is usually rather small. Frequently transitions of type 8 are radiative, i.e., the lost energy is emitted as photons with approximately the energy of the band gap. Such emisson is called edge emission.

Recombination may also occur, as is the more usual case, through recombination centers: either an electron being captured by an excited center containing a hole (transition 9) or hole being captured by an excited center containing an electron (transition 10). Transitions 9 and 10 may also be radiative.

A recombination center is a center that can act as an electron trap when empty and as a hole trap when filled. Let holes be injected into n-type material; in the trapping process the electron combines with the free hole, with release of the excess energy, thus leaving the center empty. The center can now act as an electron trap; in the trapping process an electron from the conduction band makes a transition to the empty center with release of the excess energy.

In principle all electron and hole traps can act as recombination centers; the only distinction is in the recombination probabilities involved. If a center has a large recombination probability with free electrons when empty and a small recombination probability with free holes when filled, it acts mainly as an electron trap. If the opposite is true, the center acts mainly as a hole trap. If both recombination probabilities are comparable the center acts as a recombination center[64].

2.4. Excess Carriers in Semiconductors

2.4.1. Fundamental Absorption

The fundamental absorption refers to band-to-band or to exciton transitions, i.e., to the excitation of an electron from the valence band to the conduction band. The fundamental absorption, which manifests itself by a rapid rise in absorption, can be used to determine the energy gap of the semiconductor. However, because the transitions are subject to certain selection rules, the estimation of the energy gap from the "absorption edge" is not a straightforward process even if competing absorption process can be accounted for.

Because the momentum of a photon, h/λ, (λ is the wavelength of light), is very small compared to the crystal momentum h/a (a is the lattice constant), the photon-absorption process should conserve the momentum of the electron. The absorption coefficient $\alpha(h\nu)$ for a given photon energy $h\nu$ is proportional to the probability P_{if} for the transition from the initial state to the final state and to the density of electrons in the initial state, n_i, and also to the density of available (empty) final states, n_f, and this process must be summed for all possible transitions between states separated by an energy difference equal to $h\nu$:

$$\alpha(h\nu)=A\Sigma P_{if}\, n_i\, n_f \tag{2.57}$$

In what follows, for simplicity we shall assume that all the lower states are filled and that all the upper states are empty, a condition which is true for undoped semiconductors at 0 K.

2.4.2. Allowed Direct Transitions

Let us consider between two direct valleys where all the momentum conserving transitions are allowed (Fig.2.21),i.e, the transition probability P_i is independent of photon energy.

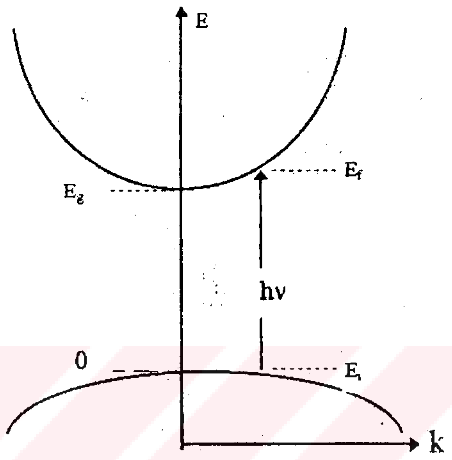

Figure 2.21. Two direct valleys where all the momentum conserving transitions are allowed.

Every initial state at E_i is associated with a final state at E_f such that

$$E_f = h\nu - |E_i| \tag{2.58}$$

But in parabolic bands,

$$E_f - E_g = \frac{h^2 k^2}{8\pi^2 m_e^*} \tag{2.59}$$

and

$$E_i = \frac{h^2 k^2}{8\pi^2 m_h^*} \tag{2.60}$$

Therefore,

$$h\nu - E_g = \frac{h^2 k^2}{8\pi^2}\left(\frac{1}{m_e^*} + \frac{1}{m_h^*}\right) \tag{2.61}$$

In momentum space the density of allowed points is uniform. The surfaces of constant energy are, to first approximation, spherical (isotropic-medium); then the volume of k-space between spheres of energy E and E+dE is $4\pi k^2$ dk. Here E is measured with respect to the edge of the parabolic band. Since a single state occupies in momentum space a volume $8\pi^3/V$ (V is the actual volume of the crystal) and there are two states per level, one finds that the number of energy states in the interval E and E+dE is

$$N(E)dE = \frac{4\pi}{h^3}(2m^*)^{3/2} E^{1/2} dE \tag{2.62}$$

For convenience, V is taken as a unit volume. The total density of states up to some energy E is

$$N = \frac{8\pi}{3h^3}(2m^* E)^{3/2} \tag{2.63}$$

Since, in general, the valleys are rotational ellipsoids instead of spherical surfaces, the effective mass is not isotropic; then an average density of state effective mass is used:

$$m^* = (m_l^* m_{t1}^* m_{t2}^*)^{1/3} \tag{2.64}$$

where m^*_l is the longitudinal effective mass and m^*_{t1} and m^*_{t2} are the two transverse masses.

Each valley contributes its own set of states from several valleys. Hence to find the density of states one must add the contributions of all the valleys. Thus in a multivalley semiconductor the number of states between, say, the bottom of the conduction band and some energy E is

$$N=\frac{8\pi}{3h^3}\Sigma_j g_j (2m_j^*)^{3/2}(E-E_j)^{3/2} \tag{2.65}$$

where g_j is the number of valleys of type j, m_j^* is the average effective mass of a j-valley, and E_j is the energy at the bottom of the j-valley. A similar treatment applies to states in the valence band.

Therefore, the density of directly associated states can then be found as

$$\begin{aligned} N(h\nu)d(h\nu) &= \frac{8\pi k^2 dk}{(2\pi)^3} \\ &= \frac{(2m_r)^{3/2}}{2\pi^2 h^3}(h\nu-E_g)^{1/2}d(h\nu) \end{aligned} \tag{2.66}$$

where m_r is the reduced mass given by

$$\frac{1}{m_r}=\frac{1}{m_e^*}+\frac{1}{m_h^*} \tag{2.67}$$

Hence the absorption coefficient which is the function of $h\nu$, α is

$$\alpha(h\nu)=A^*(h\nu-E_g)^{1/2} \tag{2.68}$$

where A^* is given by:

$$A^*=\frac{q^2\left(2\frac{m_h^* m_e^*}{m_h^*+m_e^*}\right)^{3/2}}{nch^2 m_e^*} \tag{2.69}$$

2.4.3. Forbidden Direct Transitions

In some materials, quantum selection rules forbid direct transitions at $k=0$ but allow them at $k\neq0$, the transition probability increases with k^2. In the model of Fig.2.21 this means that the transition probability increases proportionately with $(h\nu-E_g)^{1/2}$ and the absorption coefficient has the following spectral dependence:

$$\alpha(h\nu)=A(h\nu-E_g)^{1/2} \tag{2.70}$$

where A is given by

$$A=\frac{4}{3}\frac{q^2\left(\frac{m_h^* m_e^*}{m_h^*+m_e^*}\right)^{5/2}}{nc\,h^2 m_e^* m_h^* h\nu} \tag{2.71}$$

2.4.4. Optical absorption

An important technique for measuring the band gap energy of a semiconductor is the absorption of incident photons by the material. In this experiment, photons of selected wavelength are directed at the sample and the relative transmission of the various photons is observed. Since photons with energies greater than the band gap energy are absorbed while photons with energies less than band gap are transmitted, this experiment gives an accurate measure of the band gap energy.

2.4.4.1. Transmission and Absorption.

It is apparent that a photon with energy $h\nu>E_g$ can be absorbed in a semiconductor (Fig.2.22). Since the valence band contains many electrons and the conduction band has many empty states into which the electrons may be excited, the probability of the photon absorption is high. As Fig.2.22

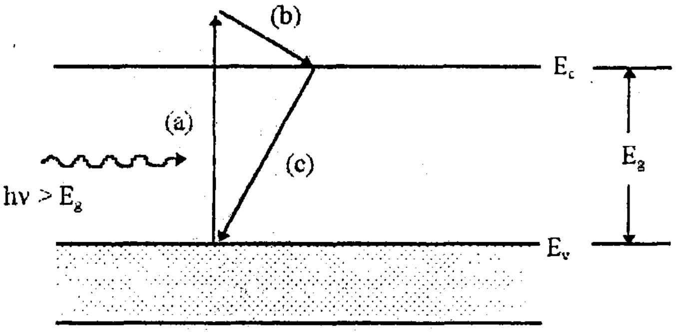

Figure 2.22. Optical absorption of a photon with $h\nu>E_g$: (a) an EHP is created during photon absorption; (b) the excited electron gives up energy to the lattice by scattering events; (c) the electron recombines with a hole in the valence band.

indicates, an electron excited to the conduction band by optical absorption may have more energy than is common for conduction band electrons (almost all electrons are near E_c unless the sample is very heavily doped). Thus the excited electron loses energy to the lattice in scattering events until its velocity reaches the thermal equilibrium velocity of other conduction band electrons. The electron and hole created by this absorption process are excess carriers; since they are out of balance with their environment, they must eventually recombine. While the excess carriers exist in their respective bands, however they are free to contribute to the conductivity of the material.

A photon with energy less than E_g is unable to excite an electron from the valence band to the conduction band. Thus in a pure semiconductor, there is negligible absorption of photons with $h\nu<E_g$. One exception to this rule is that a small amount of absorption can occur within a given band (free carrier absorption); for example, a low-energy photon can excite a conduction band electron temporarily to a higher state within the conduction band. No excess carriers are created in this process. This component of absorption is usually negligible compared with band-to-band excitation (intrinsic absorption) by photons of higher energy and most photons with $h\nu<E_g$ are transmitted

through the material. This explains why some materials are transparent in certain wavelength ranges.

2.4.4.2. Absorption constant and band gap

If a beam of photons with $h\nu > E_g$ falls on a semiconductor, there will be some predictable amount of absorption, determined by the properties of the material. We would expect the ratio of transmitted to incident light intensity to depend on the photon wavelength and the thickness of the sample. To calculate this dependence, let us assume that a photon beam of intensity I_o (photons/cm^2-sec) is directed at a sample of thickness l (Fig.2.23). The beam contains only photons of wavelength λ, selected by a monochromator. As the beam passes through the sample, its intensity at a distance x from the surface can be calculated by considering the probability of absorption within any increment dx. Since a photon which has survived to x without absorption has no memory of how far it has traveled, its probability of absorption in any dx is constant [65].

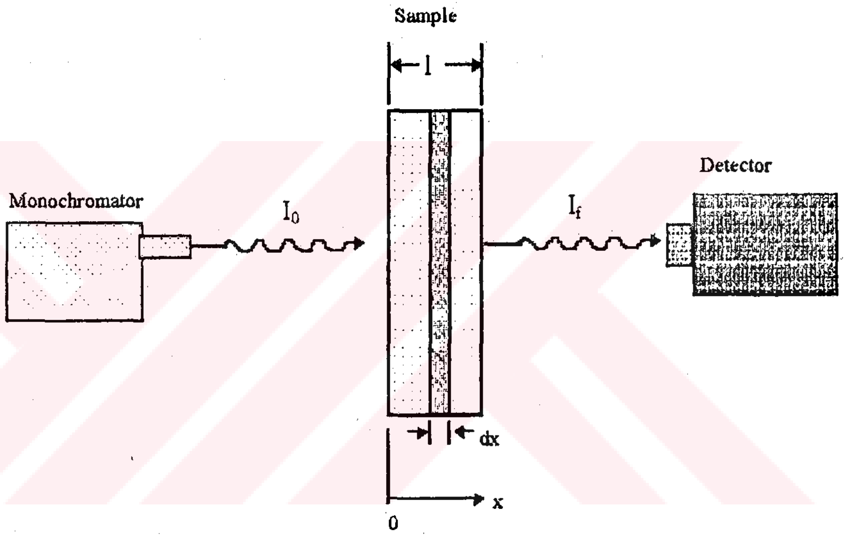

Figure 2.23. Optical absorption experiment.

Assume that a semiconductor is illuminated from a light source with $h\nu$ greater than E_g and a photon flux of I_o. As the photon flux travels through the semiconductor, the fraction of the photons absorbed is proportional to the intensity of the flux. Therefore, the number of photons absorbed within an incremental distance Δx (Fig.2.24a) is given by

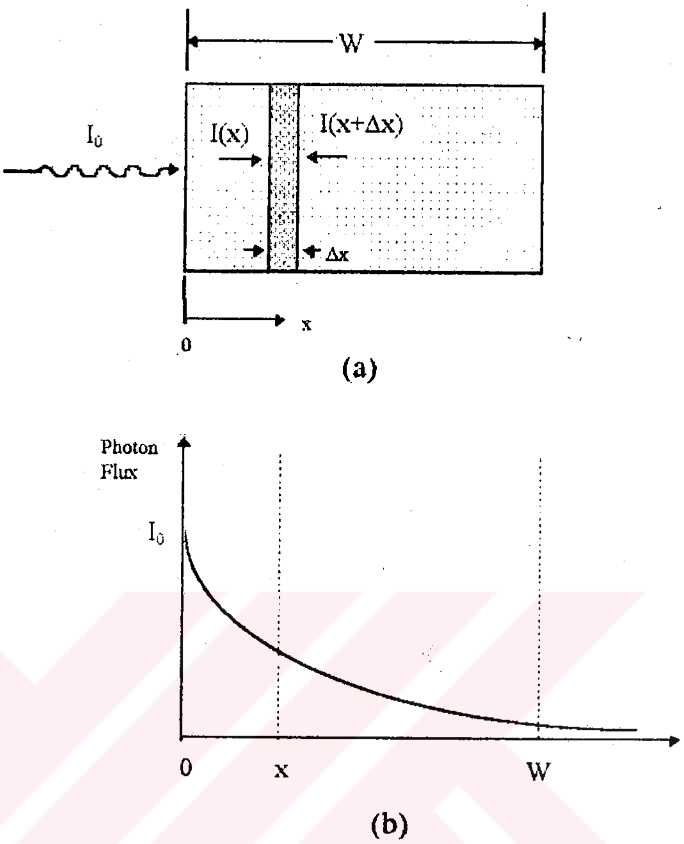

Figure 2.24 Optical absorption (a) Semiconductor under illumination (b) Exponential decay of photon flux.

$\alpha I_o(x)\Delta x$, where α is a proportionalilty constant defined as the absorption coefficient. From continuity of photon flux as shown in Fig.2.24a, we obtain

$$I(x+\Delta x)-I(x)= -\alpha I(x)\Delta x \qquad (2.72)$$

or

$$\frac{dI(x)}{dx}=-\alpha I(x) \qquad (2.73)$$

The negative sign indicates decreasing intensity of the photon flux due to absorption. The solution of Eq.2.73 with the boundary condition $I(0)=I_0$ at x=0 is

$$I(x)=I_0 e^{-\alpha x} \tag{2.74}$$

The fraction of photon flux that exists from the other end of the semiconductor at x=l (Fig.2.24b) is

$$I(l)=I_0 e^{-\alpha l} \tag{2.75}$$

As an alternative to a transmission experiment, it is possible to monitor the resistance of the sample and observe the photon energy at which absorption takes place. Since absorbed photons create EHP's and these carriers are able to participate in conduction, the conductivity of the sample will increase when photons are absorbed. This change in the conductivity with optical absorption is called photoconductivity.

Fig.2.25 indicates the band gap energies of some of the common semiconductors relative to the visible infrared and ultraviolet portions of the spectrum. We observe that GaAs, Si, Ge, and InSb lie outside the visible region so that if the eye is to be used as detector in the transmission experiment, an infrared converter tube must be used. Other semiconductors,

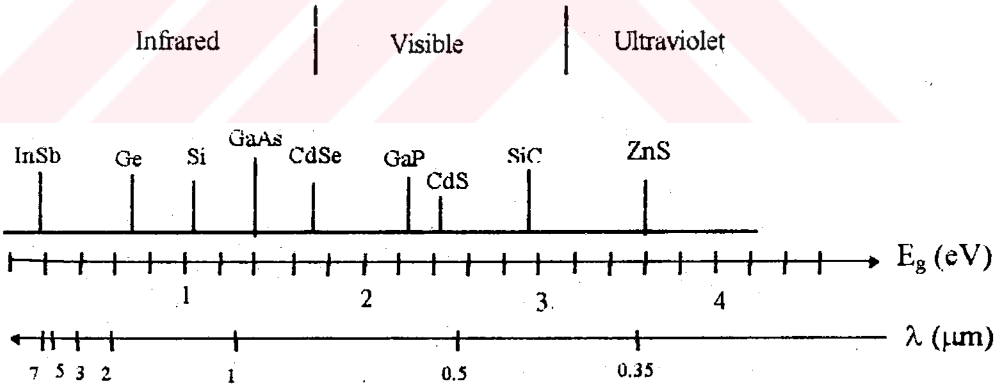

Figure 2.25. Band gaps of some common semiconductors relative to the optical spectrum.

such as GaP and CdS, have band gaps wide enough to pass photons in the visible range. It is important to note here that a semiconductor absorbs photons with energies equal to the band gap, or larger [65].

2.4.5. Carrier lifetime and photoconductivity

The conductivity of semiconducting materials depends on the number of free electrons in the conduction band and also the number of holes in the valence band. Thermal energy associated with lattice vibrations can promote electron excitations in which free electrons and/or holes are created. Additional charge carriers may be generated as a consequence of photon induced transitions in which light is absorbed, the resultant increase in conductivity is called photoconductivity. Thus, when a specimen of a photoconducting material is illuminated, the conductivity increases.

Photoconductivity is the increase in electrical conductivity of an insulating crystal caused by radiation incident on the crystal. The photoconductive effect finds practical application in television cameras, infrared detectors, light meters and indirectly in the photographic process. The direct effect of illumination is to increase the number of mobile charge carriers in the crystal. If the energy of the incident photon is greater than the energy gap E_g then each photon absorbed in the crystal will produce a free electron-hole pair. The photon is absorbed by raising to the conduction band an electron originally in the valence band. Both the hole in the valence band and the electron in the conduction band may contribute to the conductivity.

Consider a photoconductor consisting simply of a slab of semiconductor with ohmic contacts at both ends of the slab (Fig.2.26). When incident light falls on the surface of the photoconductor, electron-hole pairs are generated either by band-to-band transition (intrinsic) or by transitions involving forbidden gap energy levels (extrinsic), resulting in an increase in conductivity.

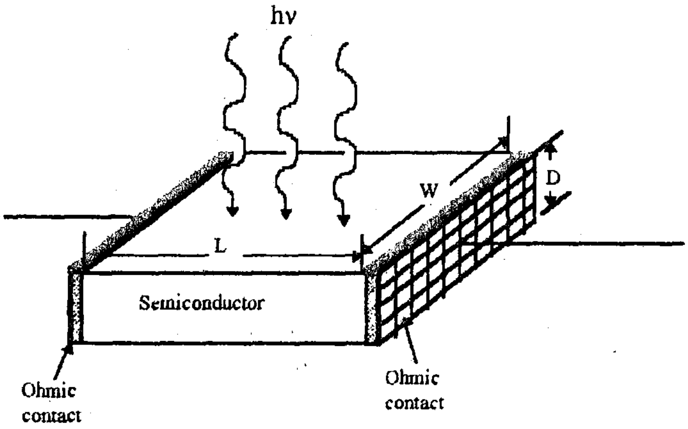

Figure 2.26. Schematic diagram of a photoconductor that consists of a slab of semiconductor and two ohmic contacts at the ends.

For the intrinsic photoconductor, the conductivity is given by

$$\sigma = q(\mu_n n + \mu_p p) \tag{2.76}$$

and the increase in conductivity under illumination is mainly due to the increase in the number of carriers. The long-wavelength cutoff for this case is given by

$$\lambda_c = \frac{1.24}{E_g} \tag{2.77}$$

For the extrinsic case, photoexcitation may occur between the band edge and an energy level in the energy gap. In this case, the long-wavelength cutoff is determined by the depth of the forbidden-gap energy level.

Consider the operation of a photocondoctor under illumination. At time zero, the number of carriers generated in a unit volume by a given photon flux is n_o. At a later time t, the number of carriers n(t) in the same volume decays by recombination as

$$n = n_0 \exp(-t/\tau) \qquad (2.78)$$

where τ is the carrier lifetime. In other words, the recombination rate is $1/\tau$. If we assume a steady flow of photon flux impinging uniformly on the surface of a photoconductor (Fig.2.25) with area A = WL, the total number of photons arriving at the surface is $(P_{opt}/h\nu)$ per unit time where P_{opt} is the incident optical power and $h\nu$ is the photon energy.

At steady state, the carrier generation rate must be equal to the recombination rate. If the detector thickness D is much larger than the light penetration depth 1/a, the total steady state carrier generation rate per unit volume is

$$G = \frac{n}{\tau} = \frac{\eta(P_{opt}/h\nu)}{WLD} \qquad (2.79)$$

where η is the quantum efficiency and n is the number of carriers per unit volume (carrier density). The photocurrent flowing between the electrodes is

$$I_p = (\sigma E)WD = (q\mu_n nE)WD = (qnv_D)WD \qquad (2.80)$$

where E is the electric field inside the photoconductor and v_D is the carrier drift velocity. Substituting n in Eq.(2.80) gives

$$I_p = q[\eta\frac{P_{opt}}{h\nu}][\frac{\mu_n \tau E}{L}] \qquad (2.81)$$

If we define the primary photocurrent as

$$I_{ph} = q[\eta\frac{P_{opt}}{h\nu}] \qquad (2.82)$$

The photocurrent gain from (2.82) is

$$\text{Gain}=\frac{I_p}{I_{ph}}=\frac{\mu_n \tau E}{L}=\frac{\tau}{t_r} \tag{2.83}$$

where $t_r = L/v_d$ is the carrier transit time. The gain depends upon the ratio of carrier lifetime to the transit time [66].

2.5. Electrode Effects

2.5.1. Energy level diagram; Work Function

Figure 2.27 shows the energy level diagram for n-type and a p-type material. The energy difference W between the vacuum level and the bottom of the conduction band is usually called the electron affinity and denoted by χ.

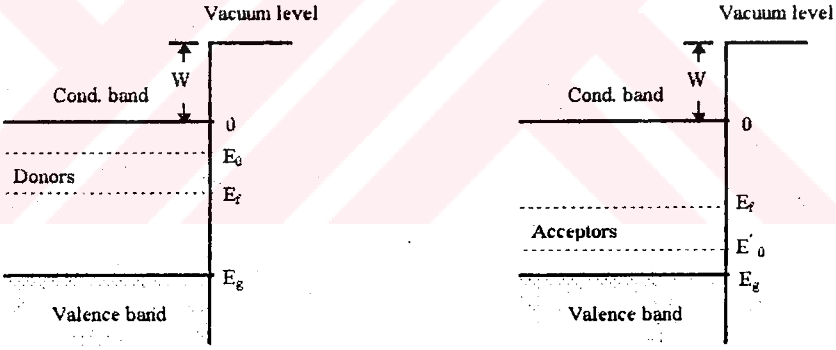

(a) (b)

Figure 2.27. (a) Energy level diagram of an n-type semiconductor. (b) Energy level diagram of a p-type semiconductor.

If the zero point is taken with respect to the bottom of the conduction band, then the work function is defined as

$$\phi=\chi-E_f \tag{2.84}$$

as in a metal, but the difference is that the Fermi level is now negative. It should be noted that E_f is obviously larger for a p-type than for an n-type semiconductor so that a p-type sample of a given material has a larger work function than an n-type sample of the same material. This is important for thermionic emission.

It should be noted that the minimum quantum energy needed to produce a photoelectron at T=0 K is $\chi + E_0$ for n-type materials and $\chi + E_g + E_0'$ for p-type materials.

2.5.2. Metal-Semiconductor Contacts

We may summarize the causes of barriers at metal-semiconductor contacts in three simple categories:

(1) Improper matching of work functions between the metal and the semiconductor,

(2) Presence of surface states on the semiconductor, producing an intrinsic surface barrier.

(3) Presence of a thin layer of a third material (such as an oxide) which in turn causes barriers for reason 1 or 2 above.

Such barriers usually demonstrate their presence by giving rise to rectification effects; the resistance to current flow is much less for one direction of the applied field than for the reverse direction.

When two substances are brought into contact a redistribution of charge occurs, finally a new equilibrium condition is reached in which the Fermi levels of the two substance are at equal heights. This rule holds not only for contacts between two metals but also for the contact between a metal and an n-type or p-type semiconductor.

A metal-semiconductor contact may either be ohmic or rectifying. The latter is a contact in which the current flows much more easily in one direction than in the opposite. We shall see that this is intimately connected with the electronic energy level diagram of the two substances.

Consider a contact between a metal and an n-type semiconductor (Fig.2.28). Let he donor concentration in the semiconductor be relatively large, and let almost all donors be ionized at room temperature. Let ϕ_m be the work function of the metal, ϕ_s the work function of the semiconductor and χ_s the electron affinity of the semiconductor. Let us first consider the case $\phi_m > \phi_s$. The situation before contact is shown in Fig.2.28a; the Fermi level of the semiconductor is then above the Fermi level of the metal by an amount $\phi_m - \phi_s$. After contact, an exchange of charge occurs, electrons from the surface layer of the semiconductor enter the metal, leaving ionized donors behind in that surface layer. After the exchange of charge is completed, the Fermi level in both materials are at the same height; this means that the energy levels in the bulk semiconductor are lowered by the amount $\phi_m - \phi_s$. As a consequence, a potential barrier is formed at the surface. On the semiconductor side the height of this barrier is thus $\phi_m - \phi_s$; on the metal side, since the Fermi levels are at the same height, the height of the barrier is shown Fig.2.28b.

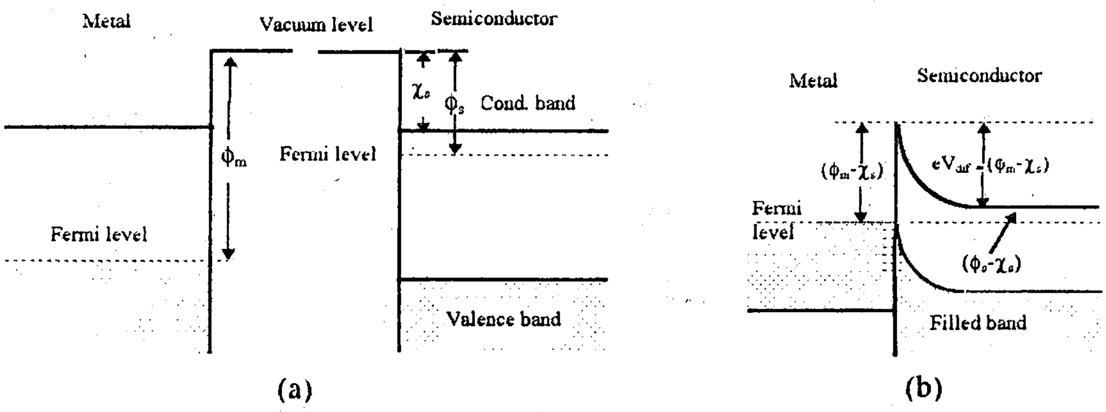

(a) (b)

Figure 2.28. Energy level diagram of a metal n-type semiconductor contact with $\phi_m > \phi_s$, where ϕ_m and ϕ_s are the work functions of metal and semicondcutor, recpectively. (a) Energy-level diagram before contact. (b) Energy-level diagram after contact. The Fermi levels are now of equal height, V_{dif} is the diffusion potential.

$$(\phi_m-\phi_s)+(\phi_s-\chi_s)=\phi_m-\chi_s \tag{2.85}$$

Expressed in volts, the height of the barrier follows from

$$eV_{dif}=\phi_m-\phi_s \tag{2.86}$$

The quantity V_{dif} is known as the diffusion potential. The potential at the interior of the semiconductor, taken with respect to the metal surface, is V_{dif}.

Up to now we have considered the case $\phi_m>\phi_s$. If $\phi_m<\phi_s$, no rectifying barrier is formed. The situation before contact is shown in Fig.2.29a, the Fermi level of the semiconductor is below the Fermi level of the metal by an amount $\phi_s-\phi_m$. An exchange of charge takes place after contact, electrons flow from the metal into the surface layer of the semiconductor, leaving a positive surface charge behind on the metal side of the contact and casing a negative surface charge at the semiconductor side of the contact. The Fermi level in the semiconductor bulk material is thereby raised by an amount $\phi_s-\phi_m$ (Fig.2.29b). If a voltage V is applied, this potential difference is not taken up in the contact area as in the previous case but is distributed across the bulk semiconductor (Fig.2.29c and d).

We see that the electrons can move across the barrier without much difficulty especially if $\phi_s - \chi_s$ is relatively small. The contact may thus be considered an ohmic contact.

We have hereby deduced a simple rule for determining whether a metal- semiconductor contact is an ohmic or rectifying contact. The contact is ohmic if $\phi_m<\phi_s$, and rectifying if $\phi_m>\phi_s$.

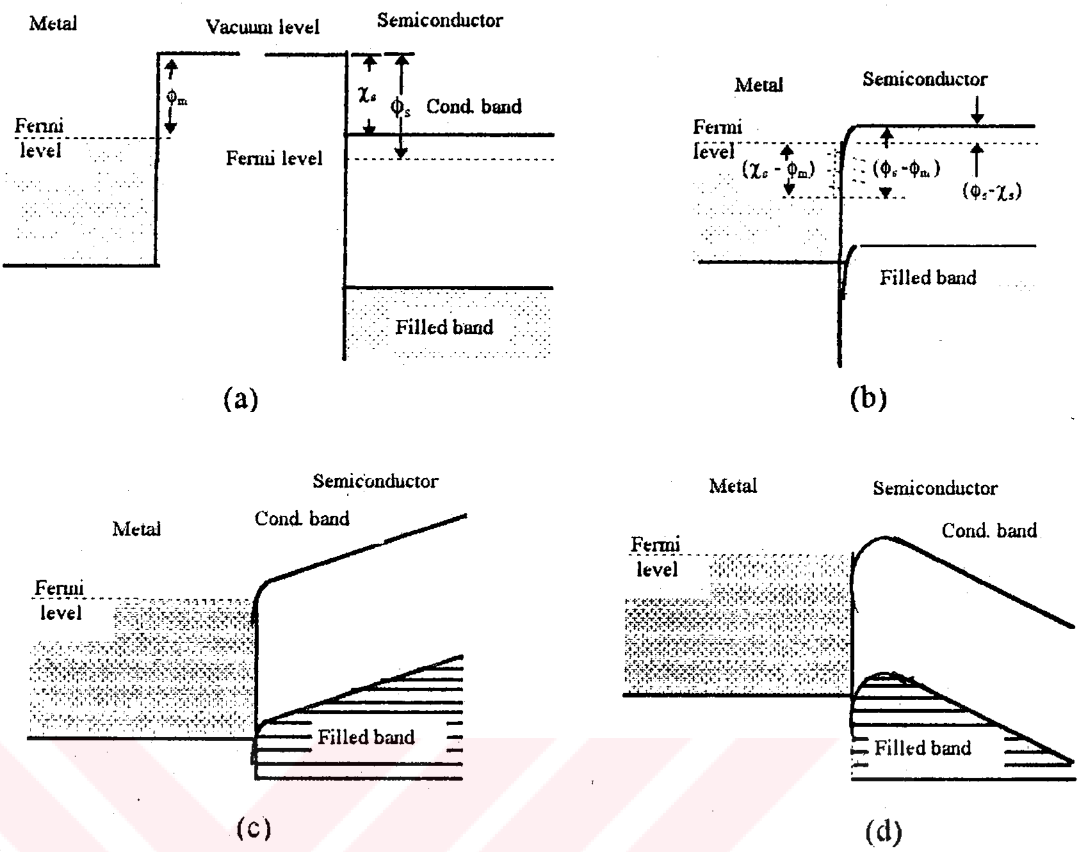

Figure 2.29. Energy level diagram of a metal n-type semiconductor contact with $\phi_m < \phi_s$, where ϕ_m and ϕ_s are work function of metal and semiconductor, respectively. (a) Energy level diagram before contact. (b) Energy level diagram after contact. This contact is ohmic. (c) A negative voltage is applied to the contact. (d) A positive voltage is applied to the contact.

After our discussion of the metal-n-type semiconductor contact, the discussion of the metal-p-type semiconductor contact can be brief. Let ϕ_m again be the work function of the metal, ϕ_s the work function of the semiconductor and E_s the depth of the top of the filled band of the semiconductor below the vacuum level. The contact is now rectifying if $\phi_m < \phi_s$ and ohmic if $\phi_m > \phi_s$.

Let us consider the latter case first. The situation before contact is shown in Fig.2.30a, the Fermi level in the semiconductor is above the Fermi level in the metal by an amount ϕ_m-ϕ_s. After contact, an exchange of charge takes place, electrons flow out of the semiconductor, leaving a positive surface charge (due to holes) behind on the semiconductor side and a negative surface charge on the metal side, thereby lowering the Fermi level in the semiconductor by an amount ϕ_m-ϕ_s (Fig.2.30b). Holes from the semiconductor can readily move into the metal and be neutralized almost instantly (because of the high electron concentration) and for opposite polarity of the applied voltage the holes formed thermally in the conduction band of the metal can readily move into the semiconductor. The contact is thus ohmic.

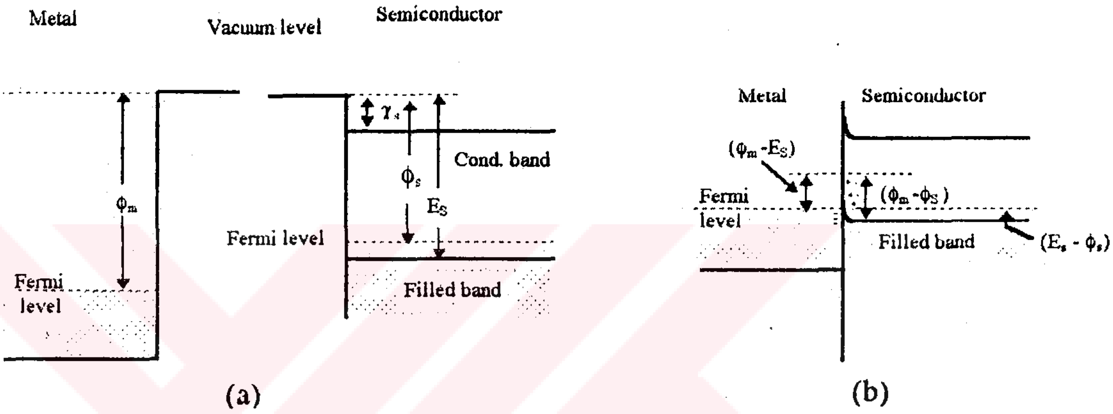

Figure 2.30. Energy level diagram of a metal p-type semiconductor contact. (a) Energy level diagram before contact (b) energy level diagram after contact if ϕ_m>ϕ_sThe contact is ohmic.

A general survey of the metal semiconductor contacts suggests three useful rules to aid in obtaining ohmic contacts to a material:

(1) Choose a metal with a smaller work function than the material if n-type, larger if p-type.

(2) Choose a metal which acts as an impurity in the material with the same conductivity characteristics as the material itself, a donor for n-type material, and an acceptor for p-type material and apply the contact in such a way as to bring about some diffusion of the contacting metal into the material.

(3) If ohmic contact is not obtained with a metal meeting the requirements of rules 1 and 2, try various means of mechanically or electrically damaging the

surface area involved in the contact. In semiconductor work, the formation of ohmic contacts has been an established procedure. It is often found that the barrier at a contact can be removed by passing a short pulse of relatively high current such as can be obtained from a condenser discharge [67].

2.6. Thermoluminescence

2.6.1. Basic thermoluminescence theory

Insulators which contain electrons trapped at defect sites are in a metastable condition. Trapped charge can be liberated by heat and will cross the potential barrier and move to a lower energy state with the emission of light. This is called thermoluminescence. The rate at which electrons or holes escape from the trap is governed by the vibrational frequency of the charge within the trap s and the height E of the potential barrier so that the overall rate of escape is proportional to s exp(-E/kT). Very naively we can see that on heating a crystal with trapped electrons the luminescence signal starts at zero (no electrons escaping) increases with increasing temperature (the Boltzman factor increases) and finally drops to zero at high temperatures when all the initial levels are empty. This maximum in the luminescence is termed a glow peak. Detailed analysis of the curve shape can give information on the trap depth, frequency factor s, number and type of electron and hole traps, electron mobility and capture cross-sections of the various levels. Since we are considering a very sensitive technique which is capable of detecting as few as 10^7 defects in a sample, we are faced with a very complex problem in a real system where there will be a total concentration of 10^{16} or more defects. The theoretical problem is still tractable since this only requires that we solve the problem with more variables but detailed comparison with experiment can no longer yield unique solutions for the variables. Historically, the theoretical approach has been either to describe a very simple idealized process or to use a digital computer to predict the possible consequence of changing the variables. Many approximations have also been suggested which correctly estimate the trap depth but not the other parameters. We shall start with the simple model of Randall and Wilkins in which the electrons are thermally excited from a single defect level to the conduction band and radiatively decay to a luminescent site as is described by Fig.2.31. We assume that no direct transitions take place from the defect to the recombination centre and the number of defect sites is small compared with the number of luminescent centres and also the recombination lifetime in the conduction band is small.

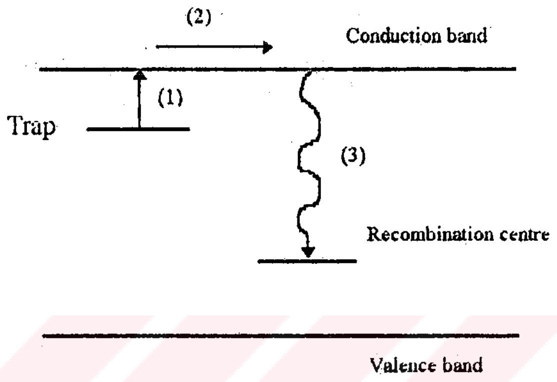

Figure 2.31. The process involved in thermoluminescence: (1) thermal excitation; (2) electronic migration and (3) luminescence

The rate of depopulation of the defect is

$$\frac{dn}{dt} = -n(N_c S v)e^{(-\frac{E}{kT})} + An_c(N-n) \tag{2.87}$$

where n is the electron concentration in the defect, N_c is the density of states in the conduction band, S is the electron capture cross-section in the conduction band and v is the electron velocity. The second term allows for the possibilty of a back reaction with A as the defect's electron capture cross section. N is the total concentration of the shallow levels and n_c the electron concentration in the conduction band [68].

2.6.2. Effect of traps on thermoluminescence

When a crystal is excited optically (with $h\nu>E_g$) or with an electron beam, deep traps can be filled. Those carriers which have been captured by the deep levels remain trapped after the excitation is terminated. The trapped carriers subsequently can be excited out of the traps either optically ($E_t<h\nu<E_g$) or thermally (E_t is the depth of the trap). The most frequently used technique is the thermal activation. The temperature at which the carrier is excited out of the trap correlates with the depth of the trapping level. When the carriers are released from the traps, they can participate in measureable events such as drifting in an electric field (thermally stimulated current) or recombining radiatively (thermoluminescence)[69].

The probability per unit time for an electron to escape from the trap is given by

$$P = s\, e^{(-\frac{E}{kT})} \tag{2.88}$$

The quantity s is given by

$$s=N_B\, v\, \sigma_t \tag{2.89}$$

where N_B is the density of states in the band into which the carriers escape, v is the carrier's thermal velocity, and σ_t is the trap's capture cross-section. The escape probability P per unit time is related to the time t spent in the trap:

$$P=\frac{1}{\tau} \tag{2.90}$$

Equation 2.88 shows that τ has a strong dependence on the depth of the trap and on the temperature.

If n_t is the density of trapped electrons, its rate of change due to thermal excitation is

$$\frac{dn_t}{dt}=-n_tP \tag{2.91}$$

If the freed electrons are not recaptured by the traps, the solution of Eq.2.91 is

$$n_t = n_{to} e^{(-\frac{t}{\tau})} \tag{2.92}$$

where n_{t0} is the initial density of trapped electrons.

CHAPTER 3

EXPERIMENTS AND MEASUREMENTS

3.1. Deposition Apparatus

In this study, the apparatus which is used for the development of the thin film samples based on the spraying pyrolysis technique has been designed and developed in our laboratory. This apparatus whose schematic diagram is given in Fig.3.1 consists of a spraying system, heater, temperature control system, and timer.

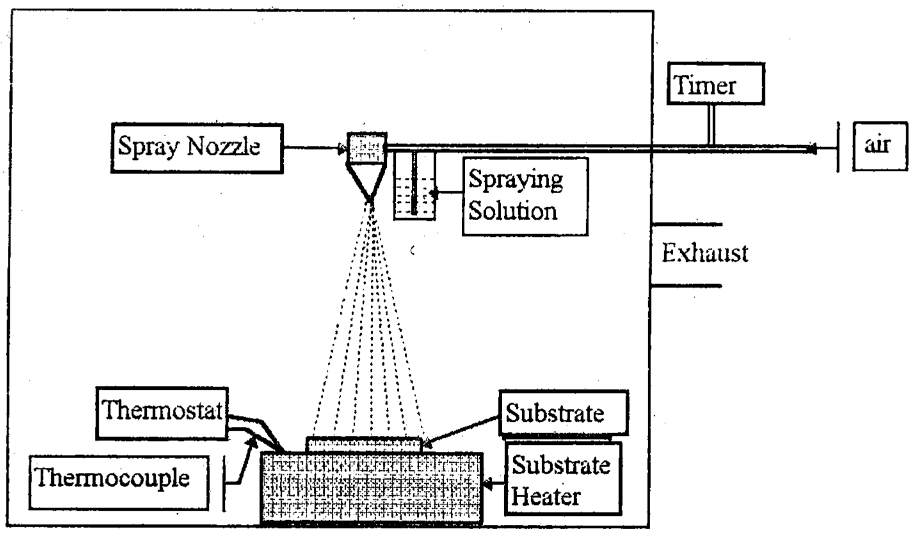

Figure 3.1. Schematic diagram of the spray pyrolysis system.

Spraying system: This is used to produce the droplets from the spraying solution. The droplets can be in different sizes depending on the geometry of the nozzle, seen in figure above, being employed to produce the droplets and also the flow rate of the carrier gas. In this study, air is used as carrier gas and the flow rate of the spraying solution is kept constant as 0.5 ml/min. On the other hand, there is another factor affecting on the size of the droplets. This is the height of the nozzle from the substrate surface. This height can be adjusted and the most suitable height, producing the highest quality samples, is found experimentally.

Heater: This is used to heat the substrates. It consists of a steel plate with resistance coils lying under it. The power of the heater is 2500 watts and it operates at 220 volts and 50 Hz (AC).

Temperature control system (thermostat): One of the most important factors which plays a vital role for producing high quality thin film samples is to keep the substrates at required temperatures. Because of this, a rather sensitive thermostat system, that is associated with an electronic circuit and operates in temperature range 0-1200 °C, is employed in the heater system. The substrate temperature is controlled to within an accuracy of $\pm 5^0$C by this thermostat system. The system operates as following: It stops the heating when the temperature of the heater plate reaches the required temperature and at the same time another switch starts the gas flow and spraying process. The droplets falling on the substrate cause a temperature drop. Thermostat system starts the heating as soon as the substrate temperature drops under a certain temperature below the required substrate temperature. This process goes on until the completion of the thin film production.

Timer: This is used to adjust the gas flow time. This time can be adjusted from 1 to 9 seconds. In this study, the spraying time was choosen as 3 seconds.

3.2 Substrate Preparation

The physical properties of the substrates on which the thin films will be formed, and the starting materials play a vital role in the development of good quality thin film samples. In this study, the crystallinity of the thin film samples is very strongly dependent on the crystal structure of the substrate and the starting material, particularly cation material such as cadmium chloride in a thiourea solution. If a cadmium chloride is used, a highly crystalline film can be developed with an amorphous substrate. Therefore, glass substrates have been used, since the glass has an amorphous crystal structure. Prior to deposition, pieces of glass substrate of dimension 1.5x2.0x0.1 cm^3 are initially cleaned. This cleaning process is carried out in four steps as seen in Fig. 3.2.

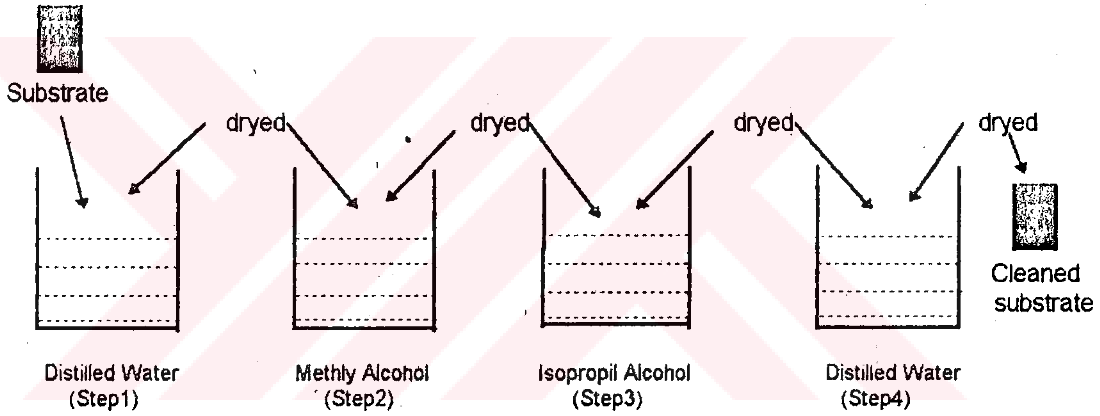

Figure 3.2. Cleaning process of the glass substrates.

All substrates used in this study have been prepared as follows:

Step 1: Firstly, the glass substrate is immersed into the distilled water to clean the dust on its surface for 15 minutes. Then it is taken out from the distilled water and dried.

Step 2: The substrate taken from the first cup and dried is immersed into the methyl alcohol and left there for 15 minutes to clean the oily substances on the surface of the substrate, and then it is taken out from this liquid and dried in air.

Step 3: The dried substrate is immersed into the third cup filled with isopropil alcohol and it is treated again for 15 minutes to obtain a smooth surface.

Step 4: Finally, the substrate is treated with the distilled water as in the first step to clean all residues remaining on the surface of the substrate from the other processes.

3.3. Spraying Solution Preparation

In this study, many CdS and ZnS thin films have been developed employing the spray pyrolysis technique. In this technique, the solution used for the production of thin film is called the 'spraying solution'. Two different spraying solutions have been prepared for the production of ZnS and CdS thin film samples. They are prepared as follows: Firstly, the required amount of salt ($CdCl_2$ or $ZnCl_2$) is weighed and stirred into a cup containing 100 ml of distilled water to form the salt solutions. After this, the required amount of $SC(NH_2)_2$ (thiourea) salt is weighed and stirred into another cup containing 100 ml of distilled water giving the thiourea solution. Finally, the spraying solutions which will be used for the production of CdS and ZnS thin film samples are obtained by mixing $CdCl_2$ and $ZnCl_2$ solutions with the thiourea solution together, respectively. The molarities of $CdCl_2$ and $SC(NH_2)_2$ salts in the spraying solutions used for developing the CdS thin films, numbered A_1 to A_9, are given in Table 3.1.

Table 3.1: Molarities of $CdCl_2$ and $SC(NH_2)_2$ salts in the spraying solutions used for the development of CdS thin films.

Sample No	A_1	A_2	A_3	A_4	A_5	A_6	A_7	A_8	A_9
Molarity of $CdCl_2$ (M)	0.1	0.1	0.05	0.1	0.1	0.05	0.1	0.1	0.05
Molarity of $SC(NH_2)_2$(M)	0.1	0.05	0.1	0.1	0.05	0.1	0.1	0.05	0.1

The molarities of $ZnCl_2$ and $SC(NH_2)_2$ salts in the spraying solutions used for developing the ZnS thin films numbered B_1 to B_9, are given in Table 3.2.

Table 3.2: Molarities of $ZnCl_2$ and $SC(NH_2)_2$ salts in the spraying solutions used for the development of ZnS thin films.

Sample No	B_1	B_2	B_3	B_4	B_5	B_6	B_7	B_8	B_9
Molarity of $ZnCl_2$ (M)	0.1	0.1	0.05	0.1	0.1	0.05	0.1	0.1	0.05
Molarity of $SC(NH_2)_2$(M)	0.1	0.05	0.1	0.1	0.05	0.1	0.1	0.05	0.1

3.4. CdS Thin Film Preparation

To develop CdS thin film samples, firstly, the spray flow rate is adjusted to about 0.5 ml min^{-1} and the height of the nozzle is fixed to 20 cm from the substrate. Then the spraying solution is sprayed onto the glass substrate which is kept at the required temperature. When the solution droplets reach the substrate surface, the following chemical reaction occurs,

$$CdCl_2 + SC(NH_2)_2 + 2H_2O \longrightarrow CdS_{solid} + 2NH_4Cl_{vapor} + CO_{2\ gas} \qquad (3.1)$$

As seen from this reaction, CdS is deposited on the substrate surface forming thin film while NH_4Cl and CO_2 leaves the system as vapour and gas, respectively. Repeating this process using the spraying solutions prepared with different molarities of $CdCl_2$ and $SC(NH_2)_2$ salts given in Table 3.1, nine different CdS thin films were developed at substrate temperatures 340, 380, and 420 °C. The thicknesses of these samples found by using the weighing method are given in Table 3.3.

Table 3.3: Thickness of the CdS thin film samples prepared at different substrate temperatures (50 ml of spraying solution has been used in the preparation of each sample).

Sample No	A_1	A_2	A_3	A_4	A_5	A_6	A_7	A_8	A_9
Substrate Temp. (°C)	340	340	340	380	380	380	420	420	420
Thickness of Samples (μm)	1.11	1.55	1.87	0.49	0.65	1.03	0.45	0.65	0.95

3.5. ZnS Thin Film Preparation

The same process followed for the production of CdS thin films is repeated for developing the ZnS thin film samples. To do this, firstly, the spray flow rate is adjusted to about 0.3 ml min^{-1} and the height of the nozzle is fixed to 15 cm from the substrate. Then, the spraying solution is sprayed onto the glass substrate whose temperature is kept at a required temperature. When the solution droplets reach the substrate surface, the following chemical reaction occurs,

$$ZnCl_2 + SC(NH_2)_2 + 2H_2O \longrightarrow ZnS_{solid} + 2NH_4Cl_{vapor} + CO_{2\ gas} \qquad (3.2)$$

As seen from this reaction, a ZnS thin film is formed on the substrate surface while NH_4Cl and CO_2 leave the system as vapour and gas, respectively. Repeating this process, using the spraying solutions prepared with different molarities of $ZnCl_2$ and $SC(NH_2)_2$ salts as given in Table 3.2, nine different ZnS thin films were developed for the substrate temperatures 440, 470, and 500 °C. The thicknesses of these samples found by using the weighing method are given in Table 3.4.

Table 3.4: Thickness of the ZnS thin film samples prepared at different substrate temperatures (75 ml of spraying solution has been used in the preparation of each sample).

Sample No	B_1	B_2	B_3	B_4	B_5	B_6	B_7	B_8	B_9
Substrate Temp. (°C)	440	440	440	470	470	470	500	500	500
Thickness of Samples (µm)	1.41	1.85	2.30	1.12	1.23	1.76	1.05	1.15	1.70

3.6. EXPERIMENTAL PROCEDURE

3.6.1. Electrical Measurements

In this study; the Van der Pauw method (70) is used to evaluate the resistivity and conductivity of the thin film samples, and the Hall mobility of the electrons which are the majority carriers at room temperature, in the dark and under white light illumination. To apply this method, four ohmic contacts A,B,C and D are prepared in the form of circular indium electrodes, with areas ~0.25 mm^2, by the evaporation method at the periphery of an irregular contour specimen of thin film in laboratory, as shown in Fig.3.3. Before making the ohmic contacts, CdS and ZnS thin film samples are etched to remove the rough surfaces and reduce the influence of surface effects as following: for etching CdS thin film samples, a solution is prepared mixing HNO_3 and

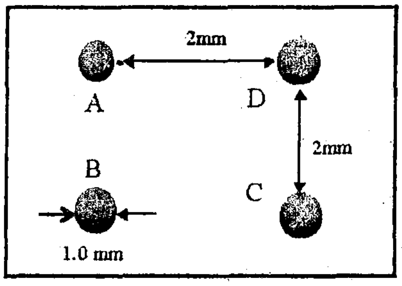

Figure 3.3. In-ohmic contacts prepared on thin film samples.

CH_3COOH with distilled water and the samples are left in this solution for 2 min. at 25 °C. For etching ZnS thin film samples the samples are put into the hydrogen peroxide solution(H_2O_2), and then they are left in there for 15 min. at 70 °C. After etching, these ZnS thin film samples are thoroughly washed alternately with KCN solution, distilled water, acetic acid, and distilled water and finally they are dried at 100 °C.

3.6.1.1. Resisitivity and conductivity measurement

The resistivity measurements are carried out in two steps. Firstly, to determine the $R_{AB,\ DC}$ the experimental set-up is performed as shown in Fig.3.4a is used. Applying an input potential V_{in} across the contacts A and B gives rise to a current I_{AB} which is measured by means of an ammeter. A potential V_{CD} appears between the contacts C and D and this potential is measured with an voltmeter. The resistance $R_{AB,CD}$ is obtained from the ratio of V_{CD} to I_{AB}. To determine the resistance $R_{BC,DA}$, Fig.3b, the input potential is applied across the contacts B and C. Then, the current I_{BC} flowing across the contacts B and C and the potential V_{DA} appearing between the contacts D and A are measured by means of an ammeter and a voltmeter, respectively. The resistance $R_{BC,DA}$ is found dividing V_{DA} by I_{BC}. These measurements are repeated five times at five different input potentials to obtain the average values of $R_{AB,CD}$ and $R_{BC,DA}$. The resistivity of the samples ρ is calculated by

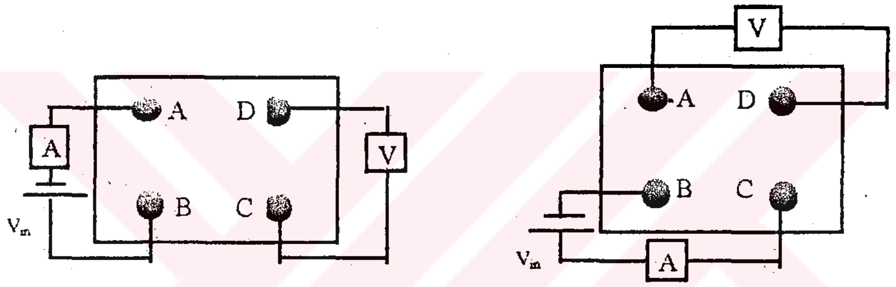

(a) (b)

Figure 3.4. Resistivity measurement set-up.

substituting the average values of these resistances in the following expression,

$$\rho = \frac{d}{\ln 2}(R_{AB,CD} + R_{BC,DA}) f(\frac{R_{AB,CD}}{R_{BC,DA}}) \qquad (3.3)$$

where f is a function (the form factor). If $R_{AB,CD}$ and $R_{BC,DA}$ are nearly equal to each other, the approximated value of f can be obtained from the following expression,

$$f = 1 - [\frac{R_{AB,CD} - R_{BC,DA}}{R_{AB,CD} + R_{BC,DA}}]^2 \frac{\ln 2}{2} - [\frac{R_{AB,CD} - R_{BC,DA}}{R_{AB,CD} + R_{BC,DA}}]^4 [\frac{(\ln 2)^2}{4} - \frac{(\ln 2)^3}{12}] \qquad (3.4)$$

The conductivities of the samples are found taking the inverse of the calculated resistivities of the samples.

3.6.1.2. Hall mobility measurement

The experiment which will be performed to determine the Hall mobility of the majority carriers(electrons) is carried out into two steps. Firstly, the resistance $R_{AC,DB}$ of the sample is measured with the experimental set-up shown in Fig.3.5a following the procedure given in section 3.6.1.1. In the second step, the same measurements are made to find the resistance $R_{AC,DB}$ placing the sample in a magnetic field having a strength of 8.75 mT and perpendicular to the surface of the sample, Fig.3.5b. The Hall mobility of the carriers is calculated substituting the average resistance difference $\Delta R_{AC,BD}$, which shows the difference between the averaged values of $R_{AC,DB}$ obtained from two different measurements, and the value of resisistivity ρ found in previous section, in the following expression,

$$\mu_H = \frac{d}{B}\frac{\Delta R_{AC,DB}}{\rho} \qquad (3.5)$$

where B is the strength of the applied magnetic field and d is the sample thickness[70].

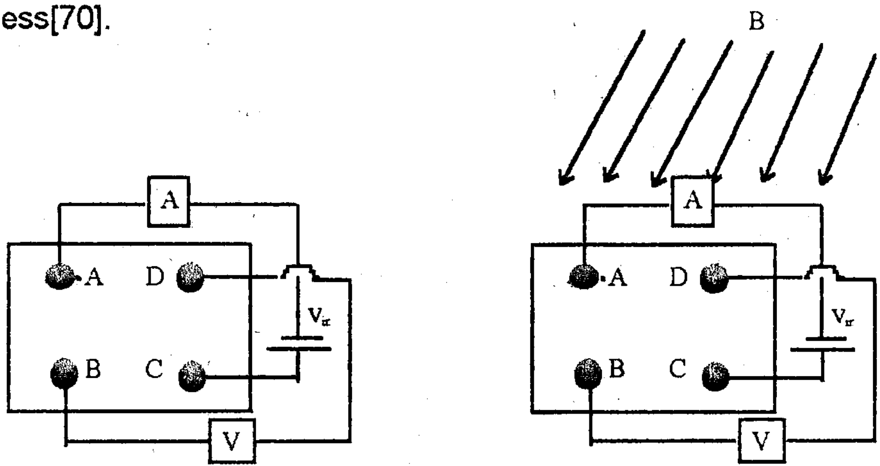

Figure 3.5. The standard configuration used for Hall effect measurements.

3.6.2. Measurements of the transit time of the minority carriers (Haynes-Shockley Experiment)

The drift mobility of the minority carriers in the CdS thin films are usually determined from their measured transit time values. To measure the transit time of the minority carriers a laboratory set-up known as Haynes-Shockley experiment was established as seen in Fig.3.6.

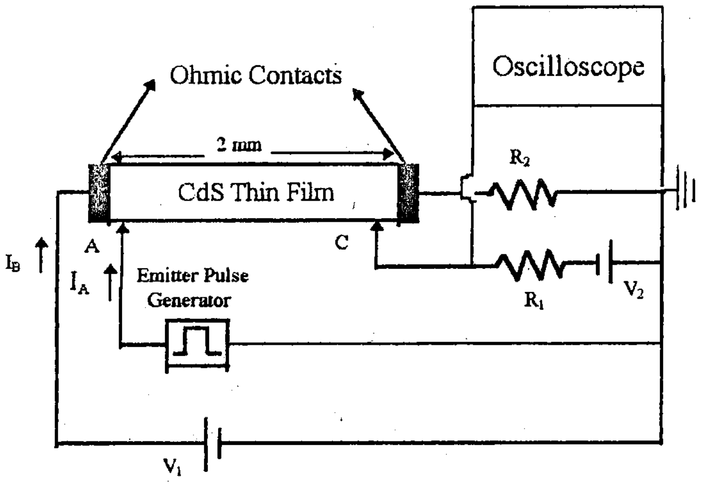

Figure 3.6. Schematic diagram of the circuit used to obtain the transit time measurements.

The CdS thin film samples used in this experiment have length of 2 mm, the ohmic contacts are formed from indium. As seen from this figure, a battery V_1 (50V) is placed in series with the plated contacts so that a direct current I_B, called the sweeping current, flows downward in the CdS thin film in the same direction of the electric field produced by this battery. An emitter pulse generator is placed in series with point A so that a current I_A flows from the point into the CdS thin film making this point an emitter of positive holes. In series with point C is placed the resistance R_1 (30Ω) and a battery V_2 (30V), so that this point is biased negatively with respect to the CdS thin film and act as a collector. The input amplifer of a Gould 4060 Model digital storage oscilloscope, to read the transit time straigth forward from the signal which will display on the screen of the oscilloscope, is connected across the resistance R_1 . At a certain instant of time a positive pulse of current I_A together with the current I_B and flows toward the collector. When these currents arrive at the collector, they produce a measurable signal on the oscilloscope, as in Fig.3.7.

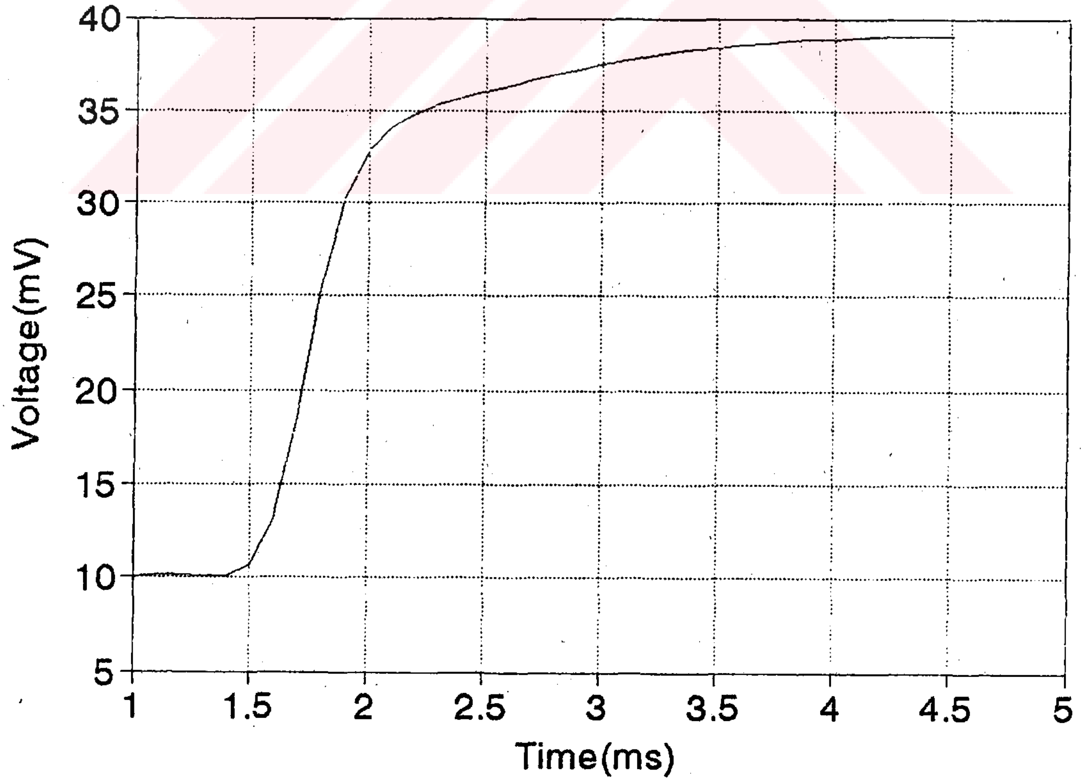

Figure 3.7. Typical trace on the oscilloscope screen (Sample No: A_1).

The transit time value of the minority carriers in each CdS thin film sample has been obtained from the curve which appears on the oscilloscope screen as mentioned above. This transit time is equal to the time needed by the current to reach its maximum value. The minority transit time values read in this way for CdS thin films samples are given in Table 3.5.

Table 3.5: The minority carrier transit time values of various CdS thin film samples.

Sample No	A_1	A_2	A_3	A_4	A_5	A_6	A_7	A_8	A_9
Transit time $(t_r)\mathrm{x}10^{-5}$ sec	4.5	6.8	5.0	5.5	4.6	5.1	4.5	5.4	5.0

3.6.3. Optical Measurements

To determine the band gap energy values of the samples, it is necessary to know the value of the absorption coefficients of the samples corresponding to different wavelengths of the photons. For this purpose, a Jasco 7800 Model Spectrophotometer, operating in a wavelength range 200-1100 nm, was used for the transmission and absorption measurements. Firstly, the transmission values (I/I_0) corresponding to different wavelengths are found for every sample by using the spectrophotometer. Then, the absorption coefficients α of every sample corresponding to different wavelengths are calculated by substituting the thickness of every sample and transmission values (I/I_0) in, the equation below,

$$\alpha = \frac{1}{d}\ln(\frac{I_0}{I}) \qquad (3.6)$$

where d is the optical path length of the sample.

3.6.4. Space Charge Limited Current Measurements

When a sufficiently large field is applied to a crystal with ohmic contacts, electrons will be injected into the material to form a current which is limited by space-charge effects related to trapping centers. When trapping centers are present, they capture many of the injected carriers thus reducing the density of free carriers. The form of the current versus voltage curve in the region of space-charge-injected currents can therefore be used to obtain information about trap densities.

Experimentally, the trap densities in CdS thin film samples are obtained from their I-V characteristic curves. To obtain the I-V characteristic curves of the thin film samples, an experimental set-up was established, this is shown in Figure 3.8.

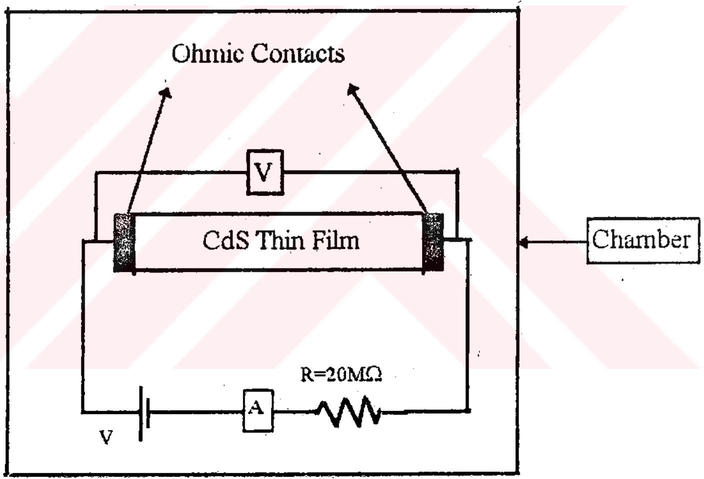

Figure 3.8. Electric circuit used to obtain the I-V characteristics of the CdS thin films.

I-V characteristic curves of the samples are obtained as follows:, a DC power supply (0-50V) is connected in series with a standard resistor (20MΩ) and the sample, as shown in figure. All measurements are carried out in the dark. A potential is applied between the ends of the sample, the supply voltage is varied from 0 to 40 volts in steps 1 volt and the currents corresponding to these voltages are recorded. Using these current and voltage values, I-V characteristic curves of the samples are plotted and V_{TFL}(trap filled limited) voltage values are found from these curves. The density of the traps N_t is obtained by substituting the V_{TFL} values into the expression,

$$eN_t = \frac{\varepsilon}{4\pi}\left(\frac{V_{TFL}}{l^2}\right) \tag{3.7}$$

where l is the electrode spacing and ε the dielectric constant.

3.6.5. Photoconductivity measurements

3.6.5.1. Photoconductivity decay method

Recombination lifetime (τ_r) is one of the best indicators of the total recombination in semiconductors. The photoconductivity decay (PCD) [71,72,73] is a proven and powerful technique to measure carrier lifetime (recombination lifetime) (τ_r) [74-76]. Generally, a single frequency laser pulse strobe lamp is used to excite or generate the excess carriers to increase the conductivity of the semiconductor material. This enhancement of the electrical conductivity under the excitation of light is called the photoconductivity effect. The duration of the strobe light is short compared with the expected lifetime of the charge carriers. Once the light pulse is removed, the excess carriers recombine, returning the sample to a quiescent condition and in the process producing a transient. Depending upon the material quality and the injection level, the transient can involve more than one recombination mechanism including (a) intrinsic radiative band-to-band recombination, (b) intrinsic band-to-band Auger recombination, (c) extrinsic defect-induced Shockley-Read-Hall (SRH), (d) trap-assisted Auger recombination, and (e) surface recombination [77-81]. Since some of these mechanisms are quite sensitive to injection level. A combination of PCD technique and lifetime modeling provides a unique opportunity to not only measure lifetime as a function of injection level but also accurately decouple various recombination mechanisms in order to understand the role of defects and distinguish the material quality [82].

3.6.5.2. Carrier Lifetime Measurements

To measure the excess carrier lifetime in the CdS thin films, a laboratory set-up was established as shown in Fig.3.9. A polished CdS thin film sample having the ohmic contacts on its ends is placed in a circuit as shown in this figure. A constant voltage (100 volt) is applied across the electrodes. A light source emitting periodic bursts of light illuminates the sample and the voltage across the resistor R_s is recorded.

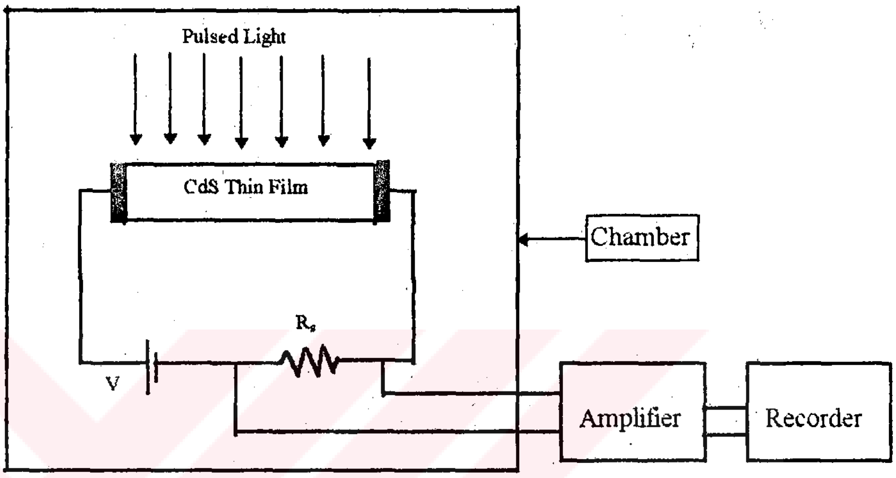

Figure 3.9. A Laboratory set-up for the measurement of lifetime in CdS thin film samples.

The effect of the light burst is to generate excess carriers in the bar, thus increasing the conductivity of the bar and reducing the voltage drop across it. The excess-carrier densities decay according to an $\exp(-t/\tau_r)$ law, resulting in an exponential rise of the voltage across the semiconductor and an exponential decay of the voltage across R_s. The time constant for this exponential can readily be measured and is equal to the recombination lifetime in the semiconductor sample [83].

When the equilibrium number of holes and electrons is disturbed by introducing additional carriers, the lifetime is a measure of the time required for the excess carriers to recombine. Their behaviour in an infinite semiconductor material with no complication is described by

$$-\frac{\partial n}{\partial t} = \frac{\Delta n}{\tau_r} \tag{3.8}$$

where n is the number of carriers present at time t, Δn excess number of carriers and τ_r carrier lifetime. When t=0, a fall in the photoconductivity can be found by integrating formula 3.8.

$$n = \Delta n \exp(-t/\tau_r) \tag{3.9}$$

Relaxation curves describing the fall of photoconductivity in the case of illumination by a square pulse are shown in Fig.3.10.

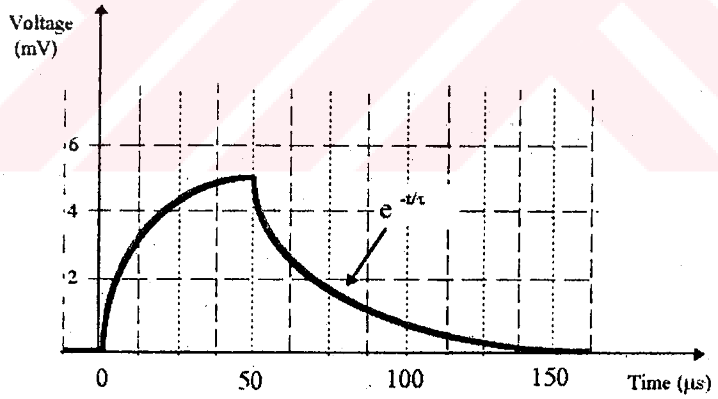

Fig.3.10. Output voltage versus time across the CdS thin film (Sample No:A_1).

The relaxation constant for recombination coincides with the lifetime of carriers and consequently, by the Eq.3.9, it becomes possible to determine experimentally τ_r from the plot of the function [84]

$$\ln\left(\frac{n}{\Delta n}\right) = f(t) \tag{3.10}$$

3.6.5.3. Photocurrent Measurements.

The quantum efficiency η of the CdS thin film samples depending on the wavelength of the photons are determined from the measured values of the photocurrents I_p. To measure the photocurrents, an experimental set-up is established as shown in Fig.3.11. A DC power supply (0-50V) is connected

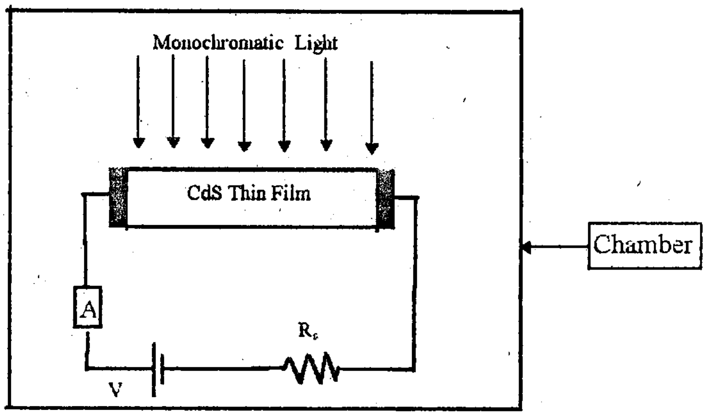

Figure 3.11. Electric circuit used to measure photocurrent of the samples.

in series with a standard resistor R_s (20MΩ). All the measurements are carried out in the dark as follows: Firstly, the voltage is adjusted to zero and alternately the sample is illuminated with monochromatic lights of wavelengths 400, 450, 500, 550, 600, 650 and 700 nm, at the same time the photocurrrents corresponding to these wavelengths are measured. Similar measurements are carried out for the voltages 5, 10, 15, 20, and 25 volts. The quantum efficiency of the CdS thin films is determined substituting the measured value of I_p in the following equation

$$\eta = [\frac{I_p}{e}][\frac{P_{opt}}{h\nu}]^{-1} \qquad (3.11)$$

where P_{opt} is the optical power at a wavelength λ (corresponding to a photon energy $h\nu$).

3.6.5.4. Spectral Response Measurement

The spectral response of CdS thin films is given by the plot of the relative response versus light wavelength. To determine the spectral response of the CdS thin films, a laboratory set- up was established as shown in Fig.3.12. A Jasco 7800 model spectrophotometer is employed to provide monochromatic light beams with different wavelengths and a constant the number of photons. A constant voltage (10 volt) is applied during the measurements. The number of the photons falling on the samples is about 10^{12} photon/cm^2 . The spectral response of every film sample is obtained according to the wavelength of the light, varying from 400 to 800 nm, by recording the output voltage across the sampling resistor R_s.

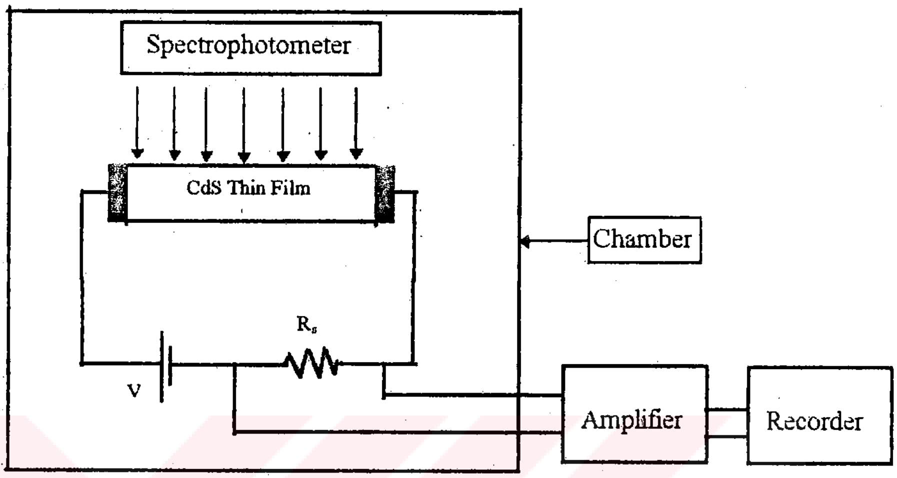

Figure 3.12. Electric circuit used to measure the spectral response of the samples.

3.6.6. Thermoluminescence Measurements

Thermoluminescence measurements of the ZnS thin film samples were performed in three steps: In the first step, the samples are exposed to β-rays emitted from (^{90}Sr-^{90}Y) radioactive source with a rate of 0.04 Gy per second for two hours. Then, these samples are placed into a Harshaw QC-3500 model manual type reader and their glow curves are obtained by increasing the temperature with a rate of 2^0C per second from room temperature to 300^0C. Finally, these glow curves are analysed with a curve fitting computer program. This program uses a linear least square minimisation procedure to determine the trap density, activation energy E_a, and frequency factor s. Two different models are used in the computer program. In the first model, the glow curve is approximated from the first order TL kinetics by the expression,

$$I = n_o s.\exp(-\frac{E_a}{kT})\exp[-\frac{s}{\beta}\frac{kT^2}{E_a}\exp(-\frac{E_a}{kT})(0.9920 - 1.620\frac{kT}{E_a})] \qquad (3.12)$$

where β is heating rate, n_o initial concentration of trapped electrons. Whereas in the second model the glow curve is approximated with the general order TL kinetics by using the expression,

$$I = n_o s.\exp(-\frac{E_a}{kT})[1 + \frac{(b-1)skT^2}{\beta E_a}\exp(-\frac{E_a}{kT})(0.9920 - 1.620\frac{kT}{E_a})]^{\frac{b}{1-b}} \qquad (3.13)$$

In our study, the first model has been used since the glow curves have only one peak.

In the second step, the experiment is carried out to obtain the glow curves of the samples according to the wavelength of the radiation emitted by the samples. This procedure is as following: firstly, the sample is exposed to a radiation as in the first step. Then, the glow curve of the sample, placing the selected filter between the photomultiplier tube and the sample, is obtained as mentioned above. This process is repeated for six filters to obtain six glow curves of the sample. The maximum intensity value is found from each glow curve. Finally, the graph of the intensity of the sample versus wavelength is plotted using these maximum intensity values. The same process is repeated for every sample. The depth of the recombination centers of the samples are found from their graphs.

In the third step, the experiment is carried out to obtain the dose-response graphics of the samples. To do this, firstly, six glow curves are obtained for each sample for six different exposure times 1, 2, 3, 4, 5, and 6 hours. Then, the maximum intensity values are found from these glow curves corresponding to the exposing times. The dose-response graphic of the sample is obtained by plotting the maximum intensity values versus exposure times.

CHAPTER 4

RESULTS AND DISCUSSIONS

4.1. Diffraction Spectra

In this study, the crystallinity of the CdS and ZnS thin film samples developed our laboratory were determined using a Philips X-ray powder diffractometer with monochromated high intensity CuKα radiation (λ=1.5405A^0). Diffraction spectra of all the samples were taken over the range of $20^{0} < 2\theta < 35^{0}$. The diffraction spectra of the samples A_1, A_4, and A_7 that have been developed with the same concentrations (Cd:S=1:1) but at different temperatures 340, 380, and 420 °C, respectively , are shown in the Fig.4.1.

As seen from this figure, the CdS thin films developed at 380 °C substrate temperature have the maximum sharp peak at 2θ = 26.6 degrees, this corresponds to diffraction from (002) plane of the hexagonal phase. The maximum peaks of the other samples A_1 and A_7 developed at temperatures below and above 380 °C, respectively, appear at the same angle, but these are smaller than that of sample A_4. The appearance of the maximum peaks of the samples at the same angle shows that each sample has the same crystal structure. On the other hand, it is well known that as the height of the peak increases the width decreases, and also the grain size of the sample increases. Because of this, sample A_4 has the largest grain size and therefore the highest quality.

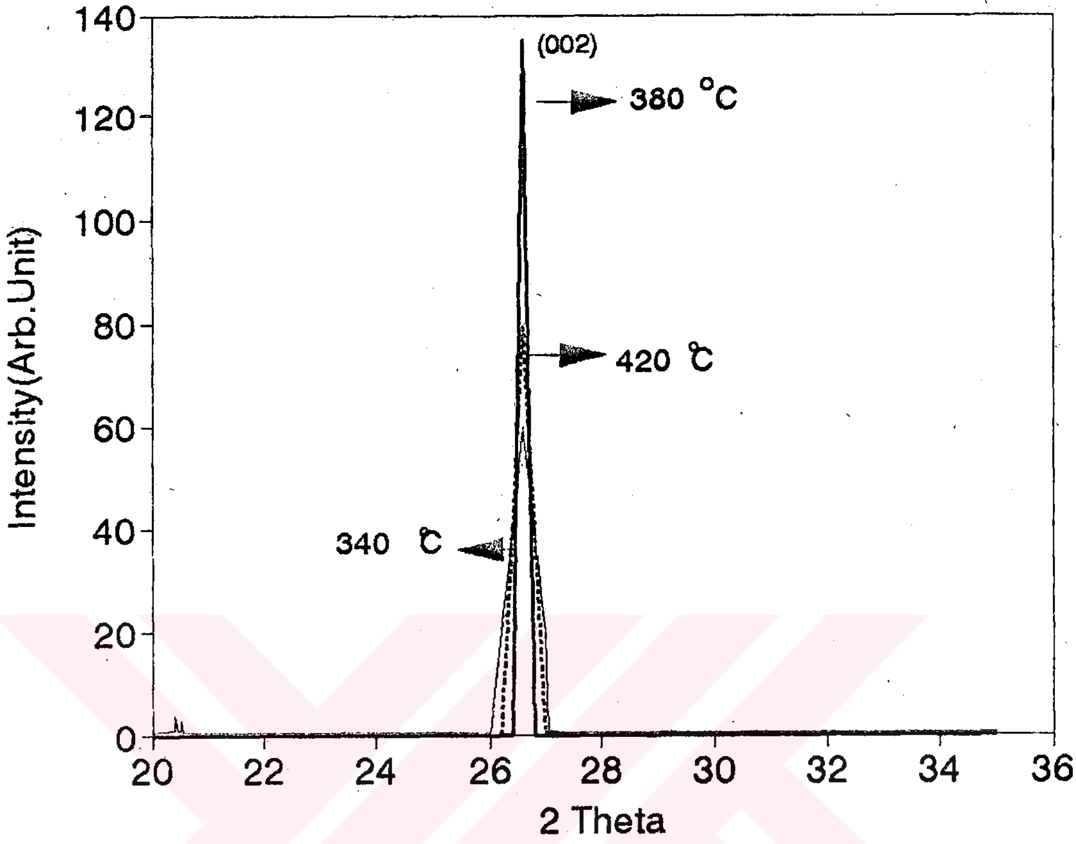

Figure 4.1. X-ray diffraction pattern of the CdS thin film samples A_1, A_4, and A_7.

Similarly, the X-ray spectra of samples A_2, A_5, and A_8, having concentration Cd:S=2:1 and developed at substrate temperatures 340, 380, and 420 °C, respectively, have been obtained. The X-ray spectra of these samples are shown in Fig.4.2. As seen from this figure, the spectra curves of these samples have three peaks. These peaks appear at the same angles in each spectrum at 2θ = 26.6, 25.0, and 27.9 degrees which correspond to diffraction from (002), (100), and (101) planes of the hexagonal phase, respectively. But the samples A_1, A_4, and A_7 have only one peak that, at 2θ=26.6 degrees. This difference is related to the excess cadmium and sulphur since these excess atoms cause new peaks to appear. The difference

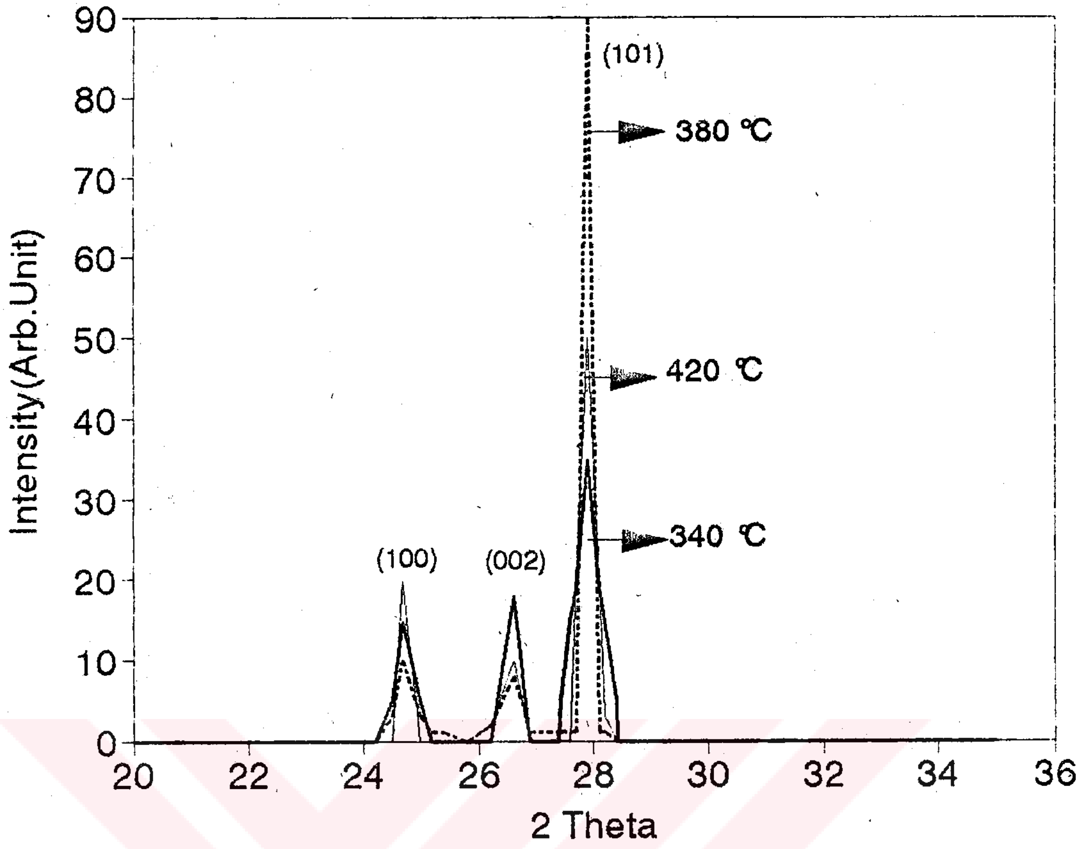

Figure 4.2. X-ray diffraction pattern of the CdS thin film samples A_2, A_5, and A_8.

in the growth planes of the two sample groups is explained with the increasing amount of excess cadmium and sulphur since the excess cadmium and sulphur plays a vital role on the growth of the grain boundaries and grain sizes of the samples. As a result we can say that the best quality CdS thin film sample which has the required crystal structure is developed at 380°C substrate temperature and with a ratio Cd:S of 1:1.

The X-ray spectra curves of the last samples A_3, A_6, and A_9 are shown in Fig. 4.3. These samples have been developed with the concentration Cd:S=1:2 and at the same temperatures as samples (A_1, A_4, and A_7) and (A_2, A_5, and A_8). As seen from this figure, each curve has three peaks each at the same angles 2θ = 26.6, 25.0, and 27.9 degrees which correspond to

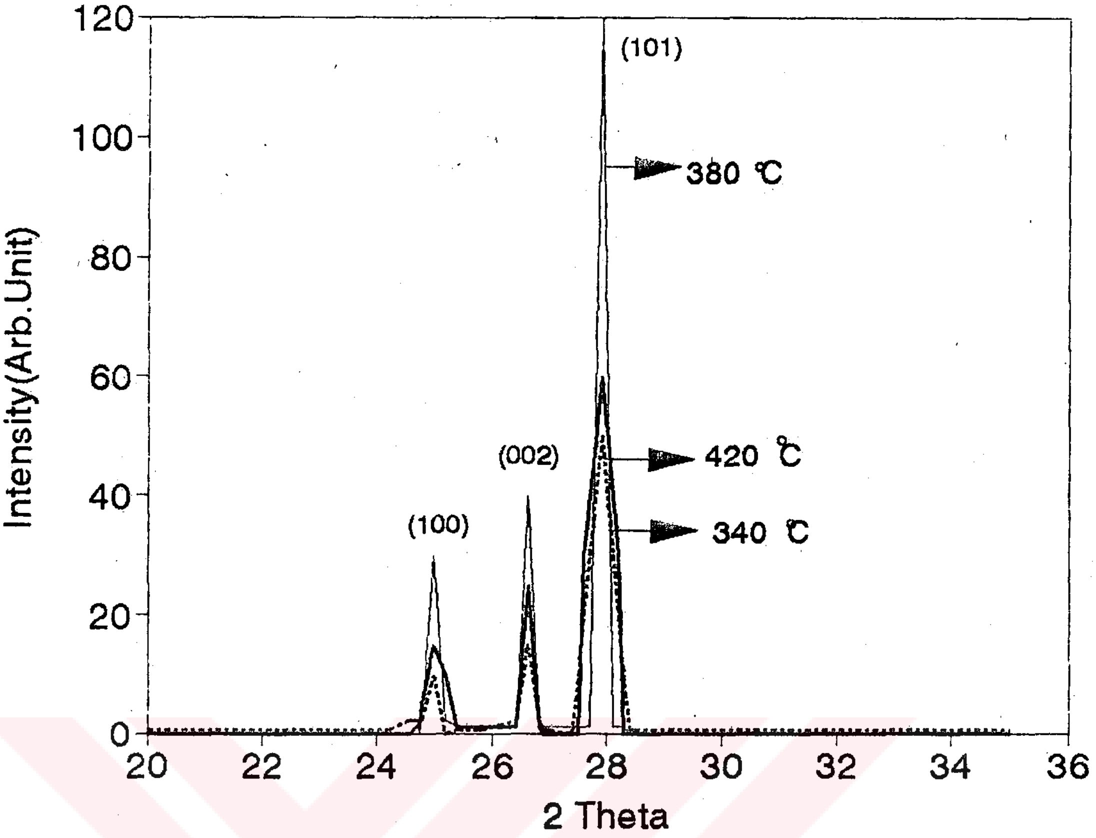

Figure 4.3. X-ray diffraction pattern of the CdS thin film samples A_3, A_6, and A_9.

to diffraction from (002), (100), and (101) planes of the hexagonal phase, respectively. Therefore, there is no difference between the crystal structure of samples (A_3, A_6, and A_9) and (A_2, A_5, and A8), and so the samples included in these two groups are expected to have similar physical properties.

In this study, the other samples that we developed are ZnS thin films. The crystallinity of these samples were investigated from their X-ray spectra. The diffraction spectra of the ZnS thin film samples B_1, B_4, and B_7 are shown in Fig. 4.4. These samples have been developed with the ratio Zn:S=1:1 and at the temperatures 440 , 470 and 500 °C, respectively.

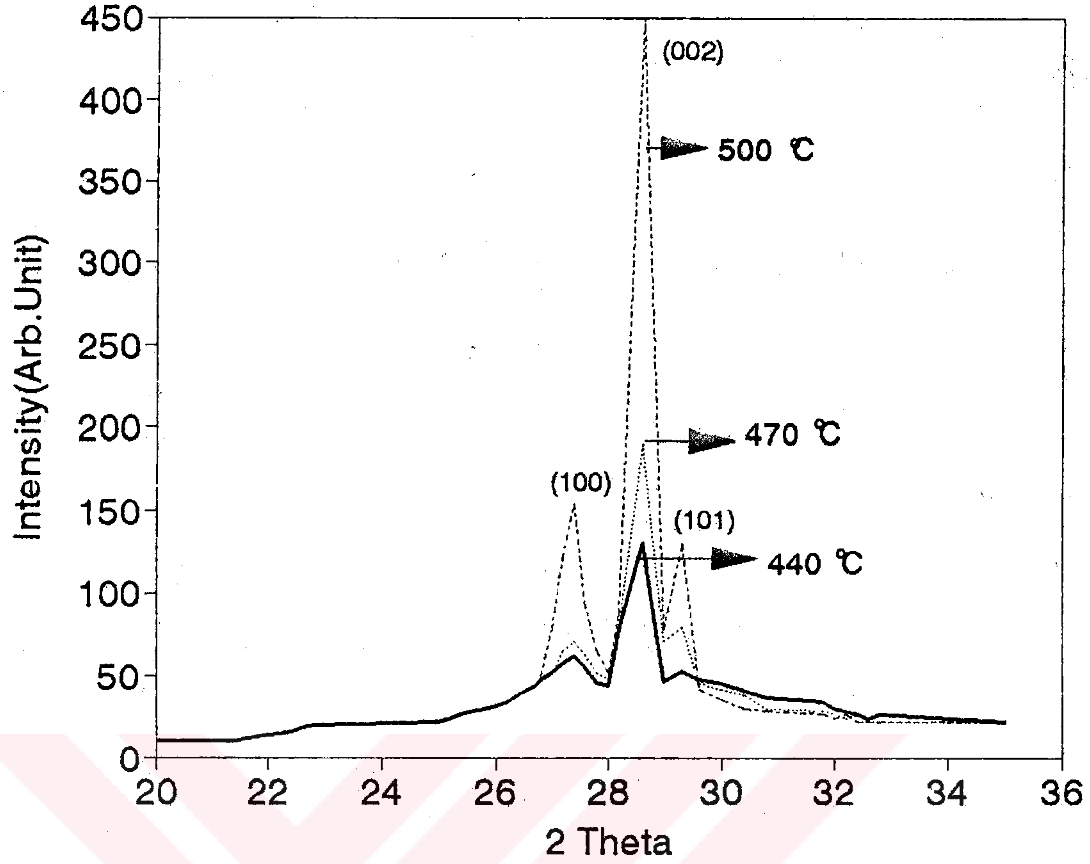

Figure 4.4. X-ray diffraction pattern of the ZnS thin film samples B_1, B_4, and B_7.

As seen from this figure, the dominant peak of each sample is seen at $2\theta=28.6$ degrees and the other peaks at 27.6 and 29.5 degrees. The existance of the peaks at $2\theta=28.6$ shows that the diffraction results from (002) plane of the hexagonal phase . This means that the ZnS thin films have a wurtzite crystal structure. The other peaks resulting from diffractions due to the hex(100) and hex(101) planes also show that the ZnS thin film samples have a wurtzite crystal structure. As seen from this figure, the increase in the heights of the peaks at 27.6 and 29.5 degrees are smaller than the increase in the height of the dominant peak at 28.6 degrees.If only heights of the peaks at 28.6 degree are compared, it is seen that the ZnS thin films developed at 500 °C substrate temperature have the highest and sharpest peaks. This means that the grain size of the samples increases with the increasing substrate temperature. As a result, we can say that the best quality ZnS thin films is developed at 500 ^{0}C substrate temperature and with the ratio of Zn:S =1:1.

The diffraction spectra of B_2, B_5, and B_8 samples which have been developed having the same ratio Zn:S=2:1 and at the same substrate temperatures 440, 470, and 500°C, respectively, are shown in Fig.4.5.

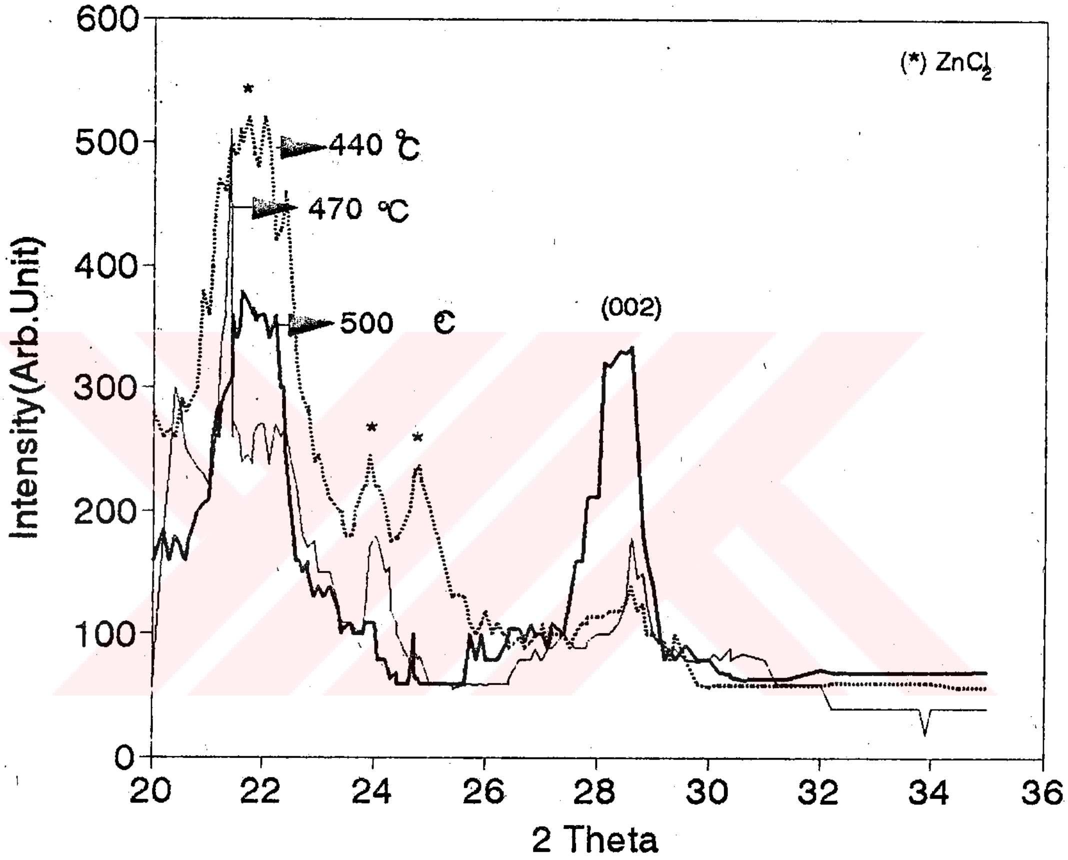

Figure 4.5. X-ray diffraction pattern of the ZnS thin film samples B_2, B_5, and B_8.

As seen from this figure, two main peaks exist at 22.0 and 28.6 degrees. The peak at 22.0 degrees shows that the $ZnCl_2$ crystals are formed during the production of the thin films. It is seen that the formation of the $ZnCl_2$ crystal decreases with the increase of the substrate temperature. This results from the molarity of $ZnCl_2$ being greater than the molarity of thiourea. The second peaks at $2\theta=28.6$ degrees show that the samples have a wurtzite crystal structure as mentioned before. In the X-ray diffraction spectrum of a good quality thin film, the peaks must exist only at $2\theta=28.6$ degrees. As a result, we can say that a good quality ZnS thin film can not be produced using the above Zn to S ratio.

The diffraction spectra of the last samples B_3, B_6, and B_9 that have been developed having the same Zn:S=1:2 at the substrate temperatures of 440, 470, and 500 °C, respectively, are shown in the Fig.4.6.

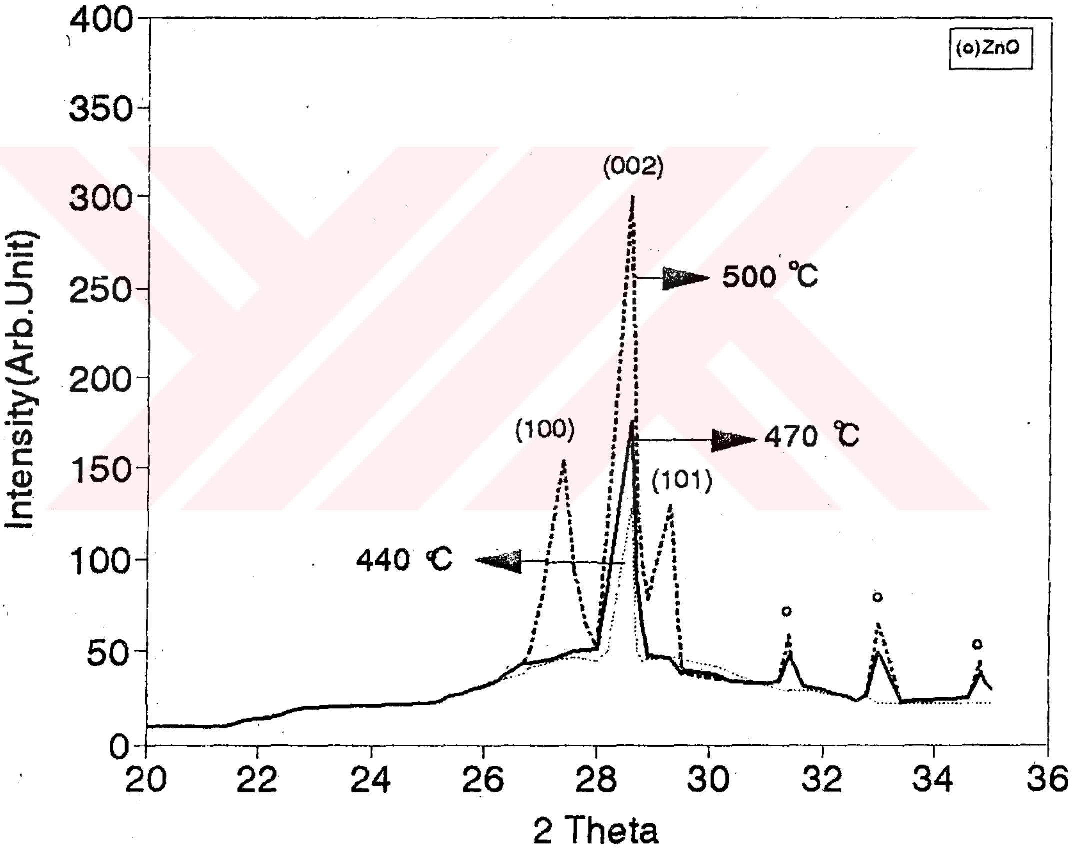

Figure 4.6. X-ray diffraction pattern of the ZnS thin film samples B_3, B_6, and B_9.

As seen from this figure, the spectrum curve of the sample developed at 440°C has only one peak which exists at 28.6 degree. Because of this, it can be said that this sample has the higher quality. On the spectrum curve of the samples four peaks exist at 28.6, 31.4, 33.2, and 35.0 degrees. The peaks at 28.6 degrees show that the wurtzite crystal structure of the ZnS thin films and the other peaks show that these thin films include a certain number of ZnO crystals. These results indicate that chemically deposited ZnS films are very sensitive the chemiabsorbed oxygen which can be converted to ZnO films by air annealing. It can not be said that these samples are of good quality since they include ZnO crystals. In the spectrum curve of the samples developed at 500 °C, six peaks are seen. The first three peaks at 27.6, 28.6, and 29.2 degrees show the wurtzite crystal structure of the ZnS thin films. The other three peaks that appear at 31.4, 33.2, and 35.0 degrees show that these thin films include ZnO crystals as in the samples developed at 470 °C. These two last thin films can attain a good quality by removing the oxygen molecules from the thin films. This can be achieved by heating the samples for about five minutes at 550°C in nitrogen.

4.2. Electrical Properties

The numerical resistivity, conductivity and Hall mobility of the CdS thin films collected in group A were calculated at room temperature using the Van der Pauw method as explained in previous sections. The calculated values of these parameters are given in Table 4.1. Samples A_1, A_4, and A_7 which have been developed with the ratio Cd:S=1:1 and at substrate temperatures 340, 380, and 420^{0}C, respectively, are grouped together in to GROUP-IA. Similarly, samples A_2, A_5, and A_8 and samples A_3, A_6, and A_9 which have been developed with different concentrations (Cd:S=2:1) and (Cd:S=1:2), respectively, and with the same temperatures as the samples developed in the first group form the second(GROUP-IIA) and third(GROUP-IIIA) groups. In Fig.4.7, the dark resistivity and Hall mobility curves represented by solid and dashed lines, respectively, of the samples in GROUP-IA, GROUP-IIA, and GROUP-IIIA are plotted versus substrate temperature using the data given in Table 4.1.

Table 4.1: The calculated values of the resistivity, conductivity and Hall mobility of the CdS thin film samples developed under different conditions.

	Resistivities		Conductivities		Hall mobilities	
Sample No	Dark $\Omega cm x 10^4$	Light $\Omega cm x 10^4$	Dark $1/\Omega cm x 10^{-7}$	Light $1/\Omega cm x 10^{-7}$	Dark $cm^2/V.s$	Light $cm^2/V.s$
A_1	258.0	225.0	3.87	4.44	35.85	62.85
A_2	272.0	242.0	3.67	4.13	11.11	26.54
A_3	298.8	261.5	3.34	3.82	5.10	12.12
A_4	181.0	152.0	5.52	6.57	2.40	7.90
A_5	221.0	192.0	4.52	5.20	1.33	3.38
A_6	198.0	167.0	5.05	5.98	18.9	24.33
A_7	231.5	174.0	4.31	5.74	1.10	2.38
A_8	245.7	221.7	4.07	4.51	1.29	2.65
A_9	228.0	216.6	4.38	4.61	1.27	2.59

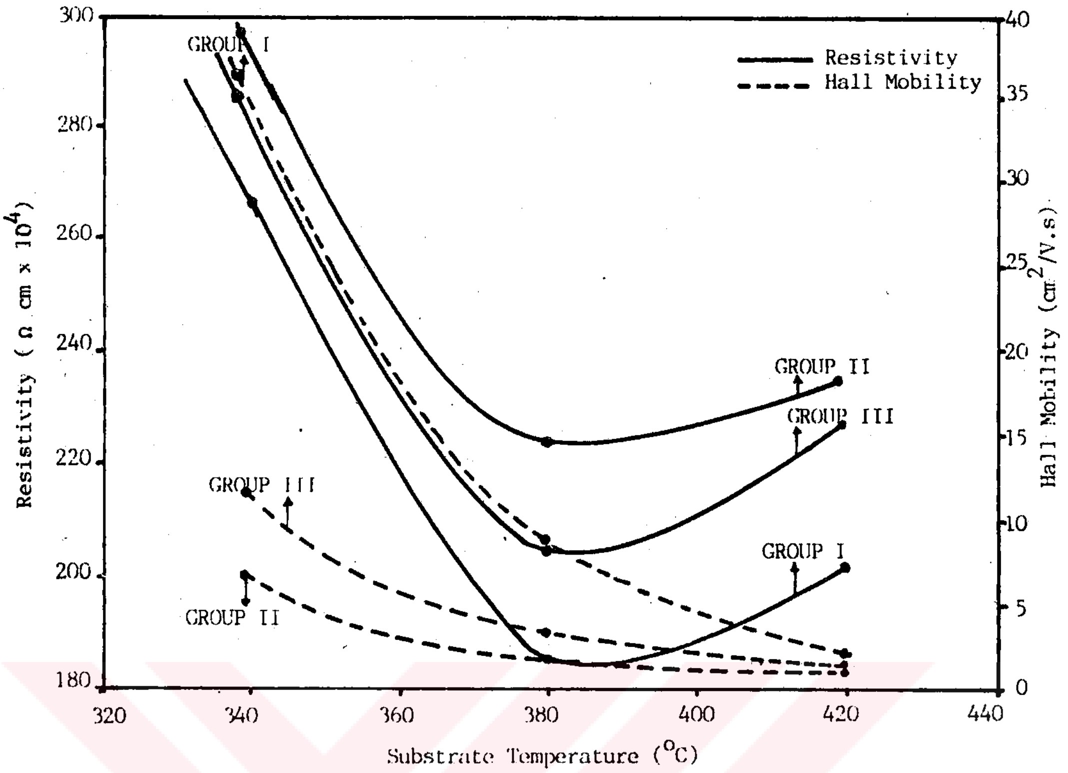

Figure 4.7. Variation of mobilities and resistivities in the dark versus substrate temperature of (300 K) CdS thin film samples in GROUP-IA, GROUP-IIA, and GROUP-IIIA.

As seen from the resistivity curves, the minimum of all these curves are at about 380^{0}C corresponding to samples A_4, A_5, and A_6. The values for these samples taken from Table 4.1 are 181, 221, and 198x 10^4 Ω-cm, respectively. Comparing these values it can be said that sample A_4 has the lowest resistivity. For the Hall mobility curves it is seen that these curves decrease continuously. In theory, they should approximate the form of a bow having a maxima at about 380^{0}C. The fact that the measured curves do not have any maxima can be explained as follows: the resistivity and Hall mobility of the sprayed CdS thin films are very sensitive to adsorbed oxygen since chemisorbed oxygen acts as an acceptor impurity. Because of this, it causes an increase in the resistivity of the thin films but a decrease in the Hall mobility. The increase in the resistivity results from the increase of the potential barrier. This increase in the potential barrier results due to the interaction of the absorbed oxygen with the grain boundaries.

The other important result seen from this figure is that the resistivity, conductivity and Hall mobility of CdS thin films are strongly dependent on the substrate temperature and molarities of $CdCl_2$ and $SC(NH_2)_2$ salts in the spraying solution. As seen from the same figure the samples included in GROUP-IA which were developed using the spraying solution with the ratio Cd:S=1:1, have the lowest resistivity. This situation results from the number of the cadmium and sulphur atoms which provide the crystal structure of the thin film. If the rate of the cadmium and sulphur atoms are equal to each other, all cadmium and sulphur atoms will make covalent bonds with each other. This means that there will be either no free cadmium or sulphur atoms in crystal. If the rate of the atoms differs from the ratio of Cd:S=1:1, there will be free cadmium atoms or sulphur atoms in crystal. The excess cadmium or sulphur atoms in CdS thin films causes the grain sizes to increase. But, excess sulphur atoms have more effective on the growth of the grain sizes than cadmium atoms. It is known that the resistivity of the CdS thin film decreases with increasing grain size. Therefore, the resisitivity of the CdS thin films developed using the ratio Cd:S=1:2 will be smaller than the resistivity of the CdS thin films developed with the ratio Cd:S=2:1. Also, excess cadmium atoms segregate at the grain boundaries and cause the resistivity of the sample to increase. Sulphur atoms do not segregate at the boundaries, but they act as a trap for the carriers together with cadmium atoms increasing the potential barrier at the grain boundaries leading to an additional increase in the resistivity.

To discuss the electrical properties of the ZnS thin films, the resistivity, conductivity and Hall mobility values have been calculated by employing the same methods used for the CdS thin films in the previous section. The calculated values of these parameters for the ZnS thin film samples B_1 to B_9 are given in Table 4.2. As for group B these samples can be collected into

Table 4.2: The calculated values of the resistivity and Hall mobility of the ZnS thin film samples developed under different conditions.

	Resistivities		Conductivities		Hall mobilities	
Sample. No	Dark Ωcmx10^6	Light Ωcmx10^6	Dark 1/Ωcmx10^{-9}	light 1/Ωcmx10^{-9}	Dark cm^2/v.s	Light cm^2/v.s
B_1	1235.0	996.0	0.81	1.0	0.033	0.052
B_2	925.81	757.50	1.08	1.32	0.054	0.077
B_3	695.5	426.52	1.52	2.34	0.076	0.098
B_4	935.0	777.0	1.05	1.28	0.032	0.038
B_5	725.0	612.0	1.37	1.63	0.039	0.047
B_6	525.0	412.0	1.90	2.42	0.046	0.068
B_7	950.7	815.0	1.06	1.22	0.015	0.032
B_8	745.0	658.0	1.34	1.51	0.033	0.045
B_9	552.0	465.0	1.81	2.15	0.038	0.058

three groups. GROUP-IB, GROUP-IIB, and GROUP-IIIB containing the samples(B_1, B_4, and B_7), (B_2, B_5, and B_8), and (B_3, B_6, and B_9), respectively. In Fig.4.8, the dark resistivity and Hall mobility curves represented by solid and dashed lines, respectively, of the samples in GROUP-IB, GROUP-IIB, and GROUP-IIIB, are plotted versus substrate temperature using the data given in Table 4.2. As seen from this figure, each resistivity curve has minimum value at 470^{0}C corresponding to samples B_4, B_5, and B_6. The Hall mobility curves of GROUP-IB and GROUP-IIIB decrease continuously. In theory, they should approximate the form of a bow having a maxima at 470^{0}C. However, the measured curves do not have any maxima. The Hall mobility curve (GROUP-IIB) is different from the others having a shape which is in agreement with the results given in literatures. The form of the measured resistivity and Hall mobility curves of the samples can be explained as follows: the resistivity and Hall mobilities of the sprayed ZnS thin films are more sensitive to adsorbed oxygen than CdS thin films. But there is no difference between the absorption mechanism of oxygen in these two thin films. The adsorbed oxygen increases the height of the potential barrier at the boundaries. Because of this, the Hall mobility of the samples decreases while

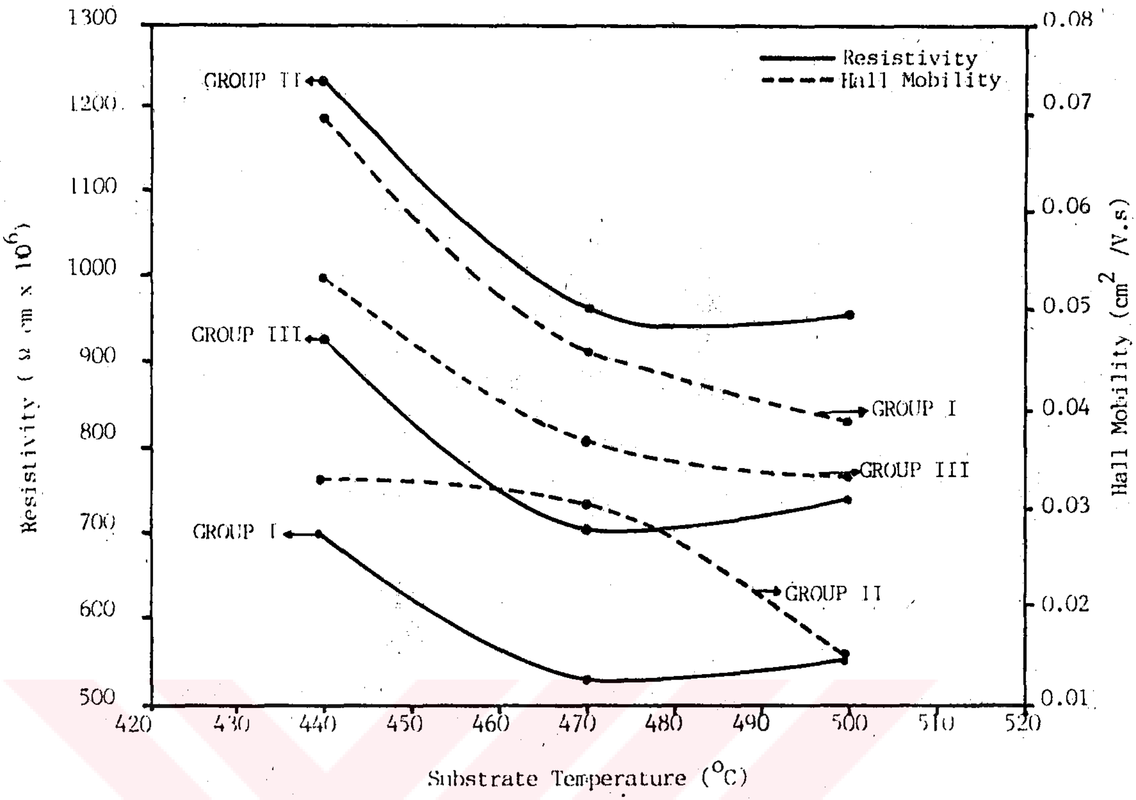

Figure 4.8. Variation of mobilities and resistivities in the dark versus substrate temperature of (300 K) ZnS thin film samples in GROUP-IB, GROUP-IIB, and GROUP-IIIB.

their resistivities increase.

The other important property of these samples, which can be obtained from these curves, is that the resistivity and Hall mobility of ZnS thin films are strongly dependent on the substrate temperature and concentration of $ZnCl_2$ and $SC(NH_2)_2$ salts in spraying solution. As seen from this figure, the samples included in GROUP-IB which were developed using the spraying solution with a ratio of Zn:S=1:1, have the lowest resistivity. This results from the number of the zinc and sulphur atoms which provide the crystal structure of the thin film. If the rate of the zinc and sulphur atoms are equal to each other, all zinc and sulphur atoms will make covalent bonds with each other. This means that there will be no free zinc or sulphur atoms in crystal. The excess zinc or sulphur atoms in ZnS thin films increases the grain sizes. But, excess sulphur atoms have a greater effect on the growth of the grain sizes than zinc atoms. As mentioned above the resistivity of the CdS thin film decreases with increasing grain size. This is also true for ZnS thin films. But, zinc atoms are much more effective than cadmium atoms at forming grain boundaries. Therefore, the resisitivity of the ZnS thin films developed using the ratio Zn:S=1:2 will be smaller than the resistivity of the ZnS thin films developed with the ratio Zn:S=2:1. Also, excess zinc atoms segregate at the grain boundaries as do cadmium atoms in CdS thin films. This causes the resistivity of the sample to increase much more. Sulphur atoms do not segregate at the boundaries, but they act as a trap for the carriers at the grain boundaries, as for cadmium atoms, increasing the potential barrier at the grain boundaries.

4.3. Sample Thickness

To investigate the relationship between the resistivity and the thickness of the CdS thin films, and also the relationship between their Hall mobilities and thicknesses, three 'A_1' samples with different thicknesses were developed. The resistivity and Hall mobility curves of these samples are plotted in Fig.4.9 versus the sample thickness. As seen from this figure, the resistivity decreases as the thickness of the sample increases. This is the expected result. The Hall mobility of the samples increases with the increasing thickness of the samples. It is suggested that the observed changes in mobility and resistivity may be a consequence of the variation of the chemisorption effect and due to the production of sulphur vacancies during the deposition which is associated with changes in the grain size with film thickness. The role of the excess cadmium and sulphur on the value of the resistivity and Hall mobilities has been explained before. The other factor that effects these two parameters is the carrier concentration. Excess cadmium and sulphur are incorporated in sprayed CdS films by varying solution composition. In the Cd-rich sprayed films, the donors are to be associated with excess Cd atoms. Thus, the excess cadmium increases the carrier concentrations in the thin film, and as a result of this, the inter-grain

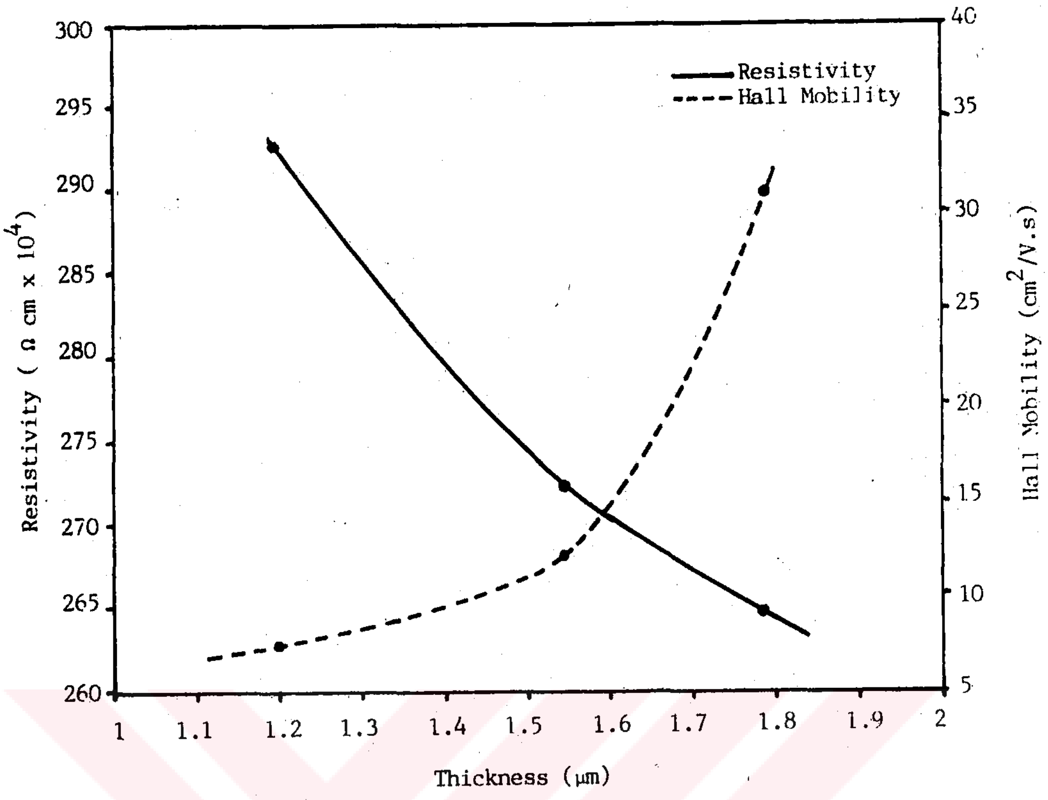

Figure 4.9. Variation in the resisitvity and Hall mobility (measured at 300 K and in the dark) of chemically sprayed CdS thin film samples with the thickness (Deposition temperature 340 °C).

barrier heights are reduced. When the inter-grain barrier heights reduce, the resistivity of the thin film decreases while Hall mobility increases, as seen in the figure. The carrier concentration of the film increases since the excess sulphur acts as an acceptor. Hence, it can be said that excess sulphur acts as a factor that decrease the resistivity of thin films while increasing the Hall mobility. Similarly, the resistivity and Hall mobility curves were obtained as for the other CdS thin film samples.

To investigate the relationship between the resistivity and the thickness of the ZnS thin films, and also the relationship between their Hall mobilities and thicknesses, three B_1 samples with different thicknesses were developed. The resistivity and Hall mobility curves of these samples are plotted in Fig.4.10 versus the sample thickness. As seen from this figure, the

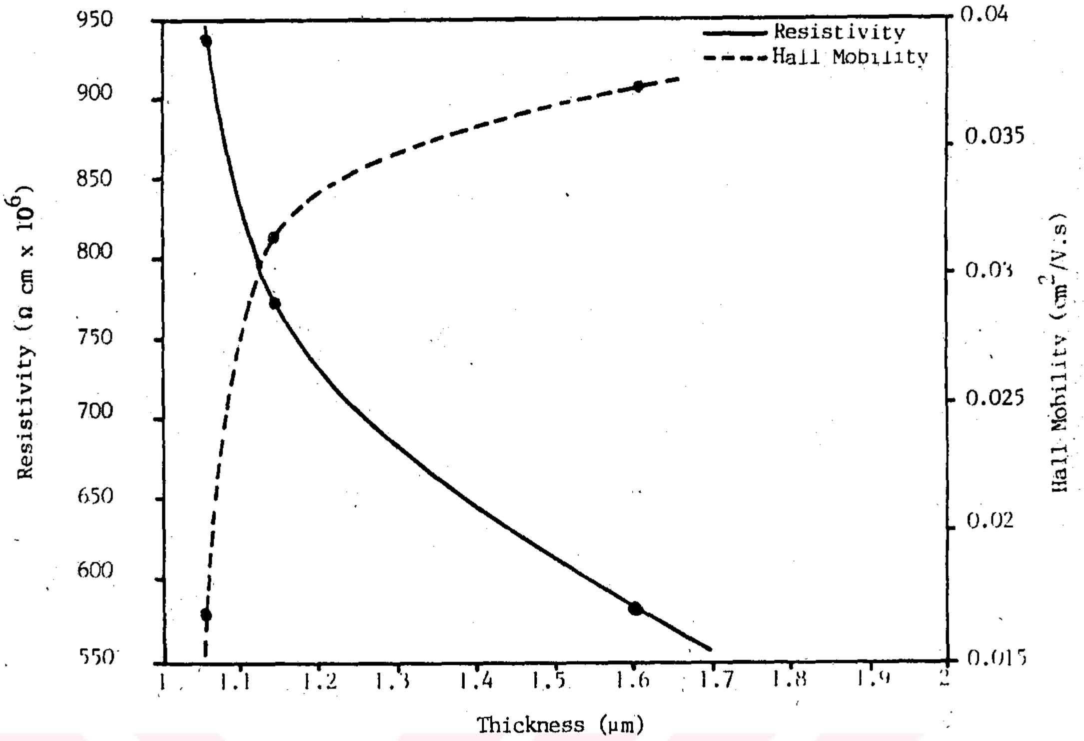

Figure 4.10. Variation in the resisitvity and Hall mobility (measured at 300 K and in the dark) of chemically sprayed ZnS thin film samples with the thickness (Deposition temperature 440 °C).

resistivity of the ZnS thin film decreases and Hall mobility of the thin film increases with the increasing thickness. This is the expected result because excess zinc acts as a donor in ZnS thin films, as does excess cadmium in CdS thin films. But, there is a difference between the resistivity and Hall mobility values of these two thin films. The resistivity values of ZnS thin films is approximately 350 times greater than the resistivity values of the CdS thin films. This again is the expected result. As it is explained in previous sections, excess zinc causes an increase in the grain boundaries much more than cadmium. Because of this , there is a greater difference between the resistivity values of these thin film samples. On the other hand, it is seen from the comparison of Hall mobilities of these two thin film samples that the Hall mobility of CdS thin films is nearly 220 greater than Hall mobility of ZnS thin films. This results from the difference between the band gap energy of these thin film samples since the resistivity of the sample increases with the band gap. Because of this, the Hall mobility of the CdS thin film samples must be greater than the Hall mobility of the ZnS thin film samples.

4.4. Optical Bandgap

The other important part of this study is to determine the optical band gap of the CdS and ZnS thin films. As an example, a curve which was obtained plotting the linear extrapolation of $(\alpha h\nu)^2$ versus $h\nu$ for sample A_1 is given in Fig.4.11. The values of the absorption coefficients of the samples which are used for plotting the extrapolation curves have been calculated as explained in Sec.3.6.3. This curve is described by Eq.2.91. The value of the energy band gap of the sample is evaluated from this curve drawing a tangent line to the curve, as seen in this figure. The crossing point of tangent line on the $h\nu$ axis is equal to the band gap energy E_g of the sample. As seen from this figure, there is negligible absorption at long wavelengths ($h\nu$ small) and considerable absorption of wavelengths shorter than hc/E_g (where c is the speed of the light). In most cases the onset of band gap absorption is sharp, and a reasonable measurement of E_g can be obtained for wide band gap semiconductors. There appears to be two regions, A and B. Region B, the exponential part, is called the Urbach edge ($10^2 < \alpha < 10^4$), and region A, the weak absorption tail ($\alpha < 10^2$ cm^{-1}), is ascribed optical excitation from defect states deep in the gap. There is no sharp delineation between these two overlapping regions.

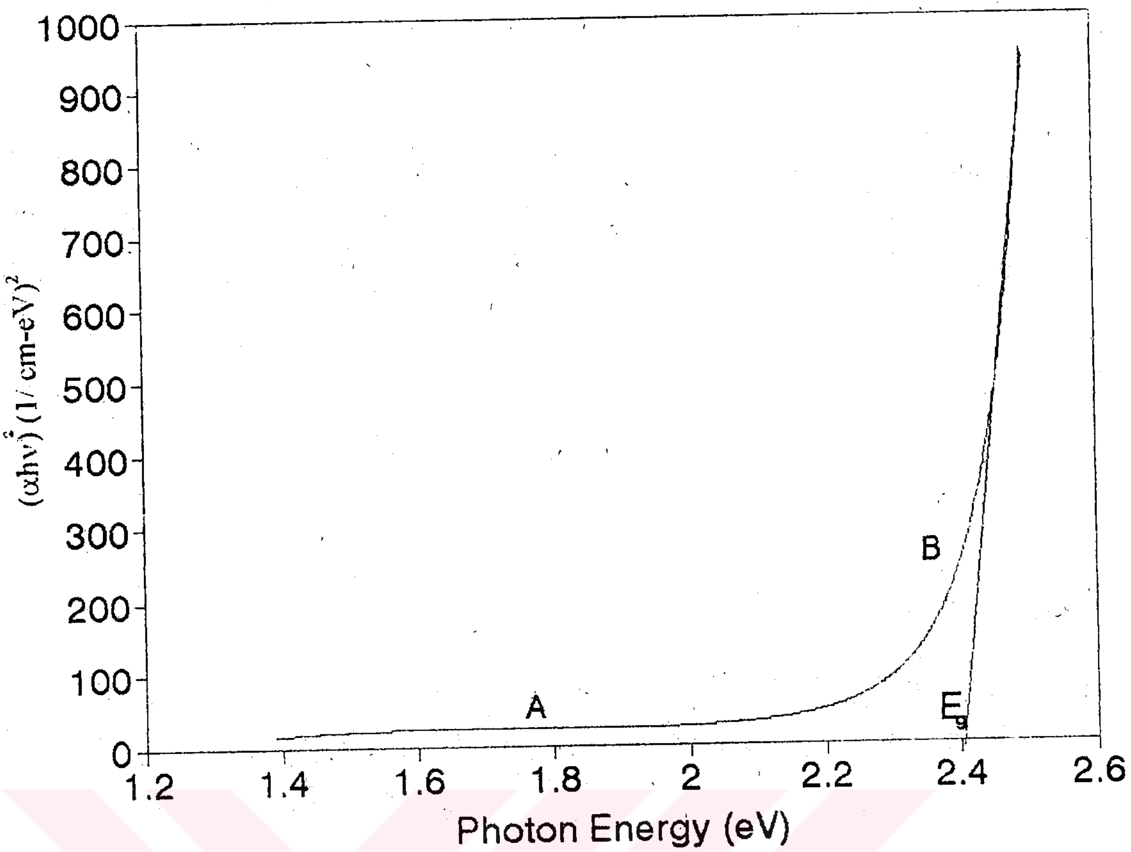

Figure 4.11. Plot of $(\alpha h\nu)^2$ against photon energy ($h\nu$) for sprayed CdS thin film (Sample No:A_1)

Similarly, the band gap energy of every CdS and ZnS thin film sample has been evaluated as explained above, the results are listed, in Table 4.3.

Table 4.3: Energy band values of various CdS and ZnS thin film samples.

CdS thin film Sample No	Band gap energy of CdS thin film(eV)	ZnS thin film Sample No	Band gap energy of ZnS thin film(eV)
A_1	2.40	B_1	3.66
A_2	2.39	B_2	3.66
A_3	2.41	B_3	3.67
A_4	2.40	B_4	3.70
A_5	2.42	B_5	3.70
A_6	2.38	B_6	3.72
A_7	2.44	B_7	3.70
A_8	2.36	B_8	3.66
A_9	2.42	B_9	3.68

As seen from this table, the band gap energy values for the CdS thin films vary from 2.36 to 2.44 eV and the average band gap energy is found to be 2.4 eV. This means that the threshold energy for photon absorption by CdS at room temperature is at about 2.4 eV. Since a 1 eV photon has a wavelength of 1.24 μm, this absorption threshold in CdS is at a wavelength of approximately 520 nm which is in the green region of the visible spectrum. Wavelengths shorter than about 520 nm are strongly absorbed by CdS, while longer wavelengths (yellow,red) are transmitted as explained above. Therefore, CdS thin film appears yellowish-orange by transmitted light.

Again, it is seen from the same table, the range of the band gap energy of the ZnS thin films varies from 3.66 to 3.72 eV. The calculated average band gap energy of ZnS thin films is 3.68 eV. This means that the threshold energy for photon absorption by ZnS at room temperature is at about 3.68 eV. This absorption threshold in ZnS is at a wavelength of approximately 338 nm, which is in the ultraviolet region. Because of this, ZnS thin films are transparent to all visible and infrared photons.

It is known that the changes in the concentrations of the salts and substrate temperatures do not have any effect on the band gap energies of the samples. The small differences between the band gap energy values of the ZnS samples are considered to be due to experimental error.

4.5. Drift Mobility

The drift mobility of the CdS thin film samples has been calculated substituting the measured values of the transit time of these samples obtained from Haynes-Shockley experiment in Eq.2.42. The transit time and the calculated drift mobility values of the CdS thin film samples are given in Table 4.4. The drift mobility curves plotted versus substrate temperature, using the drift mobility values of the samples GROUP-IA, GROUP-IIA, and GROUP-IIIA developed at different substrate temperatures 340, 380, and 420^{0}C, respectively, are seen in Fig.4.12. As seen from this figure, the shapes

Table 4.4: The transit time and drift mobility values of CdS thin film samples.

CdS thin Film Sample No	A_1	A_2	A_3	A_4	A_5	A_6	A_7	A_8	A_9
Transit Time (t_r) (10^{-3})xsec	4.5	6.8	5.0	5.5	4.6	5.1	4.5	5.4	5.0
Drift Mobility cm^2/V.s x10^{-2}	74	69.4	66	60	72.4	65.3	74	58	66

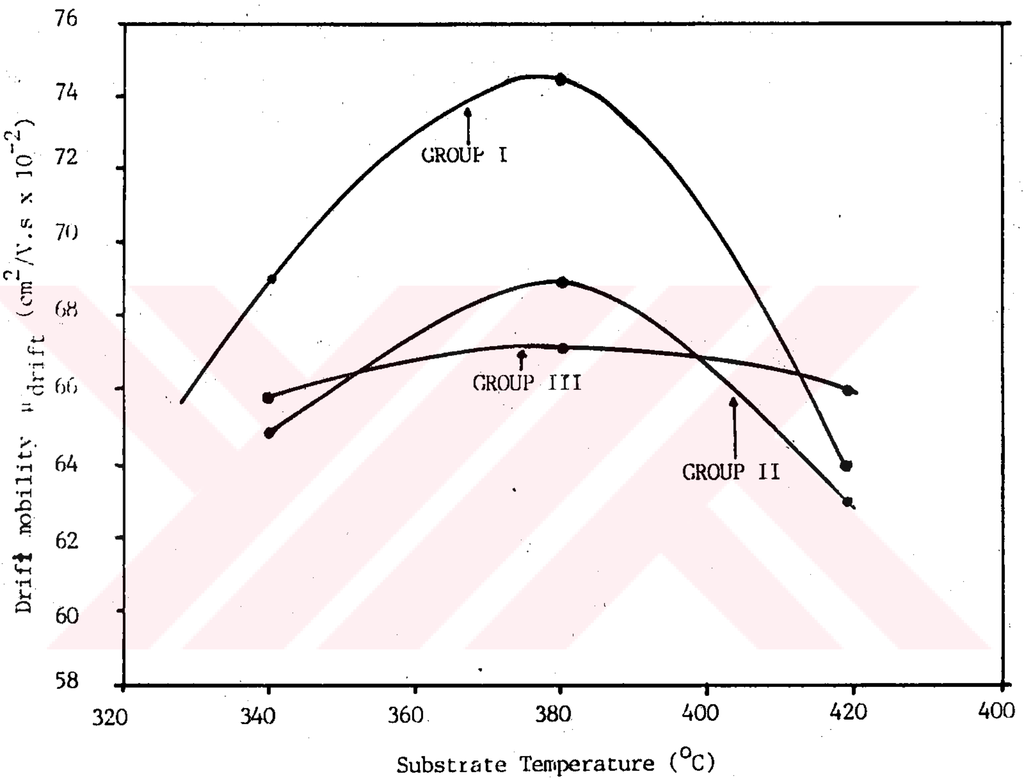

Figure 4.12. (a)The drift mobility curve obtained for GROUP-IA Cd:S=1:1, (b) for GROUP-IIA Cd:S=2:1, (c) for GROUP-IIIA Cd:S=1:2 , versus substrate temperature.

of these curves are in good agreement with theory. The drift mobility of the samples A_1, A_4, and A_7 are greater than the drift mobility of the other samples in GROUP-IIA and GROUP-IIIA and also A_4 has the largest drift mobility. If these results are compared with the drift mobility values of the samples developed under conditions of no oxygen (in a vacuum) they would have lower drift mobility values. This results from the oxygen molecules absorbed on the CdS thin film surface. These absorbed oxygen molecules create surface scattering centers and these scattering centers provide an additional potential causing the height of the electrostatic potential barrier in thin film to increase. As a result of this, the arrival time of the signal that travels from emitter to collector increases. This increase in the arrival time of the signal causes the drift mobility to decrease. Similar discussions can be given for the other samples.

4.6 Trap Density

The trap density of the CdS thin film samples is calculated by substituting the values of the V_{TFL} (trap filled limited voltage) found from their current-voltage curves in Eq.3.7. CdS thin film sample A_1 has been chosen as an example to show how the trap density of a thin film is obtained. Firstly, the I-V characteristic curve of A_1 sample is plotted, Fig.4.13. As seen from this

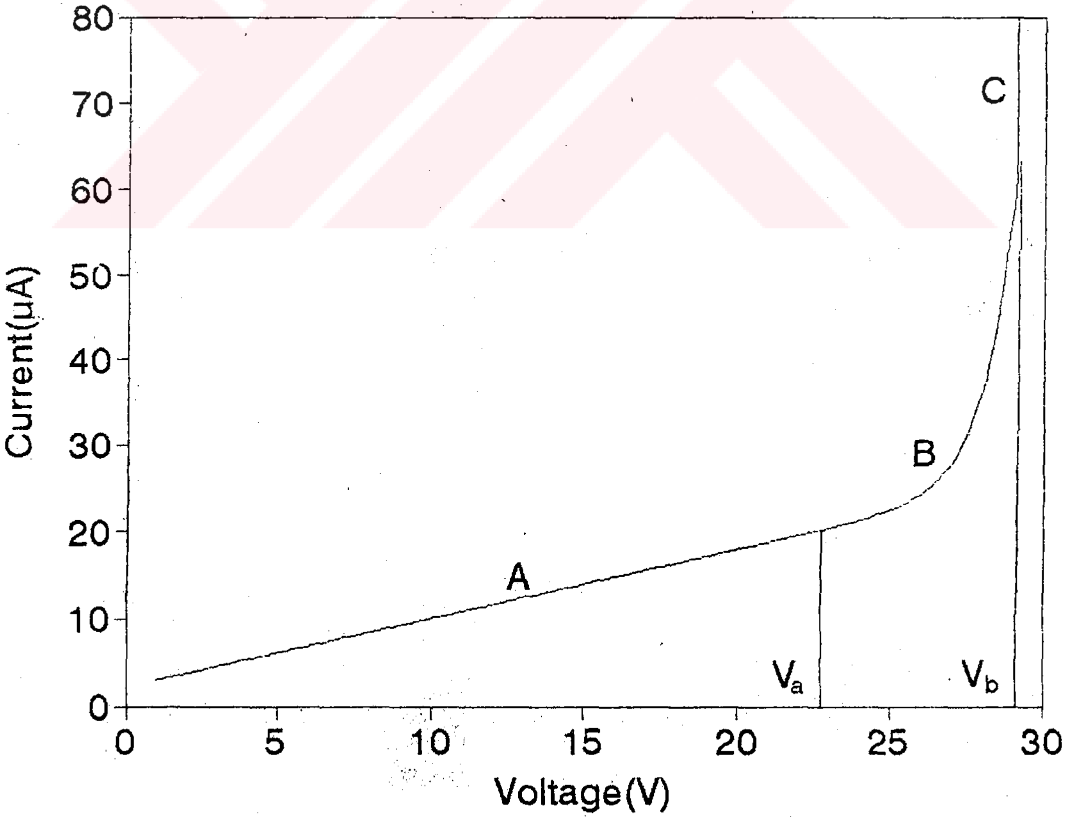

Figure 4.13. I-V characteristic curve of the CdS thin film sample A_1.

figure, the curve possesses the general characteristics predicted by the Rose-Lambert theory. The region marked A corresponds to low applied voltages where there is negligible injection of excess carriers into the thin films, and Ohm' s law holds. In region B, above a voltage V_a, the injected carrier density becomes comparable with the initially present thermal equilibrium. The current becomes space-charge limited and between V_a and V_b follows a V^2 law. The excess carrier density increases proportionally with the applied voltage and steady state Fermi level moves toward the conduction band. Region C represents voltages above V_b where the traps are completely filled. Voltage V_b is called the trap filled limited (TFL) voltage. It is concluded therefore that the steep increase in current in a space charge limited current measurement is attributed to the completion of trap filling by the injected carriers. The values of trap concentrations N_t of the other samples are computed from Eq. 3.7 in the same way. The V_{TFL} values obtained from I-V characteristics and the calculated trap concentrations of the CdS thin film samples are given in Table 4.5. As seen from this table, the trap density values of A_1, A_2, and A_3 increase from A_1 to A_3. A similar increase is seen in the trap density values of the other samples from A_4 to A_6 and from A_7 to A_9. The increase in these trap density values is caused by the excess cadmium and sulphur. The trap density values corresponding to the samples A_1 to A_9 vary between 2.35×10^{12} and 3.32×10^{12} cm^{-3}. As seen from these values, the sample developed at 340 ^{0}C has the lowest trap density and the last sample developed at 420 ^{0}C has the highest trap density. This shows that the trap

Table 4.5: The values of the trap-filling voltage and trap concentrations of the CdS thin films.

Sample No	A_1	A_2	A_3	A_4	A_5	A_6	A_7	A_8	A_9
V_{TFL} (volt)	29	32	34	35	36	38	36	38	41
Trap Density $cm^{-3}(x10^{12})$	2.35	2.59	2.76	2.89	2.92	3.08	2.92	3.08	3.32

density of the CdS thin films increases with the temperature at which the samples are developed. Increase in temperature also increases the chemiabsorbed oxygen that produces new traps at the grain boundaries on the CdS thin film surface.

4.7. Carrier Lifetime

The excess carrier lifetime of the CdS thin films can be obtained from the output voltage signal which displays on the oscilloscope screen as explained in section 3.6.5.2. As explained in that section, the voltage versus time curves of all CdS thin film samples were obtained. These curves fit to Equ. 3.10. Because of this, to find the carrier lifetime of the samples, the curves were replotted with a logV scale. The curve obtained from this graph is a straight line. As an example, the graph of logV of sample A_1 is given in Fig.4.14. The inverse of the slope of this line shows the excess carrier

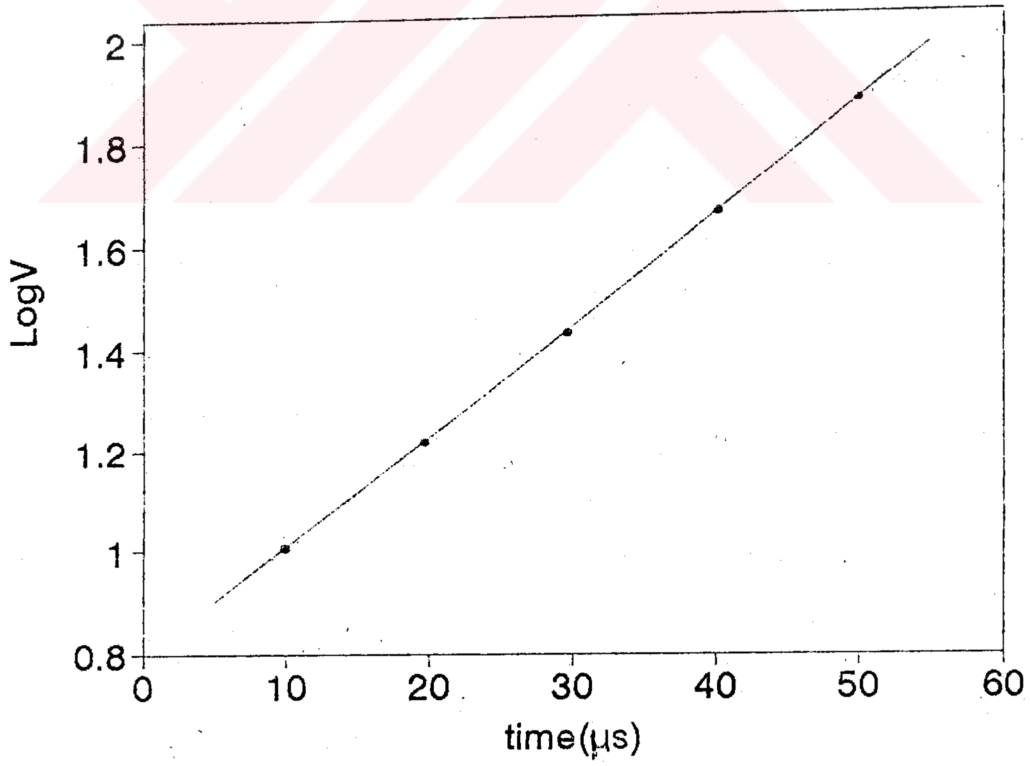

Figure 4.14. Replot of Fig.3.10 using a log scale for the voltage.

lifetime τ in the sample. Similarly, the excess carrier lifetimes of the other samples have been determined and these values are listed in Table 4.6.

Table 4.6: The carrier lifetime values of the CdS thin films.

Sample No	A_1	A_2	A_3	A_4	A_5	A_6	A_7	A_8	A_9
Carrier Lifetime (μs)	45	43	49	42	38	40	44	43	45

As seen from this table, the values of the carrier lifetime of the CdS thin film samples are more or less equal to each other. As a result, it can be said that neither temperature nor concentration of the salts have an affect on the excess carrier lifetime. On the other hand, the values found for the samples are one thousand times greater than the values given in literature. There are two possible reasons for this result: (a)-the presence of the chemiabsorbed oxygen molecules on the CdS surface provides an additional potential that causes the electrostatic potential barrier at the grain boundaries to increase, (b)- the recombination mechanism, as well as recombination at deeper levels. Finally, if these results are compared with the minority carrier lifetimes of the films, it is seen that excess carrier lifetime is smaller than the minority carrier lifetime. This situation is explained by the density of free carriers being much smaller than the density of recombination centers.

4.8. Quantum Efficiency and Spectral Response

The quantum efficiency of each CdS thin film sample according to the wavelength was calculated by substituting the values of the photocurrent (I_p) and intensity of the light falling onto sample (P_{opt}), obtained from the measurements for different input voltages, in to Eq.3.11 as described in Sec. 3.6.5.3. The quantum efficiency graphics of CdS thin film samples A_1, A_4, and A_7 including curves which are obtained for six different applied voltages are shown in Fig.4.15a, b, and c, respectively. As seen from these three graphics, all the curves reach a maximum at 500 nm. This is the expected result because these samples, as explained before, are sensitive to the photons in the wavelength range 500-550 nm. Also, as seen from the graphics, the quantum efficiency of the sample A_4 developed at 380 ^{0}C is greater than the quantum efficiencies of the samples A_1 and A_7 developed at 340 and 420 ^{0}C, respectively. The reason is that sample A_4 has a higher quality crystal structure than samples A_1 and A_7.

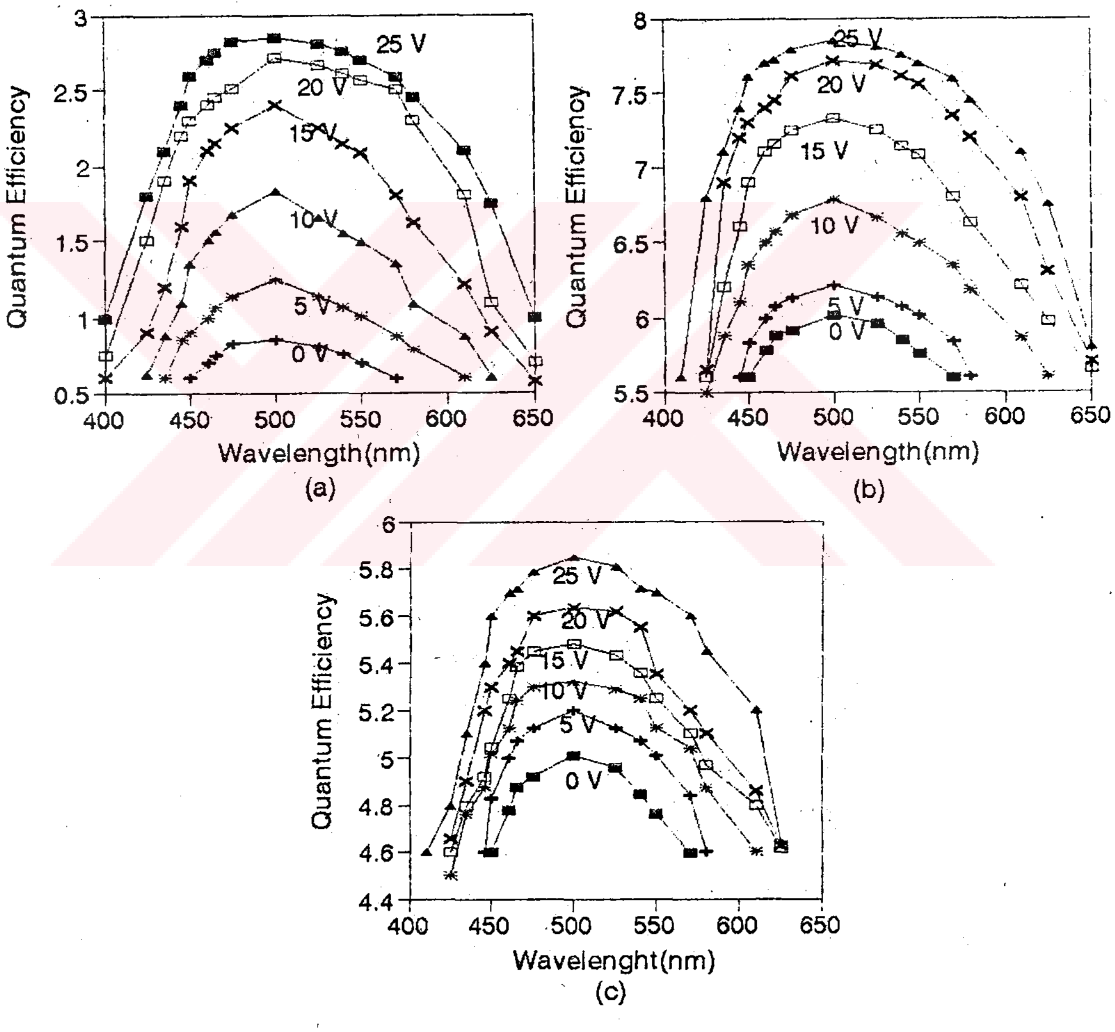

Figure 4.15. Spectral response of quantum efficiency graphics of CdS thin film sample (a)A_1, (b) A_4, and (c) A_7.

It is very important to know the spectral response of the CdS thin films, especially in their industrial applications. In this study, to discuss the physical properties of the spectral response of various samples, the spectral response curve of sample A_1 is examined as an example. The spectral response curve of this sample obtained as mentioned in Sec.3.6.5.4 is shown in Fig.4.16.

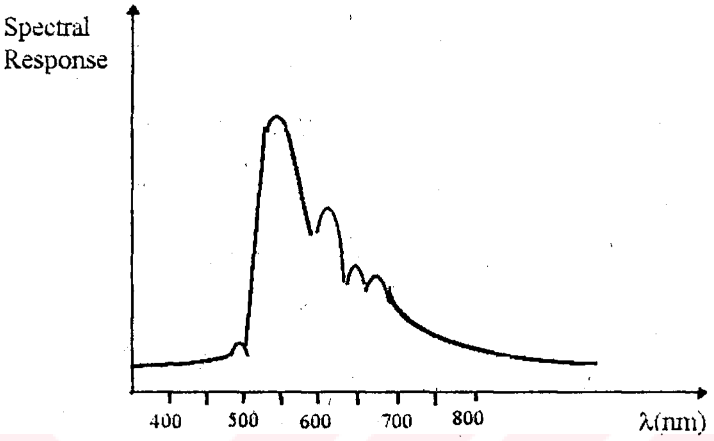

Figure 4.16. Spectral response of CdS thin film Sample No:A_1.

From this figure, it is seen that the CdS thin film sample A_1 is most sensitive to 550 nm (yellow-green), thereby closely matching the spectral response of the human eye. Also, it was seen that all the other samples are most sensitive to the same wavelength of the light. Thus, CdS thin film samples may be used effectively in light measuring applications or as a photodetector for incandescent, fluorescent, or neon light sources in the wavelength range 500-550 nm.

4.9. Thermoluminescence Properties

Finally, we studied the thermoluminescence properties of the ZnS thin film samples. Firstly, the physical properties of nine ZnS thin film samples, such as the trap concentration, activation energy, and frequency factors, were determined from the glow curves of these samples obtained by following the procedure explained in Sec.3.6.6. The glow curves of these samples are given in Fig.4.17. As seen from this figure, every curve has a maximum at

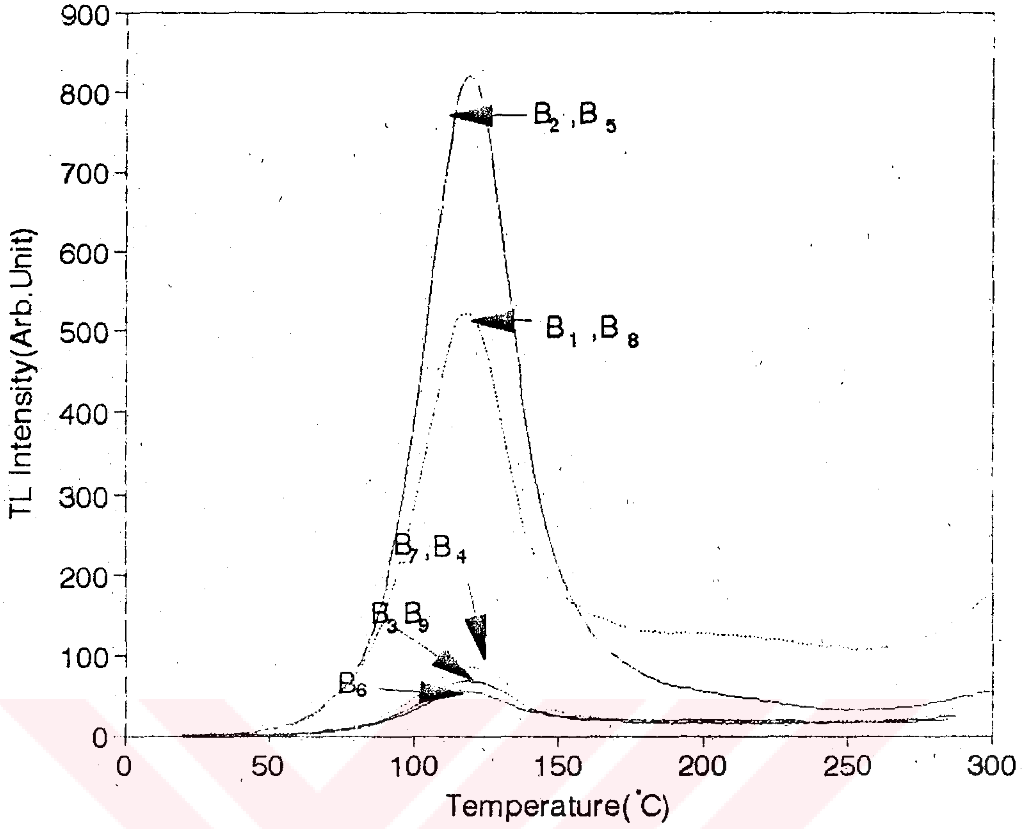

Figure 4.17. The glow curves of nine ZnS thin film samples.

approximately 120°C. This means that the number of the electrons leaving the traps reaches the maximum value at this temperature. If ZnS thin film samples are produced in a vacuum, no glow curves are observed. It is well known that only shallow trap centers exist in ZnS thin films which do not include impurities, and these centers are emptied even at very low temperatures. ZnS thin film samples developed at atmospheric conditions can include impurities as mentioned before. Therefore, these impurities can provide deep levels.

The trapping parameters (trapping depth or activation energy below conduction band, trap concentration N_t and frequency factor s) have been determined by fitting the glow curves of these samples with first order thermoluminescence kinetics. The other parameter called the lifetime (the time for the electron to be in a trap at room temperature) is obtained from the calculated values of the frequency factor and activation energy. The calculated values of all the parameters of the ZnS thin film samples are given in Table 4.7.

Table 4.7: The calculated values of parameters of the ZnS thin film samples from B_1 to B_9.

Sample No	Trap Conc. $x10^8(1/cm^3)$	Activation En. (eV)	Frequ.factor $x10^9(1/sec)$	lifetime (hour)
B_1	0.95	0.848	5.40	8.69
B_2	7.60	0.850	8.38	6.12
B_3	1.10	0.843	4.37	8.78
B_4	15.0	0.868	17.40	5.87
B_5	22.0	0.875	23.90	5.58
B_6	18.0	0.854	11.30	5.25
B_7	0.2	0.872	22.70	5.22
B_8	5.1	0.865	16.00	5.70
B_9	1.3	0.877	25.40	5.74

As seen from this table, the activation energy and lifetime of each sample is approximately equal. The frequency factor values of the samples from B_1 to B_9, vary. This is expected as the frequency factor depends on the amount of the impurities in the samples. For example, samples B_2, B_5, and B_8 which are developed at 440, 470 and 500 °C substrate temperatures, respectively, have the maximum trap concentrations as these samples have excess $ZnCl_2$ crystals which provide defects in the thin film samples and these defects act as trap centers. As a result it can be said that excess $ZnCl_2$ crytals cause the trap concentration of the samples to increase. The trap concentrations of B_1 and B_3 samples are more or less equal to each other. On the other hand, the trap concentration of the samples B_9 and B_6 are greater than the trap concentration of the samples B_7 and B_4, respectively. Another example is as follows: because samples B_9 and B_6 have excess ZnO crystals which provide defects destroying the crystal structure of the samples, these defects act as trap centers. As a result we can say that excess ZnO crystals cause the trap concentration of the samples to increase.

The second step is to investigate the recombination centers of the samples. The TL intensity curve of every sample is obtained as mentioned before. The TL intensity curves of all the samples were identical with each other. Therefore, only the TL intensity curve of one sample, B_1, is used here. This curve is seen in Fig.4.18. As seen from this figure, we can say that the curve of every samples reaches maximum at 420 nm wavelength. This wavelength corresponds to 2.95 eV which is equal to the depth energy of the recombination center. Also this result shows that the recombination centers appear deep below the conduction band.

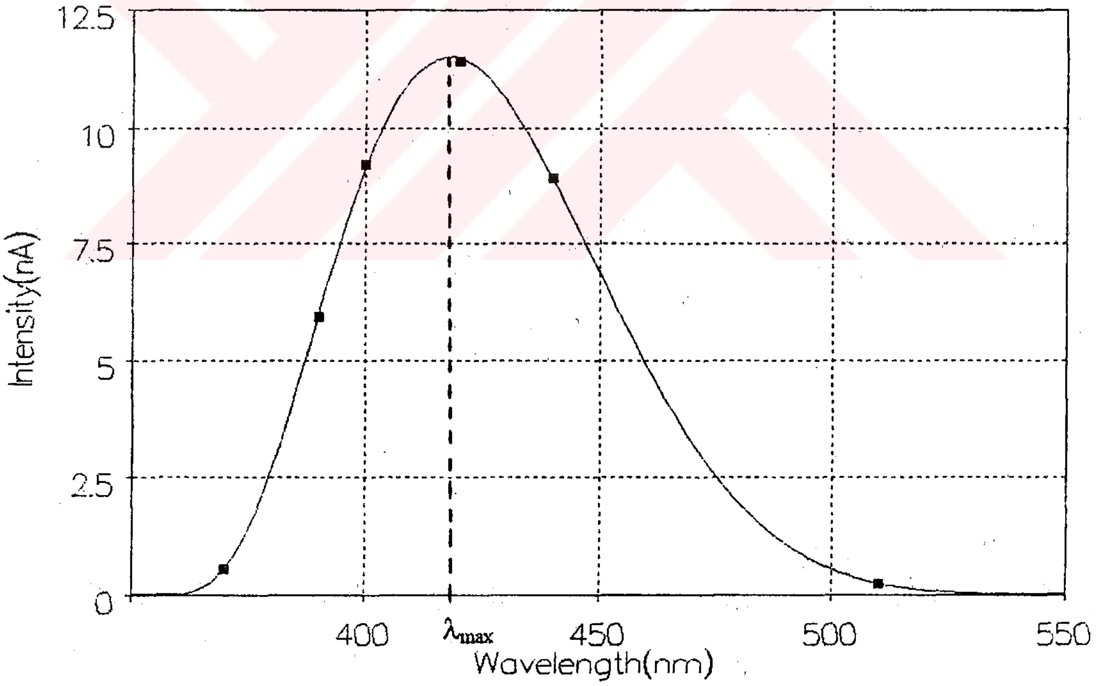

Figure 4.18. TL intensity graph of sample B_1 versus wavelength.

Finally, as mentioned in previous chapter, the dose-response graphs of the samples were obtained to show how the samples respond to the different doses. The response curves of nine samples are shown in Fig.4.19. As seen from this figure, all these curves are straight lines and their slopes are more or less equal to each other with an approximate value of 0.23 nA/Gy. This result shows that the filling probability of traps increases linearly with the radiation time. This property of the ZnS thin films gives us an opportunity to use them as a dosimeter even at room temperature.

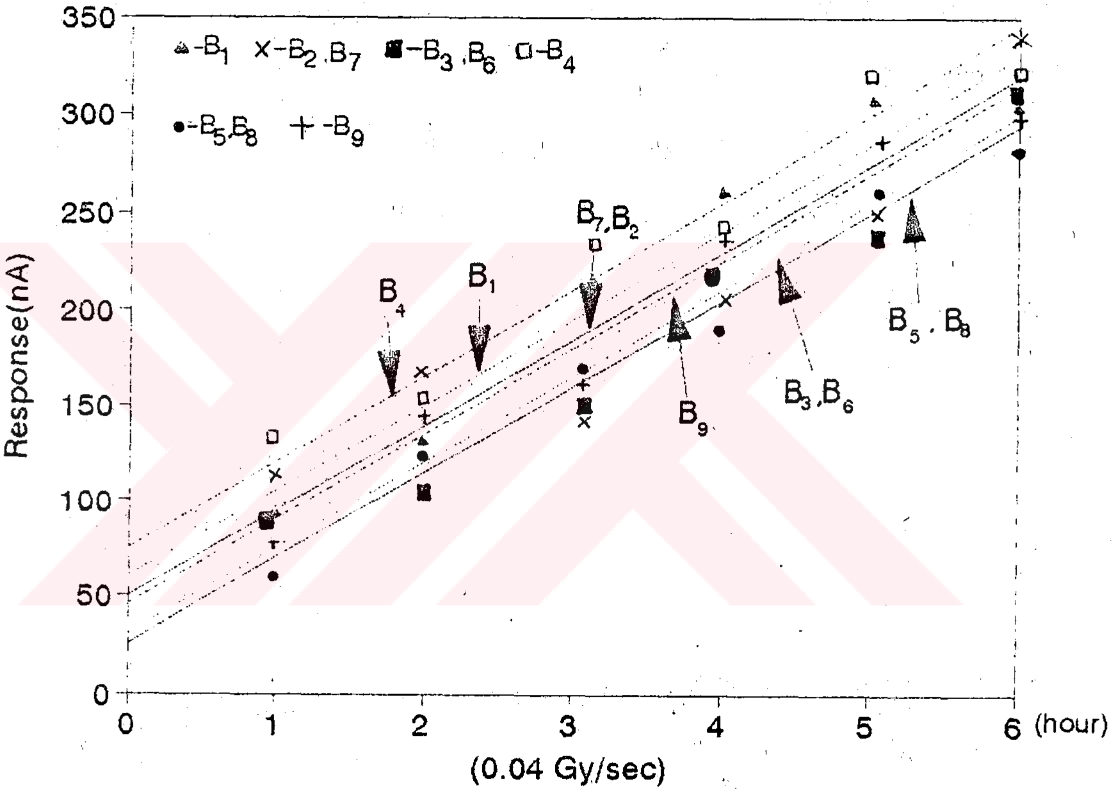

Figure 4.19. The graph of dose-response of the nine ZnS thin film samples.

CHAPTER 5

CONCLUSION

In this work, different CdS and ZnS thin films were prepared by the spray pyrolysis technique and their electrical, optical, and crystal structure were studied in detail. In addition to these studies photoconductive properties of CdS thin films and thermoluminescence properties of ZnS thin film samples were examined. The conclusions obtained from these studies can be given as follows: firstly, it was shown that the spray pyrolysis technique can be used to obtain semiconductor thin films with a very large area for solar cells and that is a very simple and low-cost method. From the measurements, it was seen that the physical properties of both CdS and ZnS thin film samples are very dependent on the thickness of the samples, the substrate temperature, and the concentrations of the salts in spraying solution. It was proved that the best quality CdS thin films are developed around at 380°C substrate temperature and the best quality ZnS thin films is developed around at 500°C substrate temperature. It was found that the chemisorption of the oxygen plays an important role in increasing the resistivity of the films. It was seen that heat treatment of the samples in nitrogen atmosphere is an important factor to increase the Hall mobility of the samples. And also it was shown that the optical band gap and the carrier lifetime and transit time of CdS of the films are independent of the substrate temperature and the concentration of the salts. From the thermoluminescence studies, it is observed that the activation energy and frequency factor of the films are independent of the substrate temperature and the concentration of the salt. But, the trap concentration of the ZnS thin films is dependent on the Zn:S ratio. And, the probability per unit time for an electron to escape from the trap is found to be about 4.6×10^{-5} sec^{-1}. Another important result obtained from the thermoluminescence study of ZnS thin films is that the ZnS thin films have only one main emission band, a violet band at about 420 nm. Under the light of this result, we can propose a model that can explain the emission band. This model is shown in Fig.5.1. As seen from this figure, oxygen molecules act as a recombination center in emission processes. However, the origin of the other energy state indicated by the dotted line is not at all certain. This state could be due to lattice defects or exciting radiation state. It is also possible that the violet emission is produced if an electron makes a direct transition from the conduction band to the oxygen recombination state. Finally, we can conclude that CdS thin films have the following advantages; high sensitivity, ease of use, and low cost. But they have the following disadvantages; narrow spectral response, and nonlinearity of resistance with illumination. ZnS thin films have the following disadvantages; high resistance, poor sensitivity and not easy to use.They have the following advantages; good dozimetric and luminescent properties.

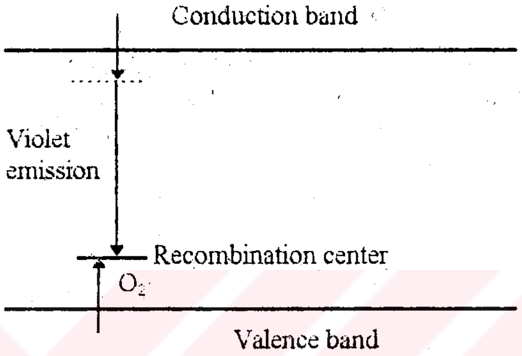

Figure 5.1. The characteristic emission bands in ZnS thin films [The violet band is centered around 420 nm (2.9 eV)].

LIST OF REFERENCES

[1] K.L.Chopra, and S.R.Das, Thin Film Solar Cells, Plenum Press, New York(1983).

[2] R.R.Chamberlin, and J.S.Skarman, Chemical Spray Deposition Process for Inprganic Films, Journal of Electrochem.Soc., 86(1966)113.

[3] Y.Y.Ma, and R.H.Bube, Journal of Electrochem.Soc., 1430(1977)124.

[4] Y.Y. Ma, Y.Y.,Fahrenbruch, A.L., and Bube, R.H., Photovoltaic Properties of n-CdS/p-CdTe Heterojunctions Prepared by Spray Pyrolysis, Appl.Phys.Lett., 423(1977)10.

[5] Touskova, J.; Kindl, D.; Tousek, J., Photovoltaic Cells on CdS/CdTe Heterojunctions, Physica Status (A) Applied Research, 142(1994)539-549.

[6] R.S.Feigelson, A.N.Diaye, S.Y.Yin, and R.H.Bube, II-VI Solid-Solution Films by Spray Pyrolysis, Journal of Appl.Phys., 3162(1977)48.

[7] S.S.Yin, A.L.Fahrenbruch, R.H.Bube, Photovoltaic Properties of ZnCdS/CdTe Heterojunctions Prepared by Spray Pyrolysis, Journal of Appl.Phys., 1294(1978)48.

[8] C.Eberspacher, A.L.Fahrenbruch, R.H.Bube, Crystallographic Polarity in the II-VI Compounds, Thin Solid films, 1(1986)136.

[9] H.Luquest, M.Perotin, A.Dhoulb, J.Bougnot, M.Savelli, Photovoltaic Properties of CdS/CdTe Heterojunctions, Solar Cells, 289(1986)13.

[10] A.C.Trevor, and R.H.Bube, Electrical Transport in ZnCdS Films Deposited by Spray Pyrolysis, Journal of Appl.Phys., 1844(1980)51.

[11] M.Abd-Lefdil, M.Rolland, J.Bougnot, M.J.M. Abadie, Studies of $Zn_xCd_{1-x}S$ Films and $Zn_xCd_{1-x}S/CuInSe_2$ Heterojunction Solar Cells, Solar Energy Mats., 307 (1986)13.

[12] M.Krunks, E.Mellikov, and E.Sork, Formation of CdS Films by Spray Pyrolysis, Thin Solid Films, 105(1986)145.

[13] P.Rajaram, R.Thangaraj, A.K.Sharma, O.P.Agnihotri, Solar Cells, 123(1985)14.

[14] H.L.Kwok, and Y.C.Chau, Carrier Density and Mobility in CdxZn1-xS Chemically Sprayed Films, Thin Solid Films, 303(1980)66.

[15] M.S.Tomar and F.J.Garcia, Japan J.Appl.Phys., 567(1980)19.

[16] Dachraoui, M., and Vedel, J., Sprayed $CdS\text{-}Cu_2S$ Solar Cells: Structural and Chemical Properties of Airless Sprayed CdS and CdZnS Layers, Solar Cells: Their Science, Technology, Applications and Economics, 15(1985)319.

[17] Lo Savio, M., Oliveri, M.E., Novel Preparation Method and Investigation of Sprayed CdS Fims, Appl.Phys.A: Solids and Surfaces, 50(1)(1990)17-21.

[18] Savio, M.L., and Oliveri, M.E., A New Procedure for Thin-Film Deposition by Solution Spraying, Appl.Phys.A., 39(1986)269-271.

[19] Brown, B.J., Bates, Clayton W.Jr., Similarities in the Chemical Mechanism of $CuInSe_2$ and CdS Thin Film, Thin Solid Films, 188(2)(1990)301-305.

[20] D.S.Albin, and S.H.Risbud, Nucleation and Growth Characteristics of Spray-Pyrolyzed CdS Thin Films, Thin Solid Films, 203(1987)147.

[21] S.Kolhe, V.J.Hasbnis, S.K.Kulkarni, M.G.Takwale, J.Mater.Sci.Letts., 49(1987)6.

[22] B.K.Gupta, O.P.Agnihotri, Sol.State Commun., 255(1977)2.

[23] Chow, L.W., Lee, Y.C., and Kwok, H.L., Structure and Electronic Properties of Chemically Sprayed CdS Films, Thin Solid Films, 81(1981)307-318.

[24] F.B.Micheletti, and P.Mark, Effects of Chemisorbed Oxygen on the Electrical Properties of Chemically Sprayed CdS Thin Films, Appl.Phys.Lett., 136(1967)10.

[25] Valyomana, A.G., Vijayakumar, K.P., Purushothaman, C., Effect of Annealing Temperatures on the Electrical Transport Properties of Spray-Pyrolysed CdS Films, Journal of Materials Science Lett., 9(1990)1025-1027.

[26] Kolhe, S., Kulkarni, S.K., Takwak, M.G., Bhide, V.G., Electrical Conduction in Sprayed CdS Films, Solar Energy Materials, 13(31)(1986)203-211.

[27] Kwok, H.L., and Siu, W.C., Carrier Concentration and Mobility in Chemically Sprayed CdS Thin Films, Thin Solid Films, 61(1979)249-257.

[28] Pence, S., Varner, E., and Bates, Clayton W.Jr., Substrate Temperature Efects on the Electrical Properties of CdS Films Prepared by Chemical Spray Pyrolysis, Materials Letters, 23(1)(1995)13-16.

[29] Mzerd, A., Sayah, D., Saunders, I.J., and Jones, B.K., Electrical Properties of $Cd_{1-y}Zn_yS$ and CdS(In) Thin Films Prepared by Prolytic Spray Technique, Phys.Stat.Sol.(A) Appl.Phys., v:119, n:2, (1990)487-494.

[30] Wu, Chen-loo, and Bube, R.H., Thermoelectric and Photothermoelectric Effects in Semiconductors: Cadmium Sulphide Films, Journal of Appl.Phys., 45(2)(1974)648-660.

[31] Valyomana, A.G., Mathew, S., Vijayakumar, K.P., Purushothuman, L., Photoconductive and Ellipsometric Studies of Spray Pyrolysed CdS Thin Films, Balletin of Materials Science, 16(1)(1993)55-61.

[32] Valyomana, A.G.; Vijayakumar, K.P., and Purushothaman, C., Effect of Annealing Temperatures on the Electrical Transport Properties of Spray-Pyrolysed CdS Films, Journal of Mat. Sci. Lett., 9(1990)1025-1027

[33] W.Dulak, H.Meczyska, Phys.Stat.Sol.(A), K.171(1986)93.

[34] S.B.Gadgill, R.Thangaraj, O.P.Agnihotri, J.Appl.D., 112(1987)20.

[35] Cong, H.N., Charter, P., Effect of Nickel Doping on the Photoelectrochemical Behaviour of Sprayed CdS Films, Journal of Electro-Analytical Chemistry and Interfacial Electro-Chemistry, 272(1) (1989)137-143.

[36] Golovanov, V., Lantto, V., Leppavuori, S., Uusimaki, A., Remes, J., Frantti, J., Surface Structure and Morphology of CdS Thin Films Deposited by Spray Pyrolysis, Evoluation of Thin Film and surface Structure and Morphology Materials Research Society Symposium Proceedings, v:355(1995), Materials Research Society, Pittsburg, PA, USA, p:507-512.

[37] Hill, R., CdS/Cu_2S Thin-Film Solar Cells: Review of Methods of Producing the CdS and Cu_2S Layers, Solid State and Electron Devices, 2 (1978)S49-S53.

[38] Ashour, A., Afifi, H.H., and Mahmoud,S.A., Effect of Some Spray Pyrolysis Parameters on Electrical and Optical Properties of ZnS Films, Thin Solid Films, 248(2)(1994)255-256.

[39] Afifi, H.H., Mahmoud, S.A. and Ashour, A., Structural Study of ZnS Thin Films Prepared by Spray Pyrolysis, Thin Solid Films, 263(2)(1995)248-251.

[40] Falcony, C., Garria, M., Ortiz, A., Alonso, C., Luminescent Properties of ZnS:Mn Films Deposited by Spray Pyrolysis, J.Appl.Phys., 72(4)(1992)1525-1527.

[41] Tohge, N., Tamaki, S., Okuyama, K., Formation of Fine Particles of ZnS From Thiourea Complexes by Spray Pyrolysis, Jpn. of Appl. Phy., Part 2; Letters, 34(2)(1995)L207-L209.

[42] Pike, R.D., Cui, H., Kershaw, R., Dwight, K., Wold, A., Blantun, T.N., Wernberg, A.A., and Gysling, H.J., Preparation of Zinc Sulfide Thin Films by Ultrasonic Spray Pyrolysis from Bis(diethyldithiocarbamato)zinc(II), Thin Solid Films, 224(1993)224-226.

[43] S.M.Sze, Semiconductors Devices, Murray Hill, New Jersey, 1985.

[44] J.T.Ronald, Fundamentals of Electronic Devices, Charles E.Merril Pubslihing Comp., Ohio, 1975.

[45] A.Barlev, Semiconductor and Electronic Devices, Technio-Israel, Ins.of Tech., Prentice Hall, 1993.

[46] J.P. McKelvey, Solid State and Semiconductor Physics, A Harper International Edition, Harper and Row, 1969.

[47] V.K.Sabhapathi et al., Optical Absorption Studies in Molybdenum Trioxide Thin Films, Phys.Stat.Sol.(a), 167(1995)148.

[48] S.B.Gadgil et al, Optical and Solar Selective Properties of Chemically Sprayed Copper Sulphide Films, IOP Publishing Ltd., (1986)112.

[49] B.N.Das and S.Ghosh, On the Photoconductivity of Painted and Sintered Cadmium Sulphide Thin Film, Chapman and Hall Ltd., (1989)1449.

[50] R.H.Bube, G.A.Dussel, Ching-Tao Ho, and L.D.Miller, DEtermination of electron trapping parameters, Journal of Applied Physics, 37(1)(1966)21.

[51] H.P.D.Lanyon and W.E.Spear, Space Charge Limited Current Flow and Deep Trapping in Selenium, Proc.Phys.Soc., 4E, (1960)1157.

[52] W.E.Spear and J.Mort, Electron and Hole Transport in CdS crystals, Proc.Phys.Soc., 81(1962)130.

[53] J.Sworakowski and G.F.Leal Ferreira, Space charge limited currents and trap filled limit in one dimensional insulators, J.Phys.D:Appl.Phys., 17(1984)135.

[54] G.A.Marlor and L.Woods, Space charge limited currents and electron traps in CdS crystals, Brit.J.Appl.Phys., 16(1965)1449.

[55] G.A.Dussel, and R.H.Bube, Electric field effects in trapping processes, J.of Appl.Phys., v:37, n:7, (1966)2797.

[56] R.H.Bube, Trap density determination by space charge limited currents, J.of Appl.Phys., v:33, n:5, (1962)1733.

[57] W.E.Spear, Transit itme measurements of charge carriers in amorphous selenium films, Proc.Phys.Soc., 7B(1957)669.

[58] Y.MAruyama and H.Inokuchi, Charge carrier mobility in anthracene single crystal, Bulletin of the Chemical Society of Japan, 40(1967)2073.

[59] G.Duggan and F.Berz, The theory of the Shockley-Haynes experiment: Contact effects, J.Appl.Phys., 53(1)(1982)470.

[60] J.R.Haynes and W.Shockley, The mobility and life if injected holes and electrons in germanium, Physical Review, 81(5)(1951)835.

[61] Solid state electronic devices, TK7871.85/S57

[62] T.E.Jenkins, Semiconductor Science growth and characterization techniques, prentice hall,1995.

[63] R.H.Bube, Photoconductivity of solids, R.E.Krieger Publishing Com. New York, 1978.

[64] A.VAN Der Ziel, Solid State Physical Electronics, Prentice Hall Inc. New Cersey, 1976.

[65] S.M.Size, Physics of semiconductor devices, murray hill,new jersey, a division of john wiley & sons ,1969

[66] P.Bhattacharya, Semiconductor Optoelectronic Devices, Prentice Hall Int. Inc.,1994.

[67] F.Gutman and L.E.Lyons, Organic Semiconductor, John Wiley and Sons, Inc, New York, 1967.

[68] P.D.Townsend, J.C.Kelly, Colour Centres and Imperfections and Semiconductor, Crane, Russak an Company, Inc. New York, 1973.

[69] I.P.Jacques, Optical process in semiconductor, Prentice-Hall, Inc. New Jersey, 1971.

[70] A.Mzerd, D.Sayah, I.J.Saunders, and B.K.Jones, Electrical properties of $Cd_{1-y}Zn_yS$ and CdS(In) thin films prepared by pyrolytic spray technique, Phys.Stat.Sol.(a), 487(1990)119.

[71] R.Fastow, and Y.Nemirovsky, The excesscarrier lifetime in p-type HgCdTe measured by photoconductive decay, J.Appl.Phys., 66(4)(1989)1705.

[72] J.Reichman, Minority carrier lifetime of HgCdTe from photoconductivity decay method, Appl.Phys.Lett., 59(10)(1991)1221.

[73] R.G.Pratt and J.Hewett, Minority carrier lifetime in n-type Bridgman grown $Hg_{1-x}Cd_xTe$, J.Appl.Phys., 54(9)(1983)5152.

[74] R.Fastow and Y.Nemirovsky, Transient and steady-state excess carrier lifetimes in p-type HgCdTe, Appl.Phys.Lett., 55(18)(1989)1882.

[75] R.K.Ahrenkiel, D.J.Dunlavy and J.Benner, Minority-carrier lifetime in GaAs thin films, Appl.Phys.Lett., 53(7)(1988)598.

[76] R.K.Ahrenkiel and D.J.Dunlavy, Time-of-flight studies of minority-carrier diffusion in $Al_xGa_{1-x}As$ homojunctions, Appl.Phys.Lett., 49(12)9.

[77] R.Fastow, D.Goren and Y.Nemirovsky, Shokley-Read recombination and trapping in p-type HgCdTe, J.Appl.Phys., 66(7)(1990)3405.

[78] S.E.Schacham and E.Finkman, Recombination mechanisms in p-type HgCdTe: Freezeout and background flux effects, J.Appl.Phys., 57(6)(1985)2001.

[79] S.K.Pang and A.Rohatgi, Record high recombination lifetime in oxidized magnetic Czochralski silicon, Appl.Phys.Lett., 59(2)(1991)195.

[80] E.Yablonovitch and T.Gmitter, Auger recombination in silicon at low carrier densities, Appl.Phys.Lett., 49(10)(1986)587.

[81] K.L.Luke, Analysis of the interaction of a laser pulse with a silicon wafer: Determination of bulk lifetime and surface recombination velocity, J.Appl.Phys., 61(6)(1987)2282.

[82] S.K.Pang and A.Rohatgi, A new methodology for separating Shockley-Read-Hall lifetime and Auger recombination coefficients from the photoconductivity decay technique, J.Appl.Phys., 74(9)(1993)5554.

[83] V.Stupelman and G.Figaretov, Semiconductor Devices, Mir.Publishers Mossow,1976.

[84] W.R.Runyan, Semiconductor measurements and instrumentation , McGraw-Hill book company, New York 1975.

CIRRICULUM VITAE

The author was born in Bursa, on March, 1963. He graduated from the primary, secondary and high schools in Bursa, in 1974, 1977, and 1980, respectively. He received the B.S. degree from physics engineering department at Gaziantep Engineering Faculty of Middle East Technical University, in 1989. He started to work as research assistant in department of physics engineering of University of Gaziantep in 1989. He also received the M.S. degree from the department of physics engineering of the University of Gaziantep, in 1992. In 1993 he was accepted to the Ph.D. program in Engineering Faculty of the University of Gaziantep.